IMPROVING A NON-LINEAR MODEL FOR SIMULATING SAND WAVES

An idealized modelling study on the effect of including suspended sediment and a critical condition for bed load transport on sand wave predictions in the North Sea

Master Thesis

February – October 2011

Author:

E. Ensing
Water Engineering & Management
University of Twente

Supervisors:

Prof.dr. S.J.M.H. Hulscher
Water Engineering & Management
University of Twente

Dr.ir. F.M. Sterlini-van der Meer
Water Engineering & Management
University of Twente

UNIVERSITY OF TWENTE.

Summary

Sand waves are bed forms that are observed in shallow seas of about 10 to 55 m deep with strong tidal currents. They only appear on a sandy bottom and they do not develop when coarse sediment covers the sea bed. They have a typical wavelength ranging from 100 to 800 m and their maximum amplitude is in the order of 5 m. Sand waves often pose a problem in shallow seas, because those seas are used for various functions. Sand waves can migrate and thereby expose pipelines, obstruct navigational routes and even expose undiscovered mines and chemical waste that may have been deposited in the past. Therefore, more insight into the behaviour of such sand waves can be put to good use.

The model that is used in this research is called the Sand Wave Code (SWC). It is a non linear model, which allows the prediction of sand waves from their initial state up to their final shape. The model can predict the sand wave shape, growth rate and migration speed and usually works with a domain of one wavelength. The domain length is determined in a linear perturbation analysis, and it is equal to the wavelength of the fastest growing mode. The main goal of this research was to improve this model, in order to be able to make better predictions of the behaviour of the sand waves.

In this research two improvements of the SWC are carried out. The first is an improvement of the suspended load transport calculation. This was necessary, because it had some shortcomings, for instance it lacked a proper scaling and the no flux boundary condition was not actually implemented at the surface. After improving all of these aspects of the suspended sediment calculation, a critical condition for the initiation of bed load transport was added to the SWC. This critical condition also works with the improved suspended sediment module and the surface gravity waves module of the model.

Hereafter, we carried out simulations to test the effect of these changes. The results of these simulations are compared with measurements from three locations in the North Sea. The results showed that the sand wave length was predicted best when suspended sediment and the critical condition were both not taken into account. However, in this case the predicted final sand wave amplitude is way too large. Including suspended sediment did not help to reduce these large amplitudes, they were even increased slightly. The results of the suspended sediment runs did show however, that the simulated concentration profiles are more physically justified. The results of the critical condition for the initiation of bed load transport were as expected. It causes shorter sand waves with a lower crest. The growth rate of the sand waves is also reduced significantly, except in the case where suspended sediment transport was also included. The resulting behavior of the bed load transport over a tidal cycle was as expected, with the bed load transport declining to zero for low flow velocities. The critical condition thus succeeded in reducing the predicted final amplitude of the sand waves, but it gave an underestimation of the sand wave length. To check whether the reduction in amplitude was not only associated with the reduction in sand wave length, simulations have been performed with the same lengths as the ones predicted in the basic simulations. The results of this showed that the critical condition was still able to predict lower values of the final sand wave amplitudes. These lower amplitudes were still too large however, so more processes are needed to help reduce this.

The Sand Wave Code has been improved significantly in this research. Especially the suspended sediment calculation has been improved. Many minor shortcomings have been improved and a new scaling has been successfully applied to the calculation. The critical condition has also been implemented successfully, even for the case with surface waves. When comparing the results to measurements at three locations in the North Sea, it can be seen that a better prediction of the final shape is obtained with the critical condition, but not with suspended sediment.

Preface

Before finishing the last course of my minor in Applied Mathematics, I started with the master program Water Engineering and Management. I finished one year of this master before I finally finished the final course for my minor and thereby bachelor. The reason for this was that this course was in the fourth quartile, and the year before that I was in Indonesia for my Bachelor Internship at LabMath-Indonesia. This was a completely different experience from the current research on sand waves at the University of Twente. With this thesis I will complete my master course at the University of Twente.

First of all I would like to thank my supervisors, because without them finishing this thesis would not have been possible. Fenneke Sterlini really helped me get the hang of the Sand Wave Code. This code was really complicated and I did not even understand the programming language of C++ when I started this research. She also gave good constructive feedback on all my reports and had useful discussions with me. Suzanne Hulscher gave really good feedback on my preparatory reports, which motivated me to come up with a good final report. During most of my research she was on a leave, which was the reason I also asked help from Pieter Roos, who sat in for Suzanne Hulscher for the interim meeting. He also really helped out with the mathematical parts of my research, on which he gave me good constructive feedback and nice suggestions. During this he was always enthusiastic and helpful, which I appreciate a lot.

I would like to thank my roommates in the graduation room for having lunch together with me during which we had nice talks and discussions. I really liked the barbecue that Felipe organized together with Jorick. I enjoyed having lunch discussions with Bert, Bart, Felipe and also Oana, who has returned to Romania. I also liked helping you guys out and want to thank you for the times you gave me some advice. I really liked the atmosphere and the employees at the WEM department. Of these employees, I would like to thank Suleyman, Kathelijne and Jolanthe for helping me out and considering my future plans.

Finally I would like to thank my family, housemates and especially my girlfriend Karlijn for supporting me and listening to me.

Erik Ensing
Enschede, October 2011

Table of Contents

List of symbols

A list of all parameters and variables used in this report.

Greek

α	Proportionality constant for the bed load transport
$\hat{\alpha}$	First scaling variable used in the flow calculation
$\tilde{\alpha}$	First scaling variable used in the concentration calculation
β_*	The difference between a water and a sediment particle
$\hat{\beta}$	Second scaling variable used in the flow calculation
$\tilde{\beta}$	Second scaling variable used in the concentration calculation
γ	Weight of τ_{bw}, depending on the angle between the surface waves and the current
Δt	Duration of one time step
Δx	Space step in x-direction
Δz	Space step in z-direction
$\Delta \tilde{z}$	Height of the top cell used in Appendix B
ϵ_v	Sediment diffusivity
$\bar{\epsilon_v}$	Sediment diffusivity in case of a constant distribution
ζ	Water surface elevation
θ_{cr}	Critical value of the Shields parameter
κ	Von Kármán constant
λ	Slope factor (inverse tangent of the angle of repose)
λ_1, λ_2	Exponents of both terms in the Ansatz of equation (4.3.22)
ν	Kinematic viscosity of water
ρ_s	Density of sediment
ρ_w	Density of water
σ	Surface gravity wave frequency
τ_b	Bed shear stress
τ_{bf}	Bed shear stress due to flow over the bottom
τ_{bw}	Additional bed shear stress due to surface gravity waves
τ_{cr}	Critical bed shear stress for the initiation of bed load transport
ψ	Angle in degrees between the surface waves and the current
ω	Tidal frequency (M2 tide)

Roman

a	Reference height used in the concentration calculation
A_1, A_2	Amplitudes of both terms in the Ansatz of equation (4.3.22)
A_v	Eddy viscosity
c	Suspended sediment concentration
c_a	Suspended sediment concentration at the reference height (a)
$C_{a,p}$	Truncated Fourier series of the reference concentration
C_p	Truncated Fourier series of the suspended sediment concentration
dt	Duration of one time step in the main loop
D_{50}	Mean sediment diameter
D_*	Dimensionless grain size
f_{eff}	Efficiency coefficient

f_w	Bed friction factor used in the calculation of τ_{bw}
g	Gravitational acceleration
h	Bed level elevation
H	Mean water depth
$\tilde{h}$	Bed level elevation plus reference height
i	Imaginary number (used in the truncated Fourier series)
i	Index of the horizontal location
j	Index of the vertical location
k	Index of the time step
L	Sand wave length
Npx	Number of cells in x-direction
Npz	Number of cells in z-direction
p	Truncation integer
P	Truncation number
Q	Threshold for the initiation of bed load transport
q_b	Bed load transport
q_{bf}	Bed load transport due to flow
q_s	Suspended load transport
s	$s-1$ is the relative density of sediment in water
S	Slip parameter
t	Time
$\hat{t}$	Scaled time in the flow calculation
$\tilde{t}$	Scaled time in the concentration calculation
t_{step}	Number of time steps within a tidal cycle
T_w	Surface wave period
u	Horizontal flow velocity
$\bar{u}$	Depth averaged mean velocity of the oscillating tidal flow
$\tilde{u}$	Scaled horizontal flow velocity in the concentration calculation
u_{bed}	Horizontal flow velocity at the bottom
u_{bf}	Horizontal flow velocity at the bottom due to the flow
u_{bw}	Horizontal flow velocity at the bottom due to surface waves
u_{cr}	Critical value of the horizontal flow velocity
u_{res}	Residual current
u_{total}	Total horizontal flow at the bottom, used in the derivation of the critical condition for the initiation of bed load transport
u_*	Bed shear velocity
w	Vertical flow velocity
$\tilde{w}$	Scaled vertical flow velocity in the concentration calculation
w_s	Sediment fall velocity
x	Horizontal location along the domain
$\hat{x}$	Scaled horizontal location in the flow calculation
$\tilde{x}$	Scaled horizontal location in the concentration calculation
z	Vertical location along the water column, starting at the bottom
$\hat{z}$	Scaled vertical location in the flow calculation
$\tilde{z}$	Scaled vertical location in the concentration calculation

1 Introduction

A model for the prediction of sand waves is improved in this research. This is done by improving the suspended sediment module, by the addition of a critical condition for the initiation of bed load transport and through some other minor improvements to the model. The improvement of the suspended sediment module consists mostly of a new scaling for the calculations and the implementation of a no flux boundary condition at the surface.

In this chapter a short description of the problem is first given. The literature study that was done prior to this research is also summarized shortly. Then the aim and objective of this research, which have been altered quite a bit during the course of the research, are given. On the basis of this, several research questions are composed. Finally, an outline of the rest of the report is presented.

1.1 Problem description

The modelling of sand waves gives us more knowledge concerning their behaviour, which has many practical applications. More insight into the contribution of different physical processes to properties of the sand waves is the main aim of this research. The main properties considered are the height, length, migration speed and growth rate of the sand waves. In practice, especially predictions on their formation and migration rates are useful (Dodd et al., 2003), but naturally also the final sand wave height is important. Sand wave migration has the capability to expose pipelines, which can cause these pipelines to bend or break. Sand waves can also obstruct navigational routes, by lowering local water depths below minimum depths required for navigation. Furthermore, along the Dutch coast artificial islands are proposed and mining is planned in order to provide sand for nourishments on the coast, while the effects of these practices are often not certain. Last but not least, sand waves also sometimes threaten the safety, as it can expose mines and chemical waste that have been deposited in the past (Németh et al., 2003).

Tidal sand waves are only observed in seas with strong tidal currents, the depth averaged tidal currents should be stronger than 0.5 m/s (Dodd et al., 2003). Sand waves appear only on a sandy bottom and they do not develop when a coarse sediment (grain size > 1 mm) covers the sea bed (Besio et al., 2003). They have a typical wavelength ranging from 100 to 800 m and their maximum height is in the order of 5 m (Hulscher, 1996). Sand waves are relatively immobile bed forms compared to the dunes and bars that occur in rivers. The reason for this is that the time-velocity asymmetry of tidal currents is generally comparatively weak. This causes a very small net bed-material transport, even though the instantaneous rates are as high as those occurring in rivers (Allen, 1980).

The model that is used in this research is called the Sand Wave Code. It is a non linear model, which allows the prediction of sand waves from their initial state up to their final shape. The model can predict the sand wave shape, growth rate and migration speed and usually works with a small domain of one wavelength. The domain length is determined in a linear perturbation analysis, and it is equal to the wavelength of the fastest growing mode. Various processes are included in the model, which were discussed in the literature report. The model currently contains three extension modules. These modules describe the addition of surface gravity waves, suspended sediment transport and sediment mixing. The suspended sediment transport calculation had some shortcomings; it lacked a proper scaling and the no flux boundary condition was not actually implemented at the surface.

Therefore, the choice was made to improve this module in this research. After improving the suspended sediment calculation, there was still some time left. This time was used to add a critical condition for the initiation of bed load transport to the Sand Wave Code. This critical condition does not only work with the basic model where only bed load transport is taken into account, but also with the improved suspended sediment module and the surface gravity waves module.

1.2 Summary of the literature study

Prior to this research, in the preparation course, a literature study had been carried out. A short summary of the findings and conclusions of this study is given here. In this literature study, the results and recommendations of the previous research were analyzed. Also, papers on the topic of sand wave evolution were consulted.

These papers and the analysis of the previous research by Sterlini (2009) showed that quite a few physical processes had not yet been included in the model. These physical processes will be summed up first. No critical value for the initiation of bed load transport was present. This means that sediment is put in motion even at small flow velocities, which does not occur according to measurements. Many researchers have used a certain critical condition for the initiation of motion in their sediment transport calculations (Allen, 1980; Bartholdy et al., 2010; Besio et al., 2003; van der Veen et al., 2006). Biological influences (Borsje et al., 2009) had not been taken into account. The variation in flow characteristics due to spring-neap tide and seasonal changes were not considered (Blondeaux and Vittori, 2010). Extreme conditions with higher velocities and therefore more sediment transport are thus not accounted for. In the Sand Wave Code, turbulence is modelled by a constant eddy viscosity and a partial slip condition at the bottom. This is a very simple estimation of the actual turbulence, while more extensive methods are available which take into account for instance the distance from the bed and the local flow velocities (Besio et al., 2006). The process of flow separation could also be added. The current model is a two-dimensional vertical model, which could be expanded to a three-dimensional model (Hulscher, 1996). When this is done, the orientation of the sand waves can be considered.

Furthermore, the modules describing suspended sediment transport, grain size sorting and surface gravity waves could not operate simultaneously (Sterlini, 2009). The model could thus also be improved by including interactions between some of these modules. Since the grain size sorting module collapses before an equilibrium is reached, only the combination of suspended sediment and surface gravity waves has been considered here. The latter combination could be carried out by describing the effect of the surface gravity waves on the flow. In the Sand Wave Code, the surface gravity waves only affect the bed shear stress and thereby the bed load transport. Since suspended sediment is transported by the flow, this would not be sufficient.

A choice on which processes to include was proposed in the literature report. This choice depended on feasibility to perform this within the time frame, expected qualitative and quantitative significance, data availability and also personal preference. Including biological influences and expanding to a three-dimensional model probably did not fit within the timeframe of this research, so these options were discarded. Improving the turbulence model was not expected to yield significant differences and flow separation was not expected to occur over sand waves. The spring-neap tide and seasonal variations were chosen not to be implemented, due to a large dependency on measurement data. As mentioned earlier, the grain size sorting model was not considered, as it did not work properly for the entire process of the sand wave evolution. It was therefore proposed to combine the modules regarding suspended sediment and surface gravity waves first, after which the critical condition for the initiation of bed load transport should be added. These additions were expected to yield very interesting results. Also, it would allow us to use the model at its full potential.

1.3 Aim and objective

The main aim of this research was to improve our understanding on the behaviour of sand waves. This was done using a modelling approach, by adding and improving processes in the model that represent physical mechanisms and comparing the results to previous findings. The new model, which includes an improved suspended sediment transport module and a critical condition for the initiation of sediment transport, should thus give us new insights into this. The research objective was initially composed using the conclusions of the literature report, but has been altered through the course of this research due to both a change of plans and time restrictions.

The following research objective has been composed:

"Improve the Sand Wave Code in order to make it predict the growth rate, final shape and migration speed of sand waves better, both by improving the suspended sediment transport module and by adding a critical condition for the initiation of sediment transport."

To check whether the growth rate, final shape and migration speed of the sand waves are predicted better, the results of the SWC are compared with three cases in the North Sea. Especially the most problematic prediction, namely predicting the final amplitude of the sand waves, is expected to be improved by adding suspended sediment and a critical condition for the initiation of bed load transport.

1.4 Research questions

The following research questions have been composed based on the research aim and objective:

- How can the suspended sediment transport module be improved?
    - Which shortcomings does the suspended sediment module of the SWC have?
    - How can the suspended sediment module be improved or expanded to overcome these shortcomings?
    - To what extent does including the new suspended sediment module have a significant effect on the prediction of the growth rate, migration speed or final shape of the sand waves?
    - What do the results of the SWC with the improved suspended sediment transport module show when compared to measurements at three sites in the North Sea?
- What is the effect of adding a critical condition for the initiation of sediment transport on the sand wave prediction?
    - Which equations should be used to describe the critical condition?
    - How can these equations be implemented in the model?
    - How significant is the effect of adding this critical condition on the prediction of the growth rate, migration speed or final shape of the sand waves?
    - What do the results show when compared to measurements at three sites in the North Sea?

1.5 Outline

We start with a description of the three cases that are used to evaluate the results of the improved Sand Wave Code (SWC) in Chapter 2. These cases both describe a location in the North Sea along with measured characteristics of the sand waves and the tidal current.

Next, in Chapter 3 the model is shortly described using a flowchart and the model parameters used in this study are presented. Basically two sets of parameters have been used in the first part of the research and each of the three cases has its own set of parameters.

In Chapter 4, an upgrade to the suspended sediment transport module is discussed. This upgrade consists of a newly introduced scaling of the suspended sediment concentration calculation, a no flux boundary condition at the top of the water column and a re-evaluation of the chosen sediment diffusivity profile. The new scaling ensures that the bed level elevation is properly taken into account in the suspended sediment calculation. In the previous version of the SWC a simple Neumann boundary condition was imposed on the surface, instead of the no flux condition as stated by Sterlini (2009). For determining the necessity and effect of the no flux boundary condition, a basic state approximation is used.

In Chapter 5, the critical condition for the initiation of bed load transport is discussed. A new expression for the bed load transport has been derived and it has been implemented in the SWC through the use of a critical bed shear stress.

Chapter 6 shows results of the three simulated North Sea. The effects of including suspended sediment, a critical condition and a combination of both are shown and the results of the simulations are compared with the measurements that were discussed in Chapter 2.

Finally, in Chapter 7 the results and limitations of the model are discussed and in Chapter 8 conclusions are drawn from this and recommendations for future research are given. In Chapter 8 the research questions are also answered and it is discussed whether the objective of the research has been reached.

2 Measurements from the North Sea

2.1 Introduction

Three cases were chosen from the literature to compare the SWC results with. The first two cases are from Van Santen (2009) and the third case is from Besio et al. (2006). All cases describe a location in the North Sea, along with characteristics of the present tidal current and properties of the occurring sand waves. The cases from Van Santen (2009) and the case from Besio et al. (2006) are described in Sections 2.2 and 2.3 respectively.

2.2 Case 1A and Case1B

Two cases were chosen from Van Santen (2009). Case 1A and 1B in our research correspond to case number “159-1” and “201”. In Figure 1 the geographical location of these cases can be seen.

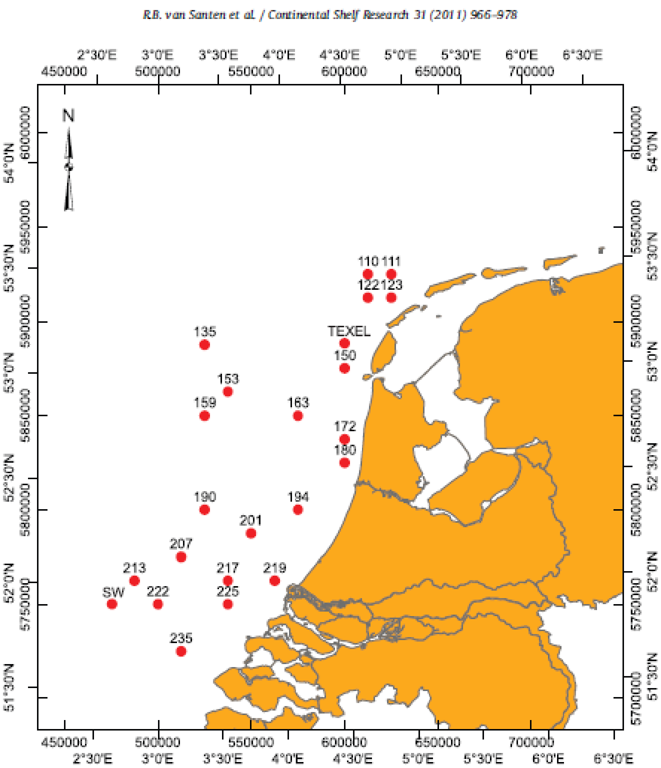

Figure 1: Geographical locations of the study areas used by Van Santen (2009) and Van Santen et al. (2011). The locations used in this research are 159 for Case 1A and 201 for Case 1B.

Van Santen (2009) gives information on environmental and tidal conditions as well as the average height and length of the measured sand waves. The data relevant for this research are shown in Table 1. The two chosen cases have a relatively high grain size and tidal velocity amplitude.

Case in this research	Number in V. Santen (2009)	Water depth (H)	Grain size (D_{50})	Tidal velocity amplitude ($\bar{u}$)	Sand wave length (L)	Sand wave height
Case 1A	159-1	27.0 m	420 µm	0.56 m/s	520 m	2.0 m
Case 1B	201	25.7 m	360 µm	0.64 m/s	400 m	3.8m

Table 1: Information on environmental conditions and sand wave characteristics for locations 159-1 and 201 from Van Santen (2009).

2.3 Case 2

The third case was taken from Besio et al. (2006). Case 2 in our research corresponds to sand waves measured from their measurement site “SW1” with tidal current measurements from site “St. 11”. In Figure 2 the geographical locations of these sites can be seen.

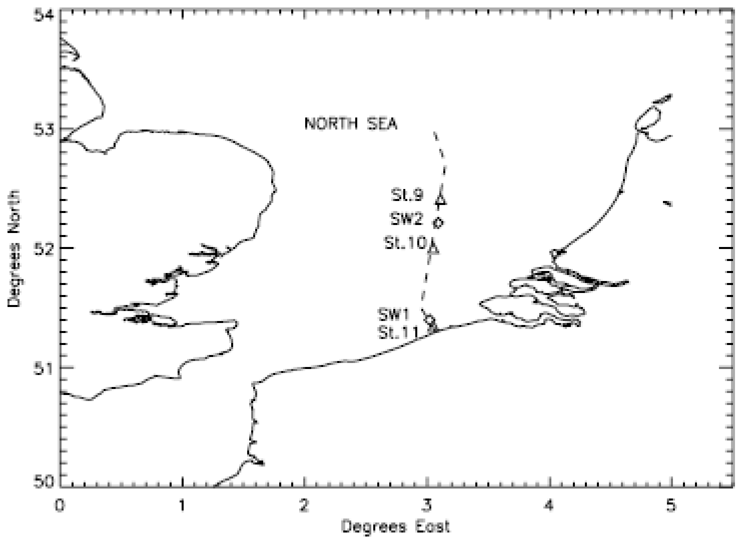

Figure 2: Study area of Besio et al. (2004) and Besio et al. (2006). In this research the sand wave measurements from site SW1 and the tidal current measurements from site St. 11 are used.

Besio et al. (2006) also give information on both the environmental and tidal conditions and the characteristics of the measured sand waves. The data relevant for this research are shown in Table 2. In addition to a velocity amplitude corresponding to the semi-diurnal tide, they state that at this location a residual current of 0.02 m/s is also present. In this research the effect of this residual current is studied individually, so for this case the simulations have been run both with and without a residual current. The sand wave length given by Besio et al. (2006) is said to vary from 165 m to 255 m with an average of 210 m, while the sand wave height varies from 2.0 m to 4.0 m with an average of 3.0 m.

Case in this research	Water depth (H)	Grain size (D_{50})	Tidal velocity amplitude ($\bar{u}$)	Residual current (u_{res})	Sand wave length (L)	Sand wave height
Case 2	20.0 m	600 μm	0.43 m/s	0.02 m/s	210 ± 45 m	3.0 ± 1 m

Table 2: Information on sand wave characteristics for site SW1 and tidal current data for site St. 11 used by Besio et al (2004) and Besio et al. (2006).

3 Model description and parameters used during this study

3.1 Short description of the model using a flowchart

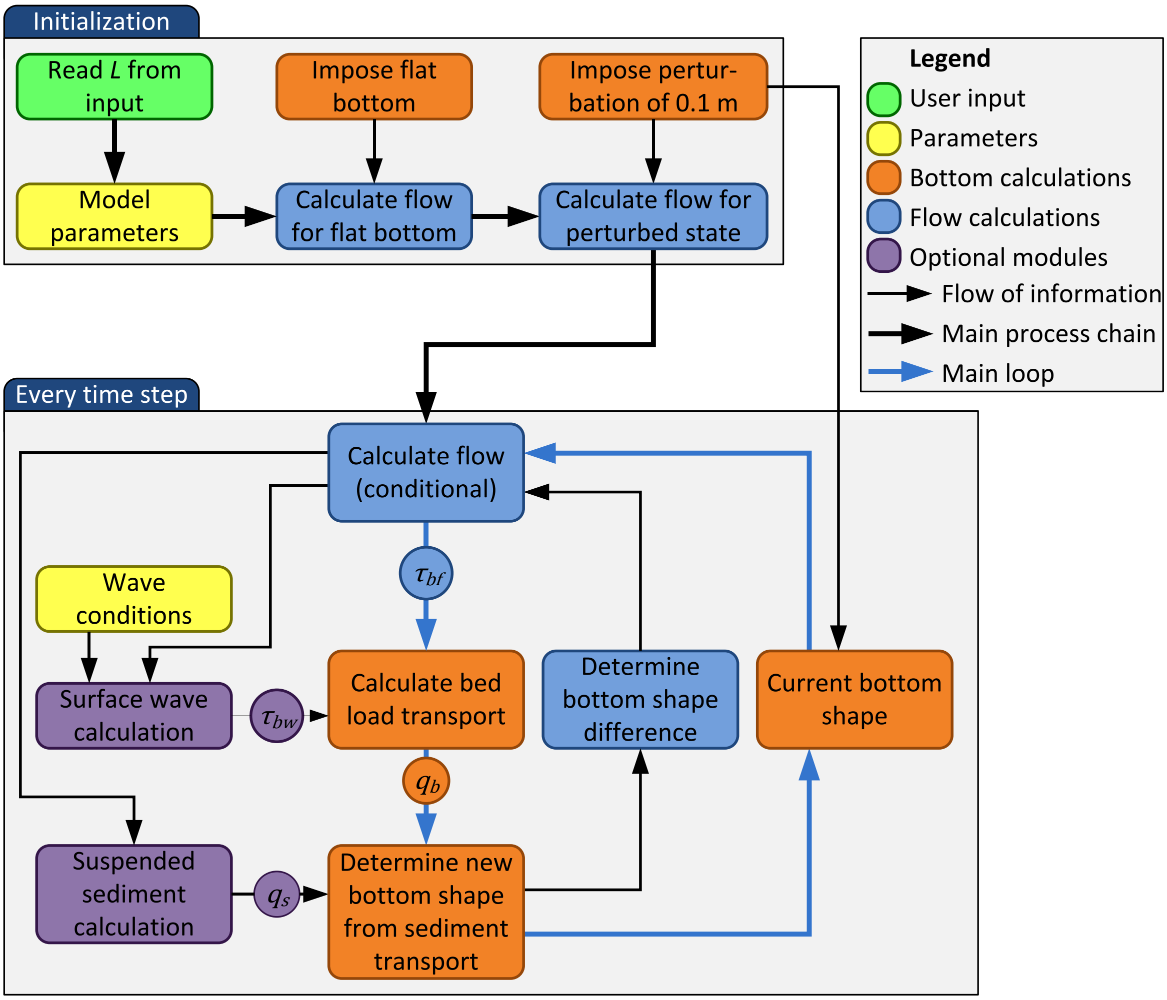

Figure 3: A flowchart showing an overview of the processes in the Sand Wave Code. The different processes are shown in boxes. The arrows between the boxes indicate the flow of information through the model.

In Figure 3 an overview of the Sand Wave Code is given in a flow chart. The initialization starts when a sand wave length (L) is given by the user. This sand wave length is inserted in the model parameters. The model parameters can be called upon from anywhere in the SWC, but it is only shown in the beginning of the process here to show that these values are loaded at the start of the initialization process. A flat bottom is then imposed, after which the flow is calculated for a flat bottom. The resulting initial flow is used in calculating the flow in the perturbed state, which is imposed next. This concludes the initialization.

After this, the model enters a loop that is rerun for each time step. The flow and bottom values resulting from the initialization are used in the first time step. In the loop, first the flow is calculated. This process is only repeated when the bottom has changed enough. The information of this is obtained from the "Determine bottom shape difference" process, which compares the bottom shape difference with a set threshold. The flow information is passed on to three other processes, namely calculating the bed load transport (q_b), the surface wave calculation and the suspended sediment calculation. When surface waves are switched on, the shear stress at the bottom due to surface waves (τ_{bw}) is first calculated and then used in the bed load transport calculation. The bed load transport calculation thus combines the bed shear stresses due to tidal flow (τ_{bf}) and surface waves (τ_{bw}). After this, it passes on the resulting bed load transport to the process that determines the new bottom shape. When suspended sediment is turned on, the suspended load transport (q_s) is also passed on to the process that determines the new bottom shape. The new bottom shape is thus determined from both the bed load transport and the suspended load transport. The new bottom shape is passed on to the process that determines the bottom shape difference and it is set to the current bottom shape. Information on the bottom shape difference and the current bottom shape are then again passed on to the flow calculation and the loop repeats until the final time step is reached. The number of time steps is given by the user and it is chosen based on the expected time of equilibrium to occur.

3.2 Model parameters used during this study

When running simulations with the Sand Wave Code (SWC), five different sets of parameters have been used. Two of these were used in the testing phase of the research in which the code was improved. The three other parameter sets correspond to the three different North Sea cases. Both of the former sets were also used by Sterlini (2009) and they both contain typical values for the North Sea. The first set, named Set 1, was used for the surface wave simulations of Sterlini (2009). The second set (Set 2) was used there for the suspended sediment simulations. In this research Set 1 has been used mostly at the start of the research. Later a switch to Set 2 has been made, which was a parameter set that was more easy to handle for the SWC in case of suspended sediment. When not mentioned otherwise, the general default parameters of Section 3.2.1 are used.

3.2.1 General default parameters

These parameters are used throughout this research, for all simulations except for the simulations for the basic state of Section 4.3.4 (see the asterisks below).

Parameter	Description	Value	Unit
ρ_s	Density of sediment	2650	kg/m³
$\bar{\epsilon_v}$	Sediment diffusivity	0.045*	m²/s
a	Reference height	$0.01 \cdot H$**	m
ω	Tidal frequency (M2 tide)	$2\pi/44700$	rad/s
Npx	Number of cells in x-direction	30	n/a
Npz	Number of cells in z-direction	20	n/a
dt	Duration of one time step in the main loop	5	weeks
t_{stap}	Number of time steps within a tidal cycle	256	n/a
Δt	Duration of one time step within a tidal cycle	149	s

Table 3: General default parameters.

* This value is used for the sediment diffusivity when the constant profile is chosen. In the simulations for the basic state of Section 4.3.4 however, a constant value of 0.09 m²/s has been used.
** The reference height is usually set to 1 percent of the water depth. In the simulations for the basic state, the reference height is set to zero for simplicity.

3.2.2 Parameter Set 1 and Set 2

During the testing phase of this research, in which the SWC was under development, the two parameter sets shown in Table 4 are used.

Parameter	Description	Value		Unit
		Set 1	Set 2	
$\boldsymbol{H}$	Mean water depth	30.0	30.0	m
$\boldsymbol{A_v}$	Eddy viscosity	0.01	0.03	m²/s
$\boldsymbol{S}$	Slip parameter	0.008	0.01	m/s
$\boldsymbol{D_{50}}$	Mean sediment diameter	250	300	µm
$\boldsymbol{\tau_{cr}}$	Critical shear stress	0.18	0.19	N/m²
$\boldsymbol{w_s}$	Sediment fall velocity	0.035	0.044	m/s
$\boldsymbol{\bar{u}}$	Depth averaged mean velocity of the oscillating tidal flow	0.5	0.5	m/s
$\boldsymbol{u_{res}}$	Residual current	0.05*	0.05*	m/s
$\boldsymbol{\lambda}$	Slope factor	1.7	2.5	-

Table 4: Parameter Set 1 and Set 2.

* The residual current is set to zero by default. In the simulations used for the results shown in Chapter 0 and Section 4.3.4 (basic state) the residual current has been set to 0.05 m/s.

3.2.3 Parameters for Case 1A, Case 1B and Case 2

In Table 5 the parameters used for the simulations of Case 1A, Case 1B and Case 2 are presented. For the eddy viscosity and the slip parameter two different combinations were used. Also, two values for the slope factor were used. The values were chosen so that the basic model (without suspended sediment or a critical condition for the initiation of bed load transport) predicted the measured sand wave length best. The values that were used for the eddy viscosity, the slip parameter and the slope factor are all typical North Sea values (Besio et al., 2008; Nemeth et al., 2007; Sterlini, 2009).

Parameter	Description	Value			Unit
		Case 1A	Case 1B	Case 2	
$\boldsymbol{H}$	Mean water depth	27.0	25.7	20.0	m
$\boldsymbol{A_v}$	Eddy viscosity	0.03	0.03	0.01	m²/s
$\boldsymbol{S}$	Slip parameter	0.01	0.01	0.008	m/s
$\boldsymbol{D_{50}}$	Mean sediment diameter	420	360	600	µm
$\boldsymbol{\tau_{cr}}$	Critical shear stress	0.23	0.21	0.29	N/m²
$\boldsymbol{w_s}$	Sediment fall velocity	0.062	0.053	0.083	m/s
$\boldsymbol{\bar{u}}$	Depth averaged mean velocity of the oscillating tidal flow	0.56	0.64	0.43	m/s
$\boldsymbol{u_{res}}$	Residual current	n/a	n/a	0.02*	m/s
$\boldsymbol{\lambda}$	Slope factor	3.0	2.5	2.5	-

Table 5: Parameters for Case 1A, Case 1B and Case 2.

* For Case 2 simulations were carried out both with and without a residual current. The runs with a residual current have “Res” in their name.

4 Upgrading the suspended sediment transport calculation

4.1 Introduction

The suspended sediment concentration and transport calculations have been upgraded in three aspects. Firstly, a new scaling has been implemented. The reason for this was that in the previous version of the SWC no scaling was present in the suspended sediment module. What is unique in this scaling is that it takes into account not only the bed level elevation, but also the reference height. Secondly, a new surface boundary condition has been implemented. What was said to be implemented in the previous version of the SWC was a no flux condition, but instead a rough approximation (a Neumann boundary condition) of this was used. This approximation was found to generate erroneous concentration profiles. Therefore, it has been replaced by an actual no flux condition. Thirdly, the evaluation of the sediment diffusivity profiles has been redone because of numerous changes to the SWC including the calculation of the sediment diffusivity itself. The results of this indicate that using the parabolic-constant profile instead of the linear profile is a safer choice.

4.2 New scaling for the suspended sediment concentration calculation

In the new version of the SWC, a new scaling is applied to the calculations regarding the suspended sediment. A proper scaling ensures that the heightening and lowering of the sand bed as a result of the present sand wave are taken into account in the calculations. This avoids that the sediment concentrations are also calculated inside of the sand wave that at locations with a positive bed level elevation as a result of the sand wave, or that calculating the concentrations is forgotten at locations with a bed level lower than the reference level. It thus ensures that the bed level is properly taken into account.

The scaling also makes it possible to take straight horizontal and vertical derivatives correctly. This means that the irregular grid formed due to the presence of the sand wave is transformed into a rectangular grid (see Figure 4). For each point in this grid, horizontal and vertical derivatives can then be taken.

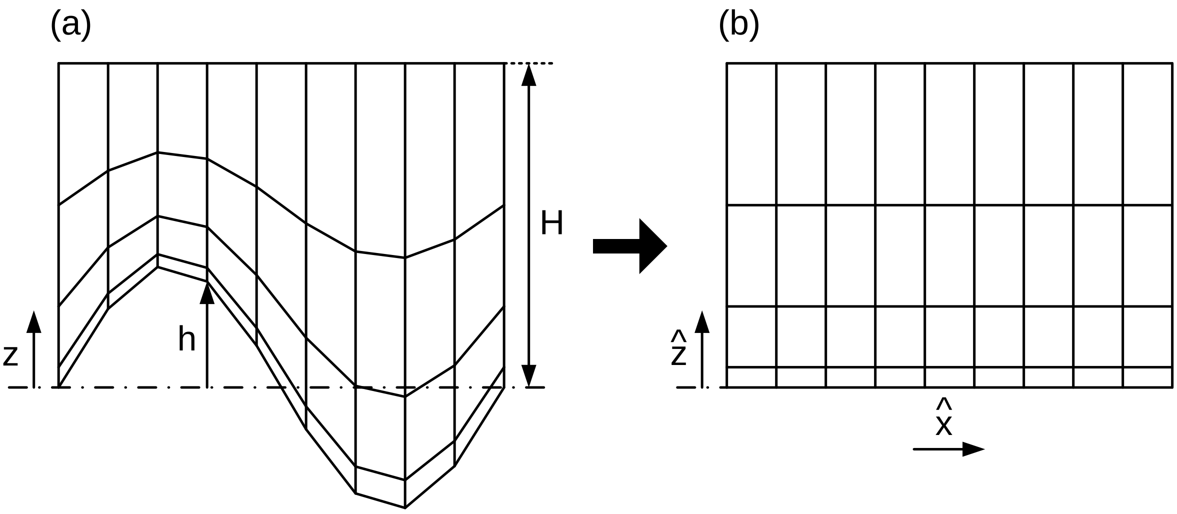

Figure 4: Schematization of the transformation from an irregular grid (a) to a rectangular grid (b). The points are distributed quadratic in the vertical (z-)direction. The bed level elevation h and the mean water depth H are also shown in the picture. Definitions of $\hat{z}$ and $\hat{x}$ are given in equation (4.2.5).

Another important point is that a linear distribution had been chosen for the sediment diffusivity ϵ_v. This means that the sediment diffusivity is not constant over the water depth. However, it has been assumed to be constant in the previous version of the model, as derivatives of ϵ_v in the vertical direction have been neglected. This can be seen in the following equation:

$$\frac{\partial c}{\partial t}+u\frac{\partial c}{\partial x}+w\frac{\partial c}{\partial z}=w_s\frac{\partial c}{\partial z}+\frac{\partial}{\partial z}\left(\epsilon_v\frac{\partial c}{\partial z}\right)+\frac{\partial}{\partial x}\left(\epsilon_v\frac{\partial c}{\partial x}\right) \tag{4.2.1}$$

Since horizontal diffusion is assumed to be negligible in comparison with the horizontal advection, it has been neglected. Also, the vertical flow velocity (w) is much smaller than the fall velocity for sediment (w_s) and can be neglected (Sterlini, 2009). This leads to the following equation:

$$\frac{\partial c}{\partial t}+u\frac{\partial c}{\partial x}=w_s\frac{\partial c}{\partial z}+\frac{\partial}{\partial z}\left(\epsilon_v\frac{\partial c}{\partial z}\right) \tag{4.2.2}$$

The last term can be further elaborated as follows:

$$\frac{\partial}{\partial z}\left(\epsilon_v\frac{\partial c}{\partial z}\right)=\frac{\partial\epsilon_v}{\partial z}\frac{\partial c}{\partial z}+\epsilon_v\frac{\partial^2 c}{\partial z^2} \tag{4.2.3}$$

When the sediment diffusivity ϵ_v is constant over the vertical direction z, the first term on the right hand side of this equation can be neglected. Thus, an extra term should be added to the equation when a parabolic-constant distribution is used instead of a constant distribution for the sediment diffusivity. In the previous version of the SWC however, this extra term was not included when a linear or parabolic-constant distribution for the sediment diffusivity was used.

4.2.1 A new transformation of z which incorporates the reference height

First, in the determination of $z(j)$-values in the previous version of the Sand Wave Code, the bed level elevation as a result of the presence of a sand wave was not taken into account. This can be fixed by expanding the equation for z (as given in equation (10.1.3), Appendix A):

$$z(j)=\big(H-0.01H-h(x)\big)\cdot\frac{j^2}{(Npz-1)^2}+0.01H+h(x) \tag{4.2.4}$$

Using this definition for z, the minimal value of z at $j=0$ equals $0.01H+h(x)$ and the maximum value at $j=Npz-1$ still equals H. The minimum value is thus $0.01H$ higher than the local bed level height ($h(x)$), of which the latter can be both positive and negative. This equation for z turned out to be problematic when applying the transformation, as will be explained below.

In the calculation of the suspended sediment concentration, a reference concentration c_a is applied at a reference height a above the bottom. The reference height is chosen as 1% of the water depth, so it is equal to $0.01H$.

In the calculation of the flow the following transformations are used for x, z and t:

$$\hat{x}=x,\quad \hat{z}=H\frac{z-h(x)}{H-h(x)},\quad \hat{t}=t \tag{4.2.5}$$

At first it was planned to use this same transformation in the suspended sediment calculation as well, but this turned out to be problematic. The problem is that when a sand wave is present, the water depth is not constant, while the reference height is (because H is constant). This meant that the reference height was not in the same proportion when compared to the water depth, leading to different values of $\hat{z}$ at different horizontal locations when a sand wave was present. This will be explained with a short example below.

We consider two locations, at location A the bed level elevation $h(x)$ is equal to zero while at location B it has a value of 2 metres. The mean water depth H is 30 metres. We check the values of $\hat{z}$ for these two locations both at the surface and at the bottom. For location A at the bottom $z = 0.01H + h(x) = 0.3 + 0 = 0.3\text{ m}$, while for location B it is $z = 0.01H + h(x) = 0.3 + 2 = 2.3\text{ m}$. Both for locations A and B at the surface ($j = Npz - 1$) $z = H = 30\text{ m}$ (see equation (4.2.4)). So:

$$\hat{z}_{A,bottom} = H\frac{z - h(x)}{H - h(x)} = 30\frac{0.3 - 0}{30 - 0} = 0.3\text{ m}$$

$$\hat{z}_{B,bottom} = H\frac{z - h(x)}{H - h(x)} = 30\frac{2.3 - 2}{30 - 2} = \frac{9}{28} \approx 0{,}3214\text{ m}$$

$$\hat{z}_{A,surface} = \hat{z}_{B,surface} = H\frac{z - h(x)}{H - h(x)} = 30\frac{30 - 0}{30 - 0} = 30\text{ m}$$

As can be seen, at location B the value for $\hat{z}$ at the bottom is larger than at location A, while the value at the surface is the same. Since at both locations the amount of grid points over the vertical is the same, the intermediate (from $j = 1$ to $j = Npz - 2$) values of $\hat{z}$ at location B also differ from the values at location A. It is a requirement that the values of $\hat{z}$ match for every location x along the domain, otherwise a rectangular grid is not obtained. Therefore, another transformation was needed for $\hat{z}$.

In order to solve the issue described above, we introduced another transformation of z, namely the following:

$$\tilde{z} = H\frac{z - \tilde{h}(x)}{H - \tilde{h}(x)} \tag{4.2.6}$$

Where $\tilde{h}(x)$ is defined as:

$$\tilde{h}(x) = h(x) + a \tag{4.2.7}$$

With a being the reference height, which equals $0.01H$ in this case. This reference height of 1 percent of the mean water depth corresponds with the minimum reference height proposed in Van Rijn (1984). With the introduction of $\tilde{z}$ the issue above is solved, which can be shown by calculating its value at the bottom for the previously described locations A and B:

$$\tilde{z}_{A,bottom} = H\frac{z - \tilde{h}(x)}{H - \tilde{h}(x)} = H\frac{z - (h(x) + 0.01H)}{H - h(x)} = 30\frac{0.3 - (0 + 0.3)}{30 - (0 + 0.3)} = 0\text{ m}$$

$$\tilde{z}_{B,bottom} = H\frac{z - \tilde{h}(x)}{H - \tilde{h}(x)} = H\frac{z - (h(x) + 0.01H)}{H - h(x)} = 30\frac{2.3 - (2 + 0.3)}{30 - (2 + 0.3)} = 0\text{ m}$$

As can also be seen from these calculations and equations (4.2.4) and (4.2.6), the value of $\tilde{z}$ ranges from 0 m at $j = 0$ to H at $j = Npz - 1$. When applying the transformation using $\tilde{z}$, a rectangular grid is thus obtained. In the next paragraph is discussed how this new transformation was used in the calculation of the suspended sediment concentrations and what other expressions this yields.

4.2.2 Derivation of the newly scaled suspended sediment equation

In this paragraph it is described how the suspended sediment equation was scaled by applying the transformation described in equation (4.2.6). The transformation was applied to the following form of the equation describing the suspended sediment concentration:

$$\overbrace{\boxed{\frac{\partial c}{\partial t}}}^{(1)} + \overbrace{\boxed{u\frac{\partial c}{\partial x}}}^{(2)} + \overbrace{\boxed{w\frac{\partial c}{\partial z}}}^{(3)} = \overbrace{\boxed{w_s\frac{\partial c}{\partial z}}}^{(4)} + \overbrace{\boxed{\frac{\partial \epsilon_v}{\partial z}\frac{\partial c}{\partial z}}}^{(5)} + \overbrace{\boxed{\epsilon_v\frac{\partial^2 c}{\partial z^2}}}^{(6)} \tag{4.2.8}$$

The third term in this equation was not neglected, because keeping it actually led to an easier equation after applying the transformation. First the following transformation will be applied to all terms individually:

$$\tilde{x} = x, \quad \tilde{z} = H\frac{z - \tilde{h}(x)}{H - \tilde{h}(x)}, \quad \tilde{t} = t \tag{4.2.9}$$

Term 1

$$\boxed{\frac{\partial c}{\partial t}} = \cancel{\frac{\partial c}{\partial \tilde{x}}\frac{\partial \tilde{x}}{\partial t}} + \cancel{\frac{\partial c}{\partial \tilde{z}}\frac{\partial \tilde{z}}{\partial t}} + \frac{\partial c}{\partial \tilde{t}}\frac{\partial \tilde{t}}{\partial t} = \frac{\partial c}{\partial \tilde{t}} \tag{4.2.10}$$

Term 2

$$\boxed{u\frac{\partial c}{\partial x}} = u\frac{\partial c}{\partial \tilde{x}}\frac{\partial \tilde{x}}{\partial x} + u\frac{\partial c}{\partial \tilde{z}}\frac{\partial \tilde{z}}{\partial x} + \cancel{u\frac{\partial c}{\partial \tilde{t}}\frac{\partial \tilde{t}}{\partial x}} = u\frac{\partial c}{\partial \tilde{x}} + u\frac{\partial c}{\partial \tilde{z}}\frac{\partial \tilde{z}}{\partial x} \tag{4.2.11}$$

In order to be able to elaborate this further, we first work the term $\partial\tilde{z}/\partial x$ out:

$$\begin{aligned}\frac{\partial \tilde{z}}{\partial x} &= \frac{\partial}{\partial x}\left(H\frac{z - \tilde{h}(x)}{H - \tilde{h}(x)}\right) = \frac{\partial}{\partial x}\left(H\frac{z - h(x) - a}{H - h(x) - a}\right) = \frac{\partial}{\partial x}\left(\frac{Hz - Hh(x) - Ha}{H - h(x) - a}\right) \\ &= \frac{\partial}{\partial x}\left(Hz\,(H - h(x) - a)^{-1} - \frac{Hh(x)}{H - h(x) - a} - Ha\,(H - h(x) - a)^{-1}\right)\end{aligned} \tag{4.2.12}$$

To this last version the derivation to x can be applied:

$$\begin{aligned}\frac{\partial \tilde{z}}{\partial x} &= \frac{\frac{\partial h(x)}{\partial x}Hz}{(H - h(x) - a)^2} - \frac{H\frac{\partial h(x)}{x}(H - h(x) - a) + Hh(x)\frac{\partial h(x)}{x}}{(H - h(x) - a)^2} - \frac{\frac{\partial h(x)}{x}Ha}{(H - h(x) - a)^2} \\ &= H\frac{\partial h(x)}{\partial x}\left(\frac{z - (H - h(x) - a) - h(x) - a}{(H - h(x) - a)^2}\right) = H\frac{\partial h(x)}{\partial x}\left(\frac{z - H}{(H - h(x) - a)}\right.\end{aligned} \tag{4.2.13}$$

This can be further elaborated by expressing z using the definition of $\tilde{z}$:

$$z = \tilde{z} - \frac{\tilde{z}\tilde{h}(x)}{H} + \tilde{h}(x) \tag{4.2.14}$$

Then the expression for $\partial\tilde{z}/\partial x$ becomes:

$$\frac{\partial\tilde{z}}{\partial x} = H\frac{\partial h(x)}{\partial x}\left(\frac{\tilde{z} - \frac{\tilde{z}\tilde{h}(x)}{H} + \tilde{h}(x) - H}{(H - h(x) - a)^2}\right) = \frac{\partial h(x)}{\partial x}\left(\frac{H - \tilde{z}\tilde{h}(x) + H\tilde{h}(x) - H^2}{\left(H - \tilde{h}(x)\right)^2}\right)$$
$$= \frac{\partial h(x)}{\partial x}\left(\frac{(\tilde{z} - H)\left(H - \tilde{h}(x)\right)}{\left(H - \tilde{h}(x)\right)\left(H - \tilde{h}(x)\right)}\right) = \frac{\partial h(x)}{\partial x}\frac{\tilde{z} - H}{H - \tilde{h}(x)} \tag{4.2.15}$$

This is the definition of the newly introduced $\tilde{\alpha}$, which is quite similar to $\hat{\alpha}$ in the flow calculation:

$$\tilde{\alpha} = \frac{\partial h(x)}{\partial x}\frac{\tilde{z} - H}{H - \tilde{h}(x)} \tag{4.2.16}$$

Term 2 now becomes:

$$u\frac{\partial c}{\partial \tilde{x}} + u\frac{\partial c}{\partial \tilde{z}}\frac{\partial \tilde{z}}{\partial x} = u\frac{\partial c}{\partial \tilde{x}} + \tilde{\alpha}u\frac{\partial c}{\partial \tilde{z}} \tag{4.2.17}$$

Term 3

$$\boxed{w\frac{\partial c}{\partial z}} = \cancel{w\frac{\partial c}{\partial \tilde{x}}\frac{\partial \tilde{x}}{\partial z}} + w\frac{\partial c}{\partial \tilde{z}}\frac{\partial \tilde{z}}{\partial z} + \cancel{w\frac{\partial c}{\partial \tilde{t}}\frac{\partial \tilde{t}}{\partial z}} = w\frac{\partial c}{\partial \tilde{z}}\frac{\partial \tilde{z}}{\partial z} \tag{4.2.18}$$

In order to be able to elaborate this further, we first elaborate the term $\partial\tilde{z}/\partial z$:

$$\frac{\partial \tilde{z}}{\partial z} = \frac{\partial}{\partial z}\left(H\frac{z - \tilde{h}(x)}{H - \tilde{h}(x)}\right) = \frac{H}{H - \tilde{h}(x)}\frac{\partial}{\partial z}\left(z - \tilde{h}(x)\right) = \frac{H}{H - \tilde{h}(x)}\frac{\partial z}{\partial z} = \frac{H}{H - \tilde{h}(x)} \tag{4.2.19}$$

This is the definition of the newly introduced $\tilde{\beta}$, which is quite similar to $\hat{\beta}$ in the flow calculation:

$$\tilde{\beta} = \frac{H}{H - \tilde{h}(x)} \tag{4.2.20}$$

Term 3 now becomes:

$$w\frac{\partial c}{\partial \tilde{z}}\frac{\partial \tilde{z}}{\partial z} = \tilde{\beta}w\frac{\partial c}{\partial \tilde{z}} \tag{4.2.21}$$

Term 2 and Term 3 combined

Terms 2 and 3 can be easily combined, when using the following definitions for $\tilde{u}$ and $\widetilde{w}$:

$$\tilde{u} = \frac{u}{\tilde{\beta}}, \quad \widetilde{w} = \frac{\tilde{\alpha}}{\tilde{\beta}}u + w \tag{4.2.22}$$

When adding up Terms 2 and 3 they then become:

$$u\frac{\partial c}{\partial \tilde{x}} + \tilde{\alpha}u\frac{\partial c}{\partial \tilde{z}} + \hat{\beta}w\frac{\partial c}{\partial \tilde{z}} = \tilde{u}\tilde{\beta}\frac{\partial c}{\partial \tilde{x}} + \tilde{\alpha}\tilde{\beta}\tilde{u}\frac{\partial c}{\partial \tilde{z}} + \tilde{\beta}w\frac{\partial c}{\partial \tilde{z}} = \tilde{u}\tilde{\beta}\frac{\partial c}{\partial \tilde{x}} + \tilde{\alpha}\tilde{\beta}\tilde{u}\frac{\partial c}{\partial \tilde{z}} + \tilde{\beta}(\widetilde{w} - \tilde{\alpha}\tilde{u})\frac{\partial c}{\partial \tilde{z}}$$
$$= \tilde{u}\tilde{\beta}\frac{\partial c}{\partial \tilde{x}} + \cancel{\tilde{\alpha}\tilde{\beta}\tilde{u}\frac{\partial c}{\partial \tilde{z}}} + \tilde{\beta}\widetilde{w}\frac{\partial c}{\partial \tilde{z}} - \cancel{\tilde{\alpha}\tilde{\beta}\tilde{u}\frac{\partial c}{\partial \tilde{z}}} = \tilde{u}\tilde{\beta}\frac{\partial c}{\partial \tilde{x}} + \tilde{\beta}\widetilde{w}\frac{\partial c}{\partial \tilde{z}} \tag{4.2.23}$$

As can be seen in the derivation above, two terms cancel each other out, which only occurs when the vertical sediment advection is not neglected.

Term 4

$$\boxed{w_s\frac{\partial c}{\partial z}} = \cancel{w_s\frac{\partial c}{\partial \tilde{x}}\frac{\partial \tilde{x}}{\partial z}} + w_s\frac{\partial c}{\partial \tilde{z}}\frac{\partial \tilde{z}}{\partial z} + \cancel{w_s\frac{\partial c}{\partial \tilde{t}}\frac{\partial \tilde{t}}{\partial z}} = w_s\frac{\partial c}{\partial \tilde{z}}\frac{\partial \tilde{z}}{\partial z} = \tilde{\beta} w_s\frac{\partial c}{\partial \tilde{z}} \tag{4.2.24}$$

Term 5

To this entire term the transformation can be applied as shown below:

$$\boxed{\frac{\partial \epsilon_v}{\partial z}\frac{\partial c}{\partial z}} = \left(\cancel{\frac{\partial \epsilon_v}{\partial \tilde{x}}\frac{\partial \tilde{x}}{\partial z}} + \frac{\partial \epsilon_v}{\partial \tilde{z}}\frac{\partial \tilde{z}}{\partial z} + \cancel{\frac{\partial \epsilon_v}{\partial \tilde{t}}\frac{\partial \tilde{t}}{\partial z}}\right)\left(\cancel{\frac{\partial c}{\partial \tilde{x}}\frac{\partial \tilde{x}}{\partial z}} + \frac{\partial c}{\partial \tilde{z}}\frac{\partial \tilde{z}}{\partial z} + \cancel{\frac{\partial c}{\partial \tilde{t}}\frac{\partial \tilde{t}}{\partial z}}\right) = \tilde{\beta}^2\frac{\partial \epsilon_v}{\partial \tilde{z}}\frac{\partial c}{\partial \tilde{z}} \tag{4.2.25}$$

However, the transformation will only be applied to a part of this term. The sediment diffusivity ϵ_v is described as a parabolic-constant value in which it is parabolically increasing for the lower part of the water column and above that constant over depth. This is expressed in the following formula:

$$\epsilon_v = \begin{cases} \kappa\beta_* u_* z\left(1-\dfrac{z}{H}\right) & \text{for } z < 0.5H \\ 0.25\kappa\beta_* u_* H & \text{for } z \geq 0.5H \end{cases} \tag{4.2.26}$$

In this equation κ is the Von Karman constant ($= 0.4$), β_* describes the difference between a water and a sediment particle and u_* is the bed shear velocity. The derivative of ϵ_v to z can be taken analytically as follows:

$$\frac{\partial \epsilon_v}{\partial z} = \begin{cases} \dfrac{\partial}{\partial z}\left(\kappa\beta_* u_* z\left(1-\dfrac{z}{H}\right)\right) = \kappa\beta_* u_*\left(1-\dfrac{2z}{H}\right) & \text{for } z < 0.5H \\ \dfrac{\partial}{\partial z}(0.25\kappa\beta_* u_* H) = 0 & \text{for } z \geq 0.5H \end{cases} \tag{4.2.27}$$

Since calculating the derivative of ϵ_v to z is more precise than numerically approximating its derivative to $\tilde{z}$, Term 5 will be implemented into the model in the following form:

$$\boxed{\frac{\partial \epsilon_v}{\partial z}\frac{\partial c}{\partial z}} = \tilde{\beta}\frac{\partial \epsilon_v}{\partial z}\frac{\partial c}{\partial \tilde{z}} \tag{4.2.28}$$

Because the derivative is taken analytically it is valid and the use of z instead of $\tilde{z}$ is permissible.

Term 6

$$\boxed{\epsilon_v\frac{\partial^2 c}{\partial z^2}} = \epsilon_v\frac{\partial c}{\partial z}\frac{\partial c}{\partial z} = \epsilon_v\left(\frac{\partial c}{\partial \tilde{z}}\frac{\partial \tilde{z}}{\partial z}\right)\left(\frac{\partial c}{\partial \tilde{z}}\frac{\partial \tilde{z}}{\partial z}\right) = \tilde{\beta}^2\epsilon_v\frac{\partial^2 c}{\partial \tilde{z}^2} \tag{4.2.29}$$

All terms together

With all of these terms together, the following equation is obtained:

$$\frac{\partial c}{\partial \tilde{t}} + \tilde{u}\tilde{\beta}\frac{\partial c}{\partial \tilde{x}} + \tilde{\beta}\tilde{w}\frac{\partial c}{\partial \tilde{z}} = \tilde{\beta} w_s\frac{\partial c}{\partial \tilde{z}} + \tilde{\beta}\frac{\partial \epsilon_v}{\partial z}\frac{\partial c}{\partial \tilde{z}} + \tilde{\beta}^2\epsilon_v\frac{\partial^2 c}{\partial \tilde{z}^2} \tag{4.2.30}$$

Dividing by $\tilde{\beta}$ gives:

$$\frac{1}{\tilde{\beta}}\frac{\partial c}{\partial \tilde{t}} + \tilde{u}\frac{\partial c}{\partial \tilde{x}} + \tilde{w}\frac{\partial c}{\partial \tilde{z}} = w_s\frac{\partial c}{\partial \tilde{z}} + \frac{\partial \epsilon_v}{\partial z}\frac{\partial c}{\partial \tilde{z}} + \tilde{\beta}\epsilon_v\frac{\partial^2 c}{\partial \tilde{z}^2} \tag{4.2.31}$$

This equation has been discretized and implemented in the Sand Wave Code. The discretization is discussed in the next paragraph.

4.2.3 Discretization of the newly scaled suspended sediment equation

In order to discretize the equation obtained in the previous paragraph, each term will again be discussed individually. The following equation gives an overview of the terms:

$$\overbrace{\boxed{\frac{1}{\tilde{\beta}}\frac{\partial c}{\partial \tilde{t}}}}^{(1)} + \overbrace{\boxed{\tilde{u}\frac{\partial c}{\partial \tilde{x}}}}^{(2)} + \overbrace{\boxed{\tilde{w}\frac{\partial c}{\partial \tilde{z}}}}^{(3)} = \overbrace{\boxed{w_s\frac{\partial c}{\partial \tilde{z}}}}^{(4)} + \overbrace{\boxed{\frac{\partial \epsilon_v}{\partial z}\frac{\partial c}{\partial \tilde{z}}}}^{(5)} + \overbrace{\boxed{\tilde{\beta}\epsilon_v\frac{\partial^2 c}{\partial \tilde{z}^2}}}^{(6)} \qquad (4.2.32)$$

In each of the discretizations, the horizontal coordinate is indicated by i and the vertical coordinate is indicated by j. The time is indicated by the integer k.

Term 1

This term is discretized using Backward Euler:

$$\boxed{\frac{1}{\tilde{\beta}}\frac{\partial c}{\partial \tilde{t}}} = \frac{c_{i,j}\big|_{t_k} - c_{i,j}\big|_{t_{k-1}}}{\Delta \mathrm{t}} \qquad (4.2.33)$$

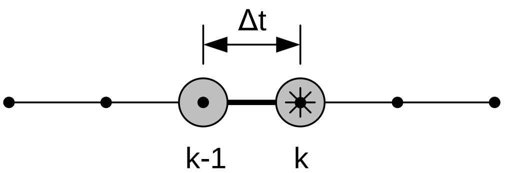

Figure 5: Schematic representation of the Backward Euler numerical discretization. The grey circles indicate the points involved in the calculation, where the circle with the asterisk is the point at which the differential equation is evaluated.

This is done because in the Sand Wave Code no values for the concentration of the next time step are known at the time of calculating the concentration at a certain time step. However, the previous time step is stored and can be used for determining the time derivative of the concentration.

Term 2

For this term, a so called upwind discretization is used:

$$\boxed{\tilde{u}\frac{\partial c}{\partial \tilde{x}}} = \begin{cases} \tilde{u}\dfrac{c_{i,j} - c_{i-1,j}}{\Delta x} & \text{for } \tilde{u} > 0 \\ \tilde{u}\dfrac{c_{i+1,j} - c_{i,j}}{\Delta x} & \text{for } \tilde{u} < 0 \end{cases} \qquad (4.2.34)$$

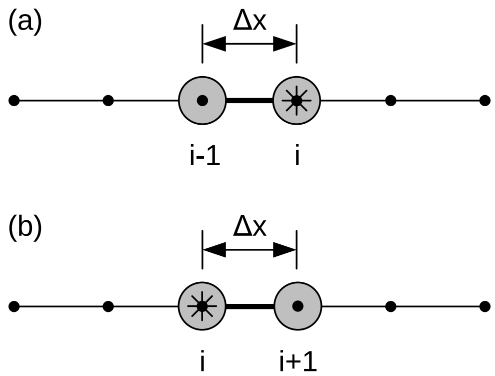

Figure 6: Schematic representation of the upwind numerical discretization in the horizontal direction. Again, the grey circles indicate the points involved in the calculation, where the circle with the asterisk is the point at which the differential equation is evaluated. In (a) the transformed horizontal flow speed ($\tilde{u}$) is positive, so the point to the left lies upstream and is used in the calculation. In (b) $\tilde{u}$ is negative and therefore the point to the right lies upstream and is used in the calculation.

Upwind means that the neighboring value on the upstream side of the considered cell is used to evaluate the space derivative. So, depending on the sign of $\tilde{u}$, the value of the concentration left or right of the considered cell is used.

Term 3

For this term upwind is also used, although not in the horizontal but in the vertical direction:

$$\boxed{\tilde{w}\frac{\partial c}{\partial \tilde{z}}} = \begin{cases} \tilde{w}\dfrac{c_{i,j} - c_{i,j-1}}{\tilde{z}_{i,j} - \tilde{z}_{i,j-1}} & \text{for } \tilde{w} > 0 \\ \tilde{w}\dfrac{c_{i,j+1} - c_{i,j}}{\tilde{z}_{i,j+1} - \tilde{z}_{i,j}} & \text{for } \tilde{w} < 0 \end{cases} \tag{4.2.35}$$

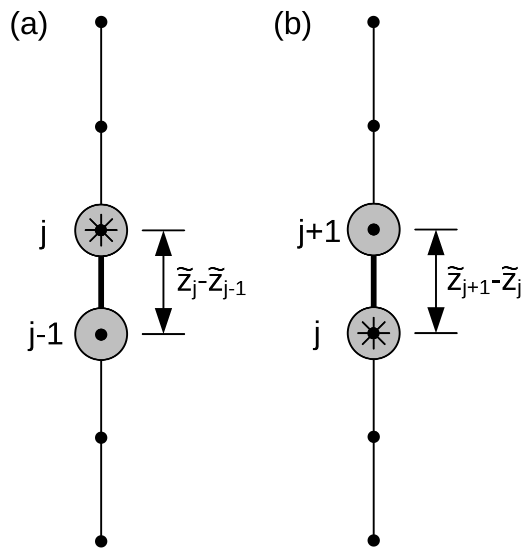

Figure 7: Schematic representation of the upwind numerical discretization in the vertical direction. Again, the grey circles indicate the points involved in the calculation, where the circle with the asterisk is the point at which the differential equation is evaluated. In (a) the transformed vertical flow speed ($\tilde{w}$) is positive, so the point to the bottom lies upstream and is used in the calculation. In (b) $\tilde{w}$ is negative and therefore the point to the top lies upstream and is used in the calculation.

Note that since $\tilde{z}$ is not evenly distributed over the vertical, we cannot simply write "$\Delta\tilde{z}$".

Term 4

For this term upwind is also used, but only in one direction, as the fall velocity only works downward:

$$\boxed{w_s\frac{\partial c}{\partial \tilde{z}}} = w_s\frac{c_{i,j+1} - c_{i,j}}{\tilde{z}_{i,j+1} - \tilde{z}_{i,j}} \tag{4.2.36}$$

Note that even though the value of w_s is always positive, the value towards the top is used in the calculation. This is because this term lies on the right hand side in equation (4.2.32) and thus works in the opposite direction when compared to Terms 1, 2 and 3.

Term 5

This term is very similar to Term 4, as a value is also multiplied with $\partial c/\partial \tilde{z}$. Since this value is always positive, as ϵ_v increases with increasing z, upwind in one direction can also be used:

$$\boxed{\frac{\partial \epsilon_v}{\partial z}\frac{\partial c}{\partial \tilde{z}}} = \frac{\partial \epsilon_v}{\partial z}\frac{c_{i,j+1} - c_{i,j}}{\tilde{z}_{i,j+1} - \tilde{z}_{i,j}} \tag{4.2.37}$$

As discussed above, the term $\partial\epsilon_v/\partial z$ is evaluated analytically, so it does not need to be discretized.

Term 6

For this term central difference is used:

$$\boxed{\tilde{\beta}\epsilon_v\frac{\partial^2 c}{\partial\tilde{z}^2}} = \tilde{\beta}\epsilon_v\frac{\left(\frac{c_{i,j+1}-c_{i,j}}{\tilde{z}_{i,j+1}-\tilde{z}_{i,j}}-\frac{c_{i,j}-c_{i,j-1}}{\tilde{z}_{i,j}-\tilde{z}_{i,j-1}}\right)}{\left(\frac{\tilde{z}_{i,j+1}\mp\tilde{z}_{i,j}}{2}-\frac{\tilde{z}_{i,j}\mp\tilde{z}_{i,j-1}}{2}\right)} = \tilde{\beta}\epsilon_v\frac{\left(\frac{c_{i,j+1}-c_{i,j}}{\tilde{z}_{i,j+1}-\tilde{z}_{i,j}}-\frac{c_{i,j}-c_{i,j-1}}{\tilde{z}_{i,j}-\tilde{z}_{i,j-1}}\right)}{\left(\frac{\tilde{z}_{i,j+1}-\tilde{z}_{i,j-1}}{2}\right)} \tag{4.2.38}$$

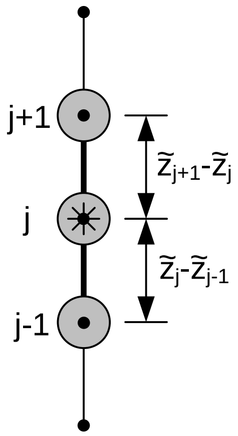

Figure 8: Schematic representation of the central difference numerical discretization in the vertical direction. Again, the grey circles indicate the points involved in the calculation, where the circle with the asterisk is the point at which the differential equation is evaluated.

4.3 New surface boundary condition: no flux

In this section the effect of implementing an actual no flux condition at the top of the water column is investigated. First the no flux condition will be described and discretized. To check the effect of this new condition and to test if it is necessary, a simplified version of the model called the basic state is used. In the basic state, the bottom remains flat. The basic state is useful, because it is so simple that an analytical solution can be derived for it as well. The results of the SWC can then be compared with this analytical solution.

4.3.1 Description and discretization of the no flux boundary condition

Sterlini (2009) states that to complete the set of boundary conditions for sediment concentrates, they disallow flux through the water surface. In the previous version of the SWC however, this boundary condition is not present. Instead, a Neumann boundary condition is used which sets the derivative of the concentration to z (thus, $\partial c/\partial z$) to zero. This means that the balance between the downward flux of the suspended sediment due to the fall velocity and the upward flux of the suspended sediment due to the diffusivity as described in the no flux condition were not both taken into account.

No flux through the water surface can be described by the following equation (Lin and Namin, 2005; Verbanck, 2000):

$$\left[cw_s+\epsilon_v\frac{\partial c}{\partial z}\right]_{z=H} = 0 \tag{4.3.1}$$

Note that the subscript states that this equation is to be evaluated at "$z = H$" instead of at "$z = H + \zeta(x,t)$", which is because the water surface elevation ($\zeta(x,t)$) is neglected in the suspended sediment calculations. In the flow calculation the elevation due to the tidal flow is neglected as well, as the rigid lid assumption is used. When applying the transformations described in Section 4.2.2, the following is obtained:

$$cw_s + \tilde{\beta}\epsilon_v \frac{\partial c}{\partial \tilde{z}} = 0 \tag{4.3.2}$$

The discretization of the no flux boundary condition was first done using a central difference approach, with the use of a so called ghost point. This approach can be found in Appendix B. As can be seen in Appendix B, the resulting formulas were far from simple. It is very hard to implement this into the SWC. Also, it is of a higher order than most things implemented in the SWC, which means it does not fit in well with the other discretizations. Implementing the no flux condition with a ghost point could thus cause instabilities in the SWC that are hard to predict. Furthermore, mistakes are bound to be made when implementing such a large equation.

Therefore, the no flux boundary condition is implemented with a first order derivative using only the top two points ($j = Npz - 1$ and $j = Npz - 2$), which does not require the use of a ghost point. This is much easier, as equation (4.3.1) can then be discretized as follows:

$$c_{i,Npz-1} \cdot w_s + \epsilon_v \left(\frac{c_{i,Npz-1} - c_{i,Npz-2}}{z_{i,Npz-1} - z_{i,Npz-2}} \right) = 0 \tag{4.3.3}$$

This could be implemented in the SWC without any further difficulties.

4.3.2 Basic state: simplification of the suspended sediment concentration equation

The basic state describes the unperturbed state in which no sand wave is present and the seabed is thus horizontally flat. Normally, in the SWC a sand wave with an amplitude of 0.10 m is imposed. In order to simulate the basic state, this small sand wave is not imposed and therefore no sand wave emerges. We are therefore dealing with a flat bottom. This is done in order to find out whether the calculation of the suspended sediment concentration works properly in a simple situation, before making it more complex by including sand waves.

That this situation is simple, implies that the associated suspended sediment concentration equation can also be simplified, which is definitely the case. We start off with the unscaled suspended sediment concentration equation:

$$\frac{\partial c}{\partial t} + u\frac{\partial c}{\partial x} + w\frac{\partial c}{\partial z} = w_s\frac{\partial c}{\partial z} + \frac{\partial \epsilon_v}{\partial z}\frac{\partial c}{\partial z} + \epsilon_v\frac{\partial^2 c}{\partial z^2} \tag{4.3.4}$$

Since no sand wave is present and the water surface elevation is not (yet) taken into account in the suspended sediment concentration calculation, there is no change in x-direction, so $\partial \ldots / \partial x = 0$:

$$\frac{\partial c}{\partial t} + w\frac{\partial c}{\partial z} = w_s\frac{\partial c}{\partial z} + \frac{\partial \epsilon_v}{\partial z}\frac{\partial c}{\partial z} + \epsilon_v\frac{\partial^2 c}{\partial z^2} \tag{4.3.5}$$

When applying the transformations described in Section 4.2.2, the following equation is obtained:

$$\frac{1}{\tilde{\beta}}\frac{\partial c}{\partial \tilde{t}} + \tilde{w}\frac{\partial c}{\partial \tilde{z}} - \tilde{\alpha}\tilde{\beta}\tilde{u}\frac{\partial c}{\partial \tilde{z}} = w_s\frac{\partial c}{\partial \tilde{z}} + \frac{\partial \epsilon_v}{\partial z}\frac{\partial c}{\partial \tilde{z}} + \tilde{\beta}\epsilon_v\frac{\partial^2 c}{\partial \tilde{z}^2} \tag{4.3.6}$$

In case of a flat bottom, $\tilde{\alpha} = 0$ (since $\partial h(x)/\partial x = 0$, see equation (4.2.16)) and $\tilde{\beta} = 1$ (since $\tilde{h}(x) = 0$, see equation (4.2.20)), so:

$$\frac{\partial c}{\partial \tilde{t}} + \tilde{w}\frac{\partial c}{\partial \tilde{z}} = w_s\frac{\partial c}{\partial \tilde{z}} + \frac{\partial \epsilon_v}{\partial z}\frac{\partial c}{\partial \tilde{z}} + \epsilon_v\frac{\partial^2 c}{\partial \tilde{z}^2} \tag{4.3.7}$$

The equation describing mass conservation of flow reads:

$$\frac{\partial u}{\partial x} + \frac{\partial w}{\partial z} = 0 \tag{4.3.8}$$

When applying the transformations of $\tilde{x}$, $\tilde{z}$ and $\tilde{t}$ (see equation (4.2.9)), this becomes:

$$\frac{\partial u}{\partial x} + \frac{\partial w}{\partial z} = \left(\frac{\partial u}{\partial \tilde{x}}\frac{\partial \tilde{x}}{\partial x} + \frac{\partial u}{\partial \tilde{z}}\frac{\partial \tilde{z}}{\partial x}\right) + \left(\frac{\partial w}{\partial \tilde{z}}\frac{\partial \tilde{z}}{\partial z}\right) = \frac{\partial u}{\partial \tilde{x}} + \tilde{\alpha}\frac{\partial u}{\partial \tilde{z}} + \tilde{\beta}\frac{\partial w}{\partial \tilde{z}} = 0 \tag{4.3.9}$$

When also applying the transformations of $\tilde{u}$ and $\tilde{w}$ (see equation (4.2.22)) we obtain:

$$\tilde{\beta}\frac{\partial \tilde{u}}{\partial \tilde{x}} + \tilde{\alpha}\tilde{\beta}\frac{\partial \tilde{u}}{\partial \tilde{z}} + \tilde{\beta}\frac{\partial(\tilde{w} - \tilde{\alpha}\tilde{u})}{\partial \tilde{z}} = \tilde{\beta}\frac{\partial \tilde{u}}{\partial \tilde{x}} + \tilde{\alpha}\tilde{\beta}\frac{\partial \tilde{u}}{\partial \tilde{z}} + \tilde{\beta}\frac{\partial \tilde{w}}{\partial \tilde{z}} - \tilde{\alpha}\tilde{\beta}\frac{\partial \tilde{u}}{\partial \tilde{z}} = \tilde{\beta}\frac{\partial \tilde{u}}{\partial \tilde{x}} + \tilde{\beta}\frac{\partial \tilde{w}}{\partial \tilde{z}} = 0 \tag{4.3.10}$$

Again $\tilde{\beta} = 1$, so:

$$\frac{\partial \tilde{u}}{\partial \tilde{x}} + \frac{\partial \tilde{w}}{\partial \tilde{z}} = 0 \tag{4.3.11}$$

Since in the basic state $\partial \ldots / \partial x = 0$, the following applies in this case:

$$\frac{\partial \tilde{w}}{\partial \tilde{z}} = 0 \tag{4.3.12}$$

This implies that $\tilde{w}$ should be constant in the vertical direction over the entire water depth. Since the bottom boundary condition states that $\tilde{w} = 0$ at the bottom, it should be zero over the entire water depth. Using this knowledge, the suspended sediment concentration equation becomes:

$$\frac{\partial c}{\partial \tilde{t}} = w_s\frac{\partial c}{\partial \tilde{z}} + \frac{\partial \epsilon_v}{\partial z}\frac{\partial c}{\partial \tilde{z}} + \epsilon_v\frac{\partial^2 c}{\partial \tilde{z}^2} \tag{4.3.13}$$

This can be simplified even further by choosing a constant value for the sediment diffusivity ϵ_v, but this has not been done as that it would show unrealistic results.

4.3.3 Basic state: analytical determination of the concentration profile

In order to check if the concentration profile generated in the SWC corresponds with the physical conditions imposed in this code, it will be compared with an analytical description of the concentration profile. The analytical derivation of the profile is only possible in a simple case, the basic state. For this case also the diffusivity ϵ_v is kept as a constant and the reference height a is set to zero.

In the basic state, when the sediment diffusivity is chosen as a constant value over the depth, the suspended sediment concentration equation (equation (4.3.4)) simplifies to:

$$\frac{\partial c}{\partial t} = w_s\frac{\partial c}{\partial z} + \epsilon_v\frac{\partial^2 c}{\partial z^2} \tag{4.3.14}$$

First the boundary conditions as used in the previous version of the model are applied. Later on, the analytical determination will also be done for a no flux condition at the surface ($z = H$). The Neumann boundary condition at the surface and the reference concentration are applied as follows in this case:

$$\frac{\partial c}{\partial z} = 0\Big|_{z=H}, \quad c = c_a\Big|_{z=h(x)+a} \tag{4.3.15}$$

It is important to note that for simplicity the reference height for this case is chosen at $a = 0$. For obtaining an analytical description of the concentration, the following truncated Fourier series is used:

$$c(z,t) = \sum_{p=-P}^{P} C_p(z) \exp(ip\omega t) \tag{4.3.16}$$

Where $C_p(z)$ is the Fourier transform of the concentration. Note that $C_{-p}(z) = C_p{}^*(z)$ (where the asterisk denotes the complex conjugate). This is a partial sum with truncation number P. The terms $\partial c/\partial t$, $\partial c/\partial z$ and $\partial^2 c/\partial z^2$ can also be written in this form:

$$\frac{\partial c}{\partial t} = \sum_{p=-P}^{P} ip\omega C_p(z) \exp(ip\omega t) \tag{4.3.17}$$

$$\frac{\partial c}{\partial z} = \sum_{p=-P}^{P} \frac{\partial C_p(z)}{\partial z} \exp(ip\omega t) \tag{4.3.18}$$

$$\frac{\partial^2 c}{\partial z^2} = \sum_{p=-P}^{P} \frac{\partial^2 C_p(z)}{\partial z^2} \exp(ip\omega t) \tag{4.3.19}$$

The reference concentration is written as a truncated Fourier series as follows:

$$c_a(t) = \sum_{p=-P}^{P} C_{a,p} \exp(ip\omega t) \tag{4.3.20}$$

When substituting these terms with their Fourier transform, the suspended sediment concentration equation becomes:

$$ip\omega C_p(z) = w_s \frac{\partial C_p(z)}{\partial z} + \epsilon_v \frac{\partial^2 C_p(z)}{\partial z^2} \tag{4.3.21}$$

The following “Ansatz” for the description of $C_p(z)$ is used:

$$C_p(z) = A_1 \exp(\lambda_1 z) + A_2 \exp(\lambda_2 z) \tag{4.3.22}$$

The derivative and second derivative to z then become:

$$\frac{\partial C_p(z)}{\partial z} = \lambda_1 A_1 \exp(\lambda_1 z) + \lambda_2 A_2 \exp(\lambda_2 z) \tag{4.3.23}$$

$$\frac{\partial^2 C_p(z)}{\partial z^2} = \lambda_1{}^2 A_1 \exp(\lambda_1 z) + \lambda_2{}^2 A_2 \exp(\lambda_2 z) \tag{4.3.24}$$

Substituting the terms in equation (4.3.21) with these descriptions gives:

$$\begin{aligned} &ip\omega(A_1 \exp(\lambda_1 z) + A_2 \exp(\lambda_2 z)) = \\ &w_s(\lambda_1 A_1 \exp(\lambda_1 z) + \lambda_2 A_2 \exp(\lambda_2 z)) + \epsilon_v\left(\lambda_1{}^2 A_1 \exp(\lambda_1 z) + \lambda_2{}^2 A_2 \exp(\lambda_2 z)\right) \end{aligned} \tag{4.3.25}$$

This can be rewritten into:

$$A_1\left\{ip\omega - \lambda_1 w_s - \epsilon_v {\lambda_1}^2\right\}\exp(\lambda_1 z) + A_2\left\{\mathrm{i}\mathrm{p}\omega - \lambda_2 w_s - \epsilon_v {\lambda_2}^2\right\}\exp(\lambda_2 z) = 0 \tag{4.3.26}$$

Since A_1 and A_2 are not both zero (otherwise another Ansatz would be more appropriate) and the exponents do not reach zero, the following must apply:

$$ip\omega - \lambda_1 w_s - \epsilon_v {\lambda_1}^2 = 0 \quad and \quad \mathrm{i}\mathrm{p}\omega - \lambda_2 w_s - \epsilon_v {\lambda_2}^2 = 0 \tag{4.3.27}$$

The values for λ_1 and λ_2 can then be determined using the quadratic formula:

$$\lambda_1 = \frac{-w_s + \sqrt{{w_s}^2 - 4\epsilon_v ip\omega}}{2\epsilon_v}, \quad \lambda_2 = \frac{-w_s - \sqrt{{w_s}^2 - 4\epsilon_v ip\omega}}{2\epsilon_v} \tag{4.3.28}$$

The first and second boundary condition (equation (4.3.15)) respectively imply:

$$\frac{\partial C_p(H)}{\partial z} = \lambda_1 A_1 \exp(\lambda_1 H) + \lambda_2 A_2 \exp(\lambda_2 H) = 0 \tag{4.3.29}$$

$$C_p(a) = A_1 \exp(\lambda_1 a) + A_2 \exp(\lambda_2 a) = C_{a,p} \tag{4.3.30}$$

Since the reference height has been chosen at $a = 0$ for the sake of simplicity in this case, equation (4.3.30) becomes:

$$A_1 \exp(\lambda_1 0) + A_2 \exp(\lambda_2 0) = A_1 + A_2 = C_{a,p} \tag{4.3.31}$$

This means that A_1 can be substituted for $C_{a,p} - A_2$ in equation (4.3.29):

$$\lambda_1\left(C_{a,p} - A_2\right)\exp(\lambda_1 H) + \lambda_2 A_2 \exp(\lambda_2 H) = 0 \tag{4.3.32}$$

$$C_{a,p}\lambda_1 \exp(\lambda_1 H) + A_2(\lambda_2 \exp(\lambda_2 H) - \lambda_1 \exp(\lambda_1 H)) = 0 \tag{4.3.33}$$

$$A_2 = -\frac{C_{a,p}\lambda_1 \exp(\lambda_1 H)}{\lambda_2 \exp(\lambda_2 H) - \lambda_1 \exp(\lambda_1 H)} = -C_{a,p}\left[\frac{\lambda_1 \exp(\lambda_1 H)}{\lambda_2 \exp(\lambda_2 H) - \lambda_1 \exp(\lambda_1 H)}\right] \tag{4.3.34}$$

Now that an expression for A_2 is obtained, A_1 can be determined easily using equation (4.3.31):

$$A_1 = C_{a,p} - A_2 = c_a + \frac{c_a \lambda_1 \exp(\lambda_1 H)}{\lambda_2 \exp(\lambda_2 H) - \lambda_1 \exp(\lambda_1 H)} = C_{a,p}\left[\frac{\lambda_2 \exp(\lambda_2 H)}{\lambda_2 \exp(\lambda_2 H) - \lambda_1 \exp(\lambda_1 H)}\right] \tag{4.3.35}$$

The analytical expression describing the concentration profile now becomes:

$$C_p(z) = C_{a,p}\left[\frac{\lambda_2 \exp(\lambda_2 H)}{\lambda_2 \exp(\lambda_2 H) - \lambda_1 \exp(\lambda_1 H)}\exp(\lambda_1 z) - \frac{\lambda_1 \exp(\lambda_1 H)}{\lambda_2 \exp(\lambda_2 H) - \lambda_1 \exp(\lambda_1 H)}\exp\,(\lambda_2 z)\right] \tag{4.3.36}$$

With λ_1 and λ_2 as defined in equation (4.3.28).

No flux boundary condition at the surface

Alternatively, an analytical expression can also be derived in the physically more realistic case of a no flux boundary condition at the surface. This boundary condition is described as follows (also see equation (4.3.1)):

$$C_p(z)w_s + \epsilon_v \frac{\partial C_p(z)}{\partial z} = 0\Bigg|_{z=H} \tag{4.3.37}$$

When using the Ansatz of equation (4.3.22) the no flux boundary condition and the same boundary condition at the reference level (equation (4.3.15), second condition), the boundary conditions can be written as:

$$C_p(z)w_s + \epsilon_v \frac{\partial C_p(z)}{\partial z} = (w_s + \epsilon_v \lambda_1)\, A_1 \exp(\lambda_1 z) + (w_s + \epsilon_v \lambda_2)\, A_2 \exp(\lambda_2 z) = 0 \tag{4.3.38}$$

$$A_1 + A_2 = C_{a,p} \tag{4.3.39}$$

Again A_1 can be substituted for $C_{a,p} - A_2$, now in equation (4.3.38):

$$(w_s + \epsilon_v \lambda_1)\left(C_{a,p} - A_2\right)\exp(\lambda_1 z) + (w_s + \epsilon_v \lambda_2)\, A_2 \exp(\lambda_2 z) = 0 \tag{4.3.40}$$

$$C_{a,p}(w_s + \epsilon_v \lambda_1) \exp(\lambda_1 H) + A_2\big((w_s + \epsilon_v \lambda_2) \exp(\lambda_2 H) - (w_s + \epsilon_v \lambda_1) \exp(\lambda_1 H)\big) = 0 \tag{4.3.41}$$

$$\begin{aligned} A_2 &= -\frac{C_{a,p}(w_s + \epsilon_v \lambda_1) \exp(\lambda_1 H)}{(w_s + \epsilon_v \lambda_2) \exp(\lambda_2 H) - (w_s + \epsilon_v \lambda_1) \exp(\lambda_1 H)} \\ &= -C_{a,p}\left[\frac{(w_s + \epsilon_v \lambda_1) \exp(\lambda_1 H)}{(w_s + \epsilon_v \lambda_2) \exp(\lambda_2 H) - (w_s + \epsilon_v \lambda_1) \exp(\lambda_1 H)}\right] \end{aligned} \tag{4.3.42}$$

Now that an expression for A_2 is obtained, A_1 can be determined easily using equation (4.3.39):

$$\begin{aligned} A_1 = C_{a,p} - A_2 &= C_{a,p} + \frac{C_{a,p}(w_s + \epsilon_v \lambda_1) \exp(\lambda_1 H)}{(w_s + \epsilon_v \lambda_2) \exp(\lambda_2 H) - (w_s + \epsilon_v \lambda_1) \exp(\lambda_1 H)} \\ &= C_{a,p}\left[\frac{(w_s + \epsilon_v \lambda_2) \exp(\lambda_2 H)}{(w_s + \epsilon_v \lambda_2) \exp(\lambda_2 H) - (w_s + \epsilon_v \lambda_1) \exp(\lambda_1 H)}\right] \end{aligned} \tag{4.3.43}$$

The analytical expression describing the concentration profile now becomes:

$$\begin{aligned} C_p(z) = C_{a,p}\Bigg[&\frac{(w_s + \epsilon_v \lambda_2) \exp(\lambda_2 H)}{(w_s + \epsilon_v \lambda_2) \exp(\lambda_2 H) - \lambda_1 \exp(\lambda_1 H)} \exp(\lambda_1 z) \\ &- \frac{(w_s + \epsilon_v \lambda_1) \exp(\lambda_1 H)}{(w_s + \epsilon_v \lambda_2) \exp(\lambda_2 H) - (w_s + \epsilon_v \lambda_1) \exp(\lambda_1 H)} \exp\,(\lambda_2 z)\Bigg] \end{aligned} \tag{4.3.44}$$

With λ_1 and λ_2 as defined in equation (4.3.28).

Determining the reference concentration analytically

In order to determine the value of the reference concentration analytically, the horizontal velocity over the bed had to be known. All values in the calculation of c_a are constants, except for the bed shear stress τ_b (see equation (4.3.45) below). The latter is determined using equation (4.3.46).

$$c_a = f_{\text{eff}} 0.015 \frac{D_{50}}{0.01 H D_*^{0.3}} \left(\frac{|\tau_b| - \tau_{cr}}{\tau_{cr}}\right)^{1.5} \tag{4.3.45}$$

$$\tau_b = \rho_w \cdot S \cdot u_{bed} \tag{4.3.46}$$

The density of water ρ_w and the slip parameter S are known constants, while the velocity at the bottom (u_{bed}) is not. The horizontal velocity consists of two components; a residual component (M0) and an M4-component. It is not easy to determine the amplitude and the residual component of u_{bed}, so a simpler technique was used. For this, the values of the horizontal velocity near the bed from the SWC output was used. This gave a time series of a full tidal cycle with 300 time steps for u_{bed}. From this, the Fourier transform was determined using the fast Fourier transform (*fft*) algorithm of MATLAB. Using this Fourier transform, the value of u_{bed} could be requested at any time during the tidal cycle. This value could then be used for calculating the bed shear stress and hence the reference concentration.

4.3.4 Basic state: comparing the analytical expressions for the concentration profile with the SWC output

The analytical expressions of the concentration profile above can be compared to the SWC output. The parameters used are those of Set 1 (see Section 3.2.2), except the reference height is set to zero and a constant sediment diffusivity of 0.09 m²/s is used.

First the SWC results are compared with the analytical solution for the case with the Neumann boundary condition at the surface (equation (4.3.15), first condition). In Figure 9 below, graphs of the concentration profiles are shown for different times during the first tidal cycle.

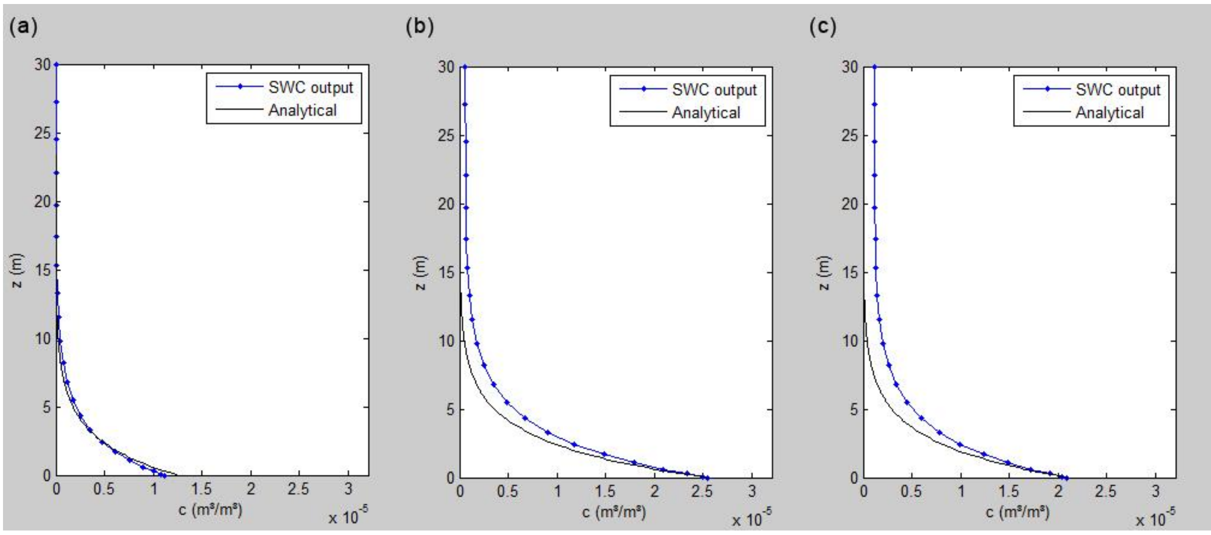

Figure 9: Graphs of the concentration profile of both the SWC output and the analytical solution in case of a Neumann boundary condition at the surface. These profiles are shown at the following times after the start of the first tidal cycle: 25 minutes (a), 3 hours and 6 minutes (b) and 8 hours and 59 minutes (c).

In Figure 9 can be seen that initially the SWC produces a quite adequate representation of the analytical solution. However, over time the simulated profile shifts to the right, only maintaining a constant concentration ($\partial c/\partial z = 0$) at the top of the water column and not a negligible value as in the analytical solution. In the analytical solution the concentration declines exponentially upwards from the bottom, which is clearly not the case for the simulated concentration. Later on it will be shown that this is due to the chosen boundary condition at the surface, which is a Neumann boundary condition and not a no flux boundary condition.

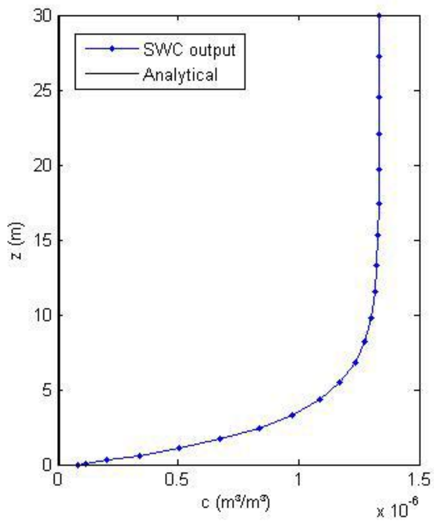

Figure 10: Concentration profiles of the SWC output and the analytical solution in case of a Neumann boundary condition at the surface, 10 hours and 46 minutes into the first tidal cycle, when the near bed horizontal velocity is about $1 \cdot 10^{-2}\ \mathrm{m/s}$.

Furthermore, in Figure 10 can be seen what happens when the near bed horizontal velocity (u_{bed}) is very low (order $1 \cdot 10^{-2}\ \mathrm{m/s}$). As can be seen, in the analytical solution the concentration is zero over the whole water column. The SWC however, simulates a very low reference concentration which increases until a certain maximum concentration is reached that remains constant in the upper part of the water column. Figure 10 clearly visualizes and (in combination with equation (4.3.15)) explains the problem shown in Figure 9 earlier. As will be shown below, this is solved when applying a no flux boundary condition at the surface.

Next, the SWC results are compared with the analytical solution for the case with the no flux boundary condition at the surface (equation (4.3.1)). In Figure 11 below, graphs of the concentration profiles using no flux are shown for different times during the first tidal cycle.

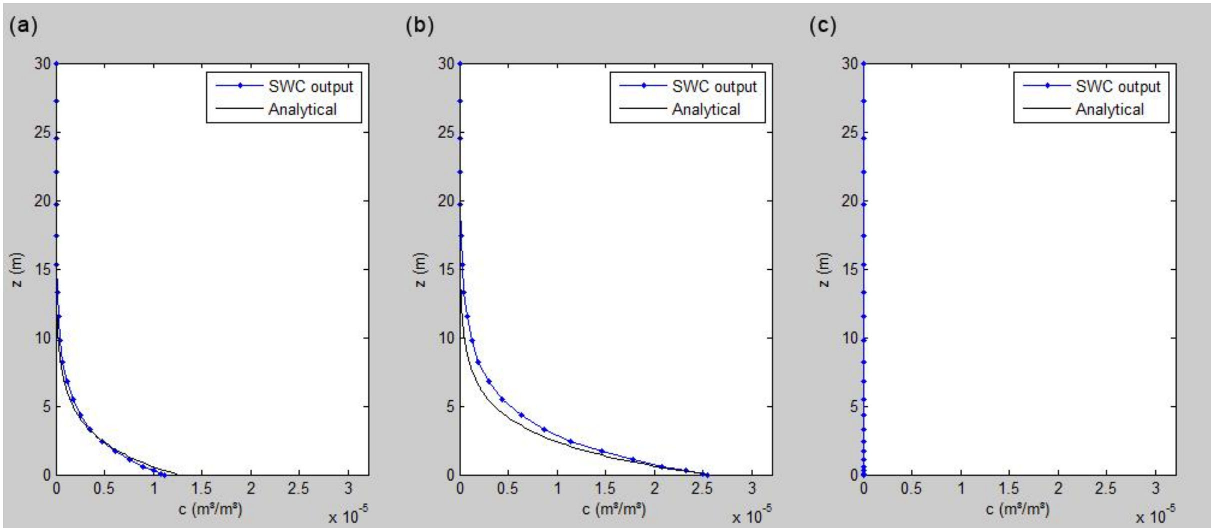

Figure 11: Graphs of the concentration profile of both the SWC output and the analytical solution in case of a no flux boundary condition at the surface. These profiles are shown at the following times after the start of the first tidal cycle: 25 minutes (a), 3 hours and 6 minutes (b) and 10 hours and 46 minutes (c).

As can be seen, when a no flux boundary condition is applied, the concentration profile of the SWC simulation no longer shifts to the right. Furthermore, the strange phenomenon where the concentration at the top of the water column was larger than that at the bottom does no longer occur, as can be seen in Figure 11c which shows the concentration profile at the same time as in Figure 10.

The no flux boundary condition at the surface which was applied without the use of a ghost point thus leads to a much better representation of the analytical profile, as can be seen when comparing Figure 9 and Figure 10 with Figure 11. The remaining differences between the numerical simulation and the analytical solution can be accounted to numerical inaccuracies caused by rounding and low order discretizations.

4.4 Re-evaluation of different sediment diffusivity models

Since a lot of changes have been applied to the Sand Wave Code, it seemed wise to reinvestigate the choice of the distribution used for describing the sediment diffusivity over the water depth. Changes that have a direct impact on this are the implementation of the new scaling of the suspended sediment calculation and the minor improvements that are discussed in Appendix A. Furthermore, taking into account the bed level elevation in the calculation of the sediment diffusivity may also have an influence on this and it is explained in Section 4.4.1 below.

4.4.1 Taking into account the bed level elevation in the diffusivity calculation

When calculating the sediment diffusivity ϵ_v the average depth H was used. This means that the bed level elevation was not taken into account. In order to properly determine the diffusivity profile however, the local depth should be used (van Rijn, 1993). The local depth is equal to $H - h(x)$. When using this local depth, the expression for the sediment diffusivity as a parabolic-constant profile becomes:

$$\epsilon_v = \begin{cases} \kappa\beta_* u_*(z - h(x))\left(1 - \dfrac{z - h(x)}{H - h(x)}\right) & \text{for } z - h(x) < 0.5\big(H - h(x)\big) \\ 0.25\kappa\beta_* u_*(H - h(x)) & \text{for } z - h(x) \geq 0.5(H - h(x)) \end{cases} \tag{4.4.1}$$

The derivative of ϵ_v to z then becomes:

$$\frac{\partial \epsilon_v}{\partial z} = \begin{cases} \kappa\beta_* u_*\left(1 - \dfrac{2(z - h(x))}{H - h(x)}\right) & \text{for } z < 0.5H \\ 0 & \text{for } z \geq 0.5H \end{cases} \tag{4.4.2}$$

4.4.2 Comparison of different sediment diffusivity models

The parameters used in this comparison are those of Parameter Set 1. Three different profiles are tested. One has a constant value over the water depth (equation (4.4.3)) and two are depth dependent, one linear (equation (4.4.4)) and one parabolic-constant (equation (4.4.5)) in which ϵ_v is parabolically increasing for the lower half of the water column and above that constant over the water depth. Examples of the three different profiles are also shown in Figure 12.

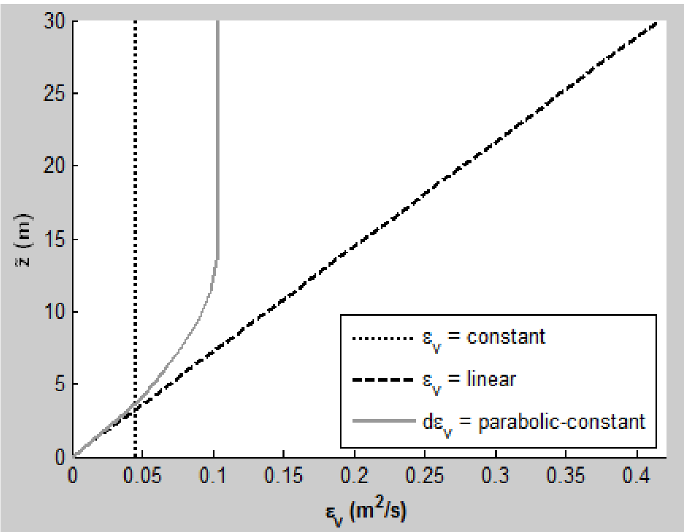

Figure 12: Examples of the three different sediment diffusivity profiles, as defined in equations (4.4.3) through (4.4.5).

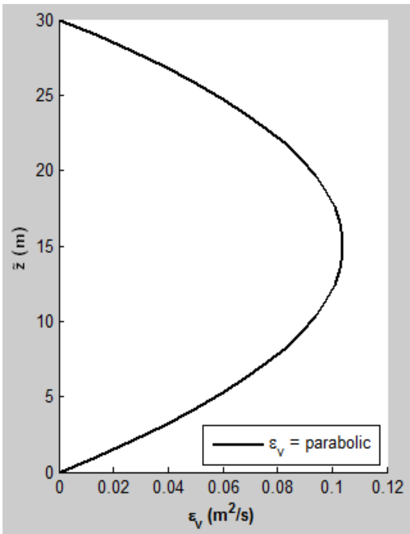

Figure 13: Example of a parabolic profile (not tested in this research).

An example of a parabolic profile is also shown in Figure 13. This profile is not tested in this research, but it is mentioned shortly at the end of this section.

$$\epsilon_{v1} = \alpha_* A_v = \overline{\epsilon_v} \tag{4.4.3}$$

$$\epsilon_{v2} = \kappa\beta_* u_* (z - h(x)) \tag{4.4.4}$$

$$\epsilon_{v3} = \begin{cases} \kappa\beta_* u_* (z - h(x)) \left(1 - \dfrac{z - h(x)}{H - h(x)}\right) & \text{for } z - h(x) < 0.5\big(H - h(x)\big) \\ 0.25\kappa\beta_* u_* (H - h(x)) & \text{for } z - h(x) \geq 0.5(H - h(x)) \end{cases} \tag{4.4.5}$$

In these equations ϵ_v is the sediment diffusifity, α_* is a constant (here chosen at 4.5), A_v is the eddy viscosity, κ is the Von Karman constant (equal to 0.4), z is the vertical coordinate and u_* is the bed shear velocity. The parameter β_* describes the difference between a water and a sediment particle, and has a maximum value of 2:

$$\beta_* = 1 + 2\left(\frac{w_s}{u_*}\right)^2 \quad \text{for } 0.1 < \frac{w_s}{u_*} < 1 \tag{4.4.6}$$

The bed shear velocity is described as follows:

$$u_* = \frac{|\tau_b|}{\tau_b} \cdot \sqrt{\frac{|\tau_b|}{\rho_w}} \tag{4.4.7}$$

First the initial growth rate has been determined for several wave lengths using 10m increments. The results of this are shown in Figure 14. As can be seen in this figure, the constant profile shows a result that is very different from the other two profiles. Compared to the linear profile, the parabolic-constant profile results in a slightly lower wave length for the fastest growing mode (240m for the linear profile and 230m for the parabolic-constant profile) as well as a slightly higher growth rate overall.

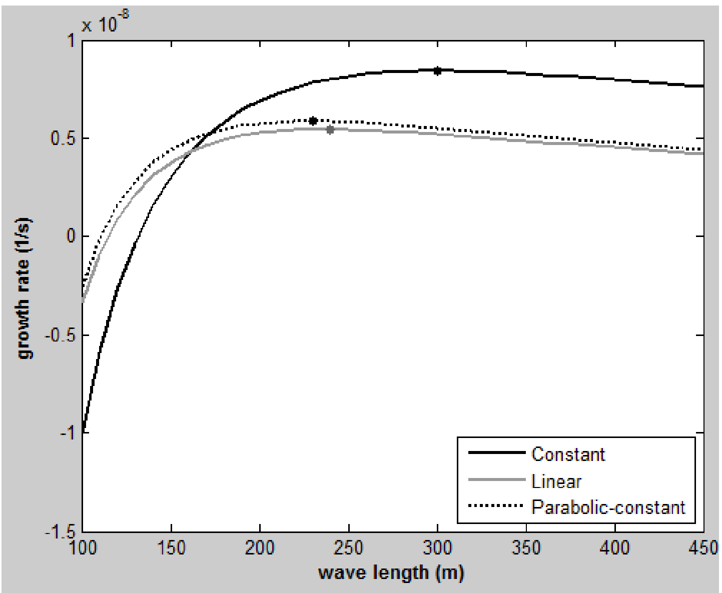

Figure 14: Initial growth rates for the three different sediment diffusivity profiles. The dots mark the wave lengths of the fastest growing modes.

Not only the initial growth of the sand wave matters, but of course also the long term development. For the FGMs of each sediment diffusivity profile a long simulation has been carried out. The results of these long runs are shown in Figure 15 below.

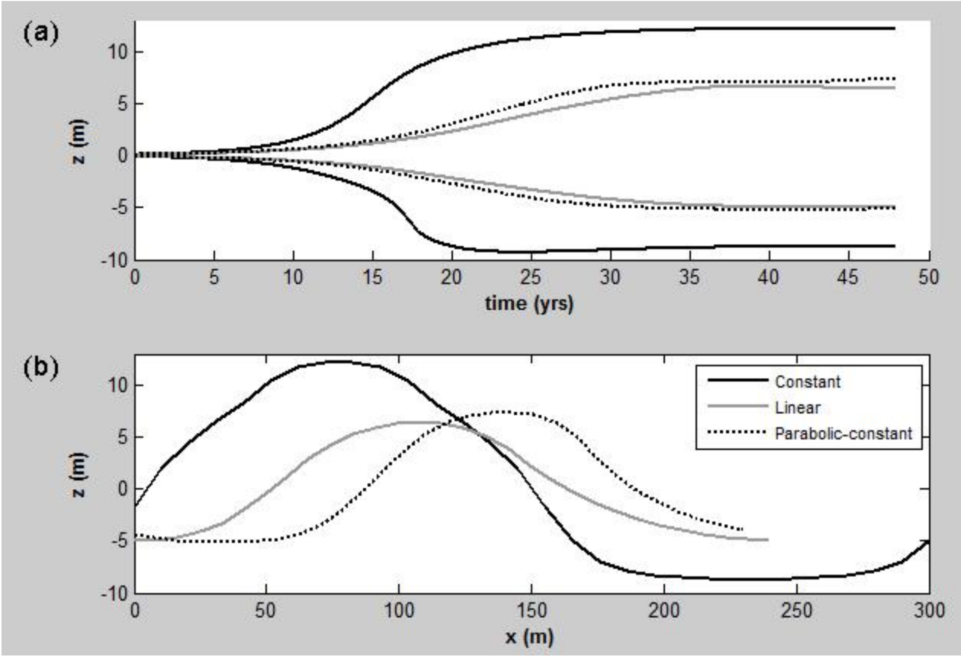

Figure 15: (a) shows the crest and trough growth and the final shapes of the sand waves are shown in (b).

As can be seen in Figure 15, the constant profile deviates very much from the other two. The crest and trough grow much faster and also reach a much higher height and depth respectively. The value of the constant profile was picked quite arbitrarily, since no good estimate of the sediment diffusivity at the bed was known. Since optimizing this constant to match the results of the other two profiles best, would be enough work for a whole new study, this was not done here. Therefore only the linear and parabolic-constant profiles were considered for use in this research.

When comparing the linear profile with the parabolic-constant profile (Figure 15b), some differences can be distinguished. First, the parabolic-constant profile resulted in a slightly higher growth rate, which caused the sand wave to reach an equilibrium situation sooner (about 4 years earlier). Also, the final crest height and trough depth are slightly larger. Lastly, the final shape with this profile showed a steeper sand wave. Furthermore, as previously mentioned the parabolic constant profile had a fastest growing mode of a slightly shorter wave length. These differences are all not very large, but they do all suggest that the use of a parabolic-constant profile results in predictions of more dangerous sand waves. Higher, steeper and shorter sand waves are namely considered as more dangerous in most cases. The safe choice from a designer's perspective would therefore be to use the parabolic-constant profile. In this research the goal is to improve the model and thereby make more realistic predictions. Fortunately the parabolic constant profile also seems to be the most realistic profile. According to Van Rijn (1993), a parabolic distribution is most satisfactory in a physical sense, mainly because it is based on a linear shear stress distribution and a logarithmic velocity profile. An example of such a distribution can be seen in Figure 13. The parabolic distribution has the disadvantage of yielding a zero-concentration at the water surface however, which is not realistic because mixing coefficients based on the analysis of measured concentration profiles by Coleman (1970) were more in accordance with the parabolic-constant distribution. This is why I will build upon the version of the model with the parabolic-constant profile for the sediment diffusivity.

5 Critical condition for the initiation of bed load transport

5.1 Introduction

In the previous version of the Sand Wave Code (SWC), no critical condition for the initiation of sediment transport was used for the bed load transport. In this section we will describe how a critical condition is included in the equations that are implemented in the SWC.

5.2 New description of the bed load transport in case of a critical condition

In the previous version of the model, the following equations for bed load transport were used when surface waves were excluded and included respectively:

$$q_{bf} = \alpha\left|\tau_{bf}\right|^{1/2}\left[\tau_{bf} - \lambda\left|\tau_{bf}\right|\frac{\partial h}{\partial x}\right] \tag{5.2.1}$$

$$q_b = \alpha\left|\tau_{bf}\right|^{1/2}\left(\left|\tau_{bf}\right| + \gamma\left|\tau_{bw}\right|\right)\left[\frac{\tau_{bf}}{\left|\tau_{bf}\right|} - \lambda\frac{\partial h}{\partial x}\right] \tag{5.2.2}$$

The latter equation has been derived using a third order dependency of the sediment transport on the total horizontal near bed velocity u_{total}. The same method is used here to derive a sediment transport equation that includes a critical value of the bed shear stress. We start off with expressions for the velocity in x-direction ($\vec{u}$) and the velocity in y-direction ($\vec{v}$).

$$\vec{u} = u_{bf} + u_{bw}\cos(\psi)\sin(\sigma t) \tag{5.2.3}$$

$$\vec{v} = u_{bw}\sin(\psi)\sin(\sigma t) \tag{5.2.4}$$

A velocity in y-direction exists, because there can be an angle (ψ) between the direction of the current and the direction of the surface waves. The direction of the current is assumed to be dominant, and is therefore taken as the x-direction, which is also the only horizontal direction the SWC uses. The third order of u_{total} is formally given by the following expression:

$$u_{total}{}^3 = |\vec{u}|^2\,\vec{u} \tag{5.2.5}$$

When introducing a critical value of the horizontal velocity at the bed (u_{cr}), this can be changed to the following expression:

$$|\vec{u}|^2\,\vec{u} = (|\vec{u}| - u_{cr})^3\,\mathcal{H}(|\vec{u}| - u_{cr})\,\frac{\vec{u}}{|\vec{u}|} \tag{5.2.6}$$

Here $\mathcal{H}(\cdot)$ is the Heaviside function, which has a value of one for a positive argument and zero otherwise. Note that the critical value of the horizontal velocity at the bed (u_{cr}) is subtracted from the length of the velocity vector. This means that the remainder of the horizontal velocity, after this subtraction, contributes to the bed load transport. When the remaining velocity becomes zero or negative, the bed load transport is zero, because then the velocity is below the critical condition. The Heaviside function takes care of the latter. The length of the velocity vector ($|\vec{u}|$) can be derived as follows:

$$|\vec{u}| = \sqrt{\vec{u}^2 + \vec{v}^2} = \sqrt{\left(u_{bf} + u_{bw}\cos(\psi)\sin(\sigma t)\right)^2 + (u_{bw}\sin(\psi)\sin(\sigma t))^2}$$
$$= \sqrt{{u_{bf}}^2 + 2u_{bf}u_{bw}\cos(\psi)\sin(\sigma t) + {u_{bw}}^2\cos^2(\psi)\sin^2(\sigma t) + {u_{bw}}^2\sin^2(\psi)\sin^2(\sigma t)} \quad (5.2.7)$$
$$= \sqrt{{u_{bf}}^2 + 2u_{bf}u_{bw}\cos(\psi)\sin(\sigma t) + {u_{bw}}^2\sin^2(\sigma t)}$$

Since the absolute value of the bed shear stress τ is proportional to the square of the horizontal velocity at the bed ${u_{bed}}^2$, all velocity terms can be replaced by their corresponding bed shear stress terms in equations (5.2.7) and (5.2.3). Since τ is proportional to ${u_{bed}}^2$, but not completely equal, a proportionality constant α is introduced in the expression for ${u_{total}}^3$. The new expressions for $\vec{u}$ and $|\vec{u}|$ are given in equations (5.2.8) and (5.2.9) respectively.

$$\vec{u} = \sqrt{\tau_{bf}} + \sqrt{\tau_{bw}}\cos(\psi)\sin(\sigma t) \quad (5.2.8)$$

$$|\vec{u}| = \sqrt{\left|\tau_{bf}\right| + 2\sqrt{\left|\tau_{bf}\right|}\sqrt{\tau_{bw}}\cos(\psi)\sin(\sigma t) + \tau_{bw}\sin^2(\sigma t)} \quad (5.2.9)$$

Note that the absolute value of the bed shear stress due to flow (τ_{bf}) is used here. The reason for that is that in the SWC the sign of τ_{bf} is used to indicate the direction of bed load transport. This means that it merely has the same sign as u_{bf}. Since negative bed shear stresses have no physical meaning, the absolute value is used here. The values of the bed shear stress due to surface waves (τ_{bw}) and the critical bed shear stress (τ_{cr}) are always positive.

We take the third order of u_{total} and average over a surface wave:

$$\langle u_{total}\rangle^3 = \alpha\left\langle\left(|\vec{u}| - \sqrt{\tau_{cr}}\right)^3 \mathcal{H}\left(|\vec{u}| - \sqrt{\tau_{cr}}\right)\frac{\vec{u}}{|\vec{u}|}\right\rangle \quad (5.2.10)$$

Where $\vec{u}$ and $|\vec{u}|$ are as given in equations (5.2.8) and (5.2.9) respectively. Note that the proportionality constant α is taken outside the averaging parentheses, because it is a constant.

It is not possible to solve equation (5.2.10) analytically, because of the Heaviside function. Averaging over a surface wave period should therefore be done numerically. This means that the surface wave period should be divided in a finite number of time steps. The value of ${u_{total}}^3$ is calculated for each of these time steps, the values for all time steps are then summarized and the total sum is divided by the amount of time steps. This is represented by the following equation:

$$\langle u_{total}\rangle^3 = \alpha\frac{1}{T_W}\sum_{t=0}^{T_W}\left(|\vec{u}| - \sqrt{\tau_{cr}}\right)^3 \mathcal{H}\left(|\vec{u}| - \sqrt{\tau_{cr}}\right)\frac{\vec{u}}{|\vec{u}|} \quad (5.2.11)$$

The new equation for the bed load transport q_b then becomes:

$$q_b = \alpha\frac{1}{T_W}\sum_{t=0}^{T_W}\left(|\vec{u}| - \sqrt{\tau_{cr}}\right)^3 \mathcal{H}\left(|\vec{u}| - \sqrt{\tau_{cr}}\right)\left[\frac{\tau_{bf}}{\left|\tau_{bf}\right|} - \lambda\frac{\partial h}{\partial x}\right] \quad (5.2.12)$$

Note that $\vec{u}/|\vec{u}|$ has been replaced by $\tau_{bf}/\left|\tau_{bf}\right|$. They both indicate the direction of the bed load transport.

Just like in the suspended sediment calculation, the critical shear stress is determined using the following equations:

$$\tau_{cr} = (\rho_s - \rho_w) g D_{50} \theta_{cr} \tag{5.2.13}$$

$$\theta_{cr} = \frac{0.24}{D_*} + 0.055(1 - \exp(-0.02 D_*)) \tag{5.2.14}$$

$$D_* = \left(\frac{g(s-1)}{\nu^2}\right)^{1/3} D_{50} \tag{5.2.15}$$

We now have a new equation that describes the bed load transport when a critical condition for the initiation of sediment motion is included, which also works when surface waves are included. This equation can be implemented in the SWC to see what the effect of this critical condition is on both the development and final shape of sand waves.

6 Results of the three simulated North Sea cases

In this Chapter the results of the three simulated North Sea cases are presented. First an overview of the performed runs and their results is given. Various simulations have been carried out for all three North Sea cases discussed in Chapter 2. After this, the effect of including suspended sediment, a critical condition for the initiation of bed load transport and both of these additions together will be discussed in more depth. Both the initial growth rates from which the fastest growing mode (FGM) is determined and the total sand wave development of the FGM will be discussed. While presenting the results, the values are already compared to the measured sand wave heights and lengths shown in Chapter 2.

6.1 Overview of the performed runs and their results

An overview of the runs carried out for each of the North Sea cases is given in Table 6. The runs labelled "Basic" are simulations without any of the additions, which are used as a reference here. The abbreviations "SS", "CSS" and "Res" respectively stand for "suspended sediment", "critical shear stress" and "residual current". To clarify this further, in Table 6 it is shown what is and is not turned on for all the simulations. In the runs of Case 1A, Case 1B and Case 2, the corresponding parameters from Section 3.2.3 (page 9) have been used. In Table 7 the sand wave characteristics resulting from the runs described in Table 6 are shown. It shows the length of the fastest growing mode, the final amplitude (consisting of the crest height and the trough depth), the crest/trough ratio and the maximum slope of the sand wave.

Run	Suspended sediment	Critical condition	Residual current
Case 1A Basic	No	No	No
Case 1A SS	Yes	No	No
Case 1A CSS	No	Yes	No
Case 1A SS+CSS	Yes	Yes	No
Case 1B Basic	No	No	No
Case 1B SS	Yes	No	No
Case 1B CSS	No	Yes	No
Case 1B SS+CSS	Yes	Yes	No
Case 2 Basic	No	No	No
Case 2 Res	No	No	Yes
Case 2 CSS	No	Yes	No
Case 2 CSS+Res	No	Yes	Yes
Case 2 SS	Yes	No	No
Case 2 SS+Res	Yes	No	Yes
Case 2 SS+CSS	Yes	Yes	No
Case 2 SS+CSS+Res	Yes	Yes	Yes

Table 6: Overview of runs performed for all three North Sea cases.

From Table 7, some general findings are already clearly visible. It can be seen that the Basic case, in which suspended sediment and the critical condition have not been taken account, gives the best predictions of the measured sand wave lengths of 520, 400 and 210 m (respectively for Case 1A, Case 1B and Case 2). In most cases the predicted sand wave length is reduced when suspended sediment or the critical condition are included. This results in a severe underprediction of the sand wave length in case of the critical condition. In Case 2 the predicted FGM was actually less than 100 metres. If we would use an FGM shorter than 100 m, the shallow water approximation would not hold, so instead a sand wave length of 100 m is used in the long simulations.

Run	FGM (m)	ampli-tude (m)	crest height (m)	trough depth (m)	crest/trough ratio (-)	maximum slope (°)
Case 1A Basic	520	24.1	+15.5	-8.6	0.70	17.9
Case 1A SS	470	24.6	+17.0	-7.6	0.62	17.3
Case 1A CSS	350	19.5	+12.0	-7.5	0.75	17.3
Case 1A SS+CSS	410	19.8	+15.9	-3.9	0.49	27.2
Case 1B Basic	440	21.8	+14.4	-7.4	0.67	21.1
Case 1B SS	610	31.2	+20.3	-10.9	0.63	16.7
Case 1B CSS	320	19.2	+12.4	-6.8	0.70	21.1
Case 1B SS+CSS	650	26.8	+22.8	-4.0	0.26	26.2
Case 2 Basic	210	11.3	+6.9	-4.4	0.65	16.1
Case 2 Res	200	9.0	+5.7	-3.3	0.64	22.0
Case 2 SS	190	10.6	+6.4	-4.2	0.77	18.4
Case 2 SS+Res	180	8.6	+5.4	-3.2	0.65	21.0
Case 2 CSS	100	4.2	+2.9	-1.3	0.75	17.6
Case 2 CSS+Res	100	3.9	+2.6	-1.3	0.47	27.4
Case 2 SS+CSS	100	6.4	+4.7	-1.7	0.35	43.9
Case 2 SS+CSS+Res	100	4.3	+3.3	-1.0	0.32	39.7

Table 7: Sand wave properties resulting from the runs described in Table 6.

The predictions of the final sand wave amplitude are often way too large. Amplitudes of a factor 10 too large are predicted. Only in Case 2 the amplitude reaches a reasonable value when the critical condition is included. The critical condition results in a reduction of the final sand wave amplitude in all three cases. Including suspended sediment results in an increased final amplitude in Case 1A and Case 1B, but in a decreased final amplitude in Case 2. In Case 2 the residual current leads to a reduction in the final amplitude in each case (Basic, SS, CSS and CSS+Res).

A rather alarming yet logical finding is that the maximum slopes found in all the simulations are way too large. In the simulations of Case 2 with a combination of including suspended sediment and the critical condition the slopes even reach about 40°, which is very unrealistic. This finding is logical though, because the predicted amplitude was way too large while the predicted sand wave lengths were very close to the measured sand wave lengths. A larger amplitude on the same domain logically leads to a higher slope. In the simulations of "Case 2 SS+CSS" and "Case 2 SS+CSS+Res" however, the amplitude was rather low while the slope is extremely high. This is probably because these simulations were rather unstable, which can be seen in the results of section

6.2 Basic model and residual current

In this section the results of the runs without suspended sediment and a critical condition are presented. For Case 2, also the case with a residual current is performed. The effect of this will be discussed as well.

A short overview of the results is shown in Figures 16 and 17, which contain the initial growth rate for different wave lengths (a), the crest and trough growth of the sand waves in time (b) and the final shape of the sand wave (c).

The predicted lengths of the fastest growing mode lie very close to their measured values. The effect of the chosen model parameters on this will be discussed in Section 7.1.1. For Case 1A and Case 2 the

FGM was exactly the same as the averaged measured sand wave length, while for Case 1B the predicted sand wave length was 40 m larger.

The final sand wave amplitudes that have been found in these simulations are way too large. They are three to twelve times to large, depending on the case. In Case 2 the amplitude reduced by about 2 metres when the residual current is included. Also, the predicted sand wave length is slightly lower with a residual current. Perhaps a residual current should also be present in Case 1A or Case 1B, but no value of it was reported by Van Santen (2009).

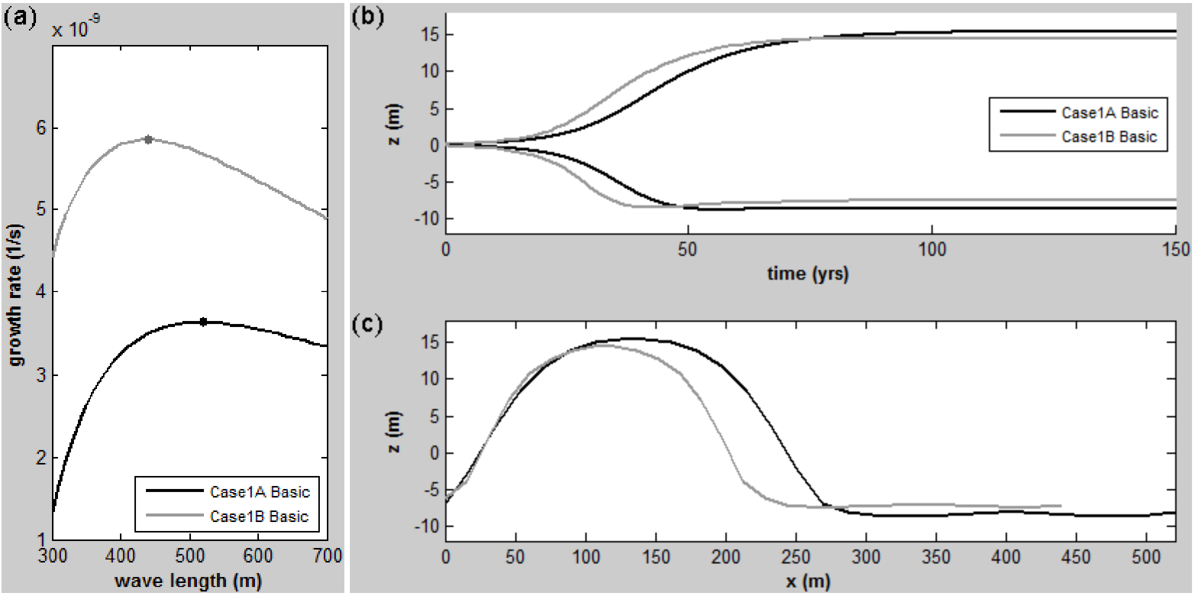

Figure 16: Basic model results for Case 1A and Case 1B. (a) shows the initial growth rate for different wave lengths, where the dot indicates the FGM, (b) shows the crest and trough growth of the FGM in time and (c) shows the equilibrium sand wave shape for the two simulations. The shown legends apply to all three figures. The codes shown in the legends correspond with the codes shown in Tables 6 and 7.

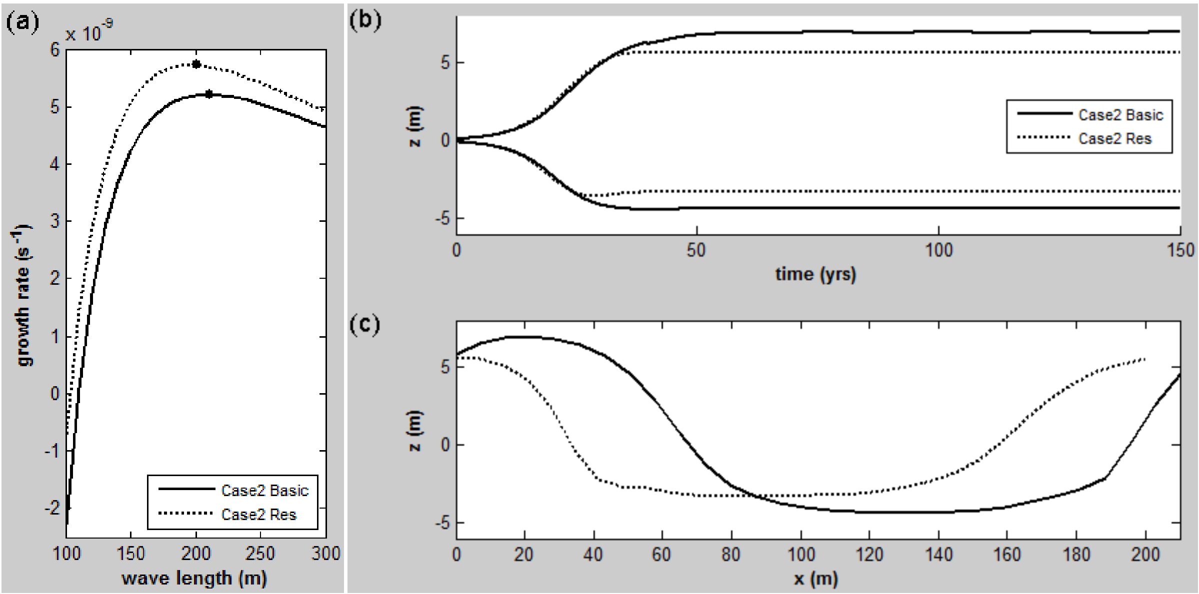

Figure 17: Basic model results for Case 2, both with and without a residual current. (a) shows the initial growth rate for different wave lengths, where the dot indicates the FGM, (b) shows the crest and trough growth of the FGM in time and (c) shows the equilibrium sand wave shape for the two simulations. The shown legends apply to all three figures. The codes shown in the legends correspond with the codes shown in Tables 6 and 7.

Furthermore, in Figures 16 and 17 it can be seen that the sand waves reach a very steady equilibrium. It can also be seen that the slope on the downstream side (to the right) of the crest is higher in case of a residual current for Case 2. Under these circumstances a velocity skewed sand wave develops.

6.3 The new suspended sediment module

As can be seen in Figures 18 and 19, when suspended sediment is included slightly shorter sand waves develop in Case 1A and Case 2. For these two cases, the final sand wave amplitude does not change very much with respect to the results without suspended sediment. In Case 1B the fastest growing mode becomes much larger when suspended sediment is included, and consequently the final amplitude increases a lot (about 10 metres). I say consequently, because a longer sand wave length often yields a larger sand wave height, because the height to length ratio remains relatively the same. That being said, the slightly shorter sand waves in Case 1A and Case 2 were thus expected to yield sand waves with a lower amplitude. However, the amplitude in Case 1A increased, despite the decrease in FGM of 50 m. The slight drop in amplitude in Case 2 is also most likely associated with the slight decrease in sand wave length.

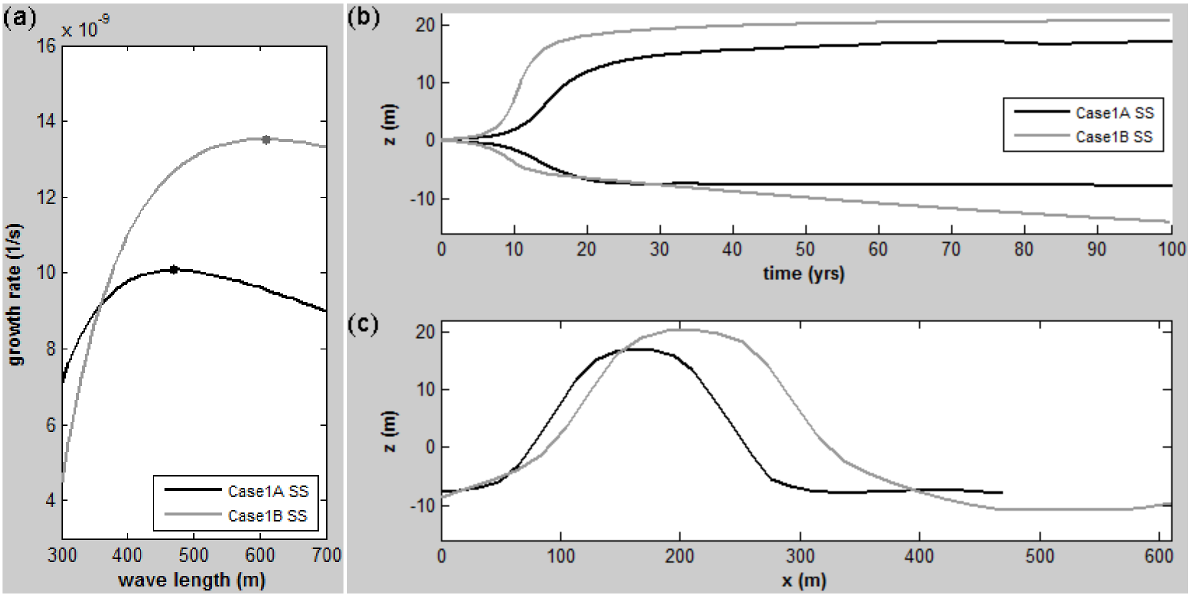

Figure 18: Influence of suspended sediment load on the sand waves for Case 1A and Case 1B. (a) shows the initial growth rate for different wave lengths, where the dot indicates the FGM, (b) shows the crest and trough growth of the FGM in time and (c) shows the equilibrium sand wave shape for the two simulations. The shown legends apply to all three figures. The codes shown in the legends correspond with the codes shown in Tables 6 and 7.

The residual current of Case 2 again resulted in a decrease of the final amplitude of about the same magnitude as in the basic model results (Figure 19b). Also, the predicted FGM shortens slightly due to the residual current. However, in this case the shortening is relatively so small (10 metres) that it is probably not the only cause for the decrease in amplitude of 2 m.

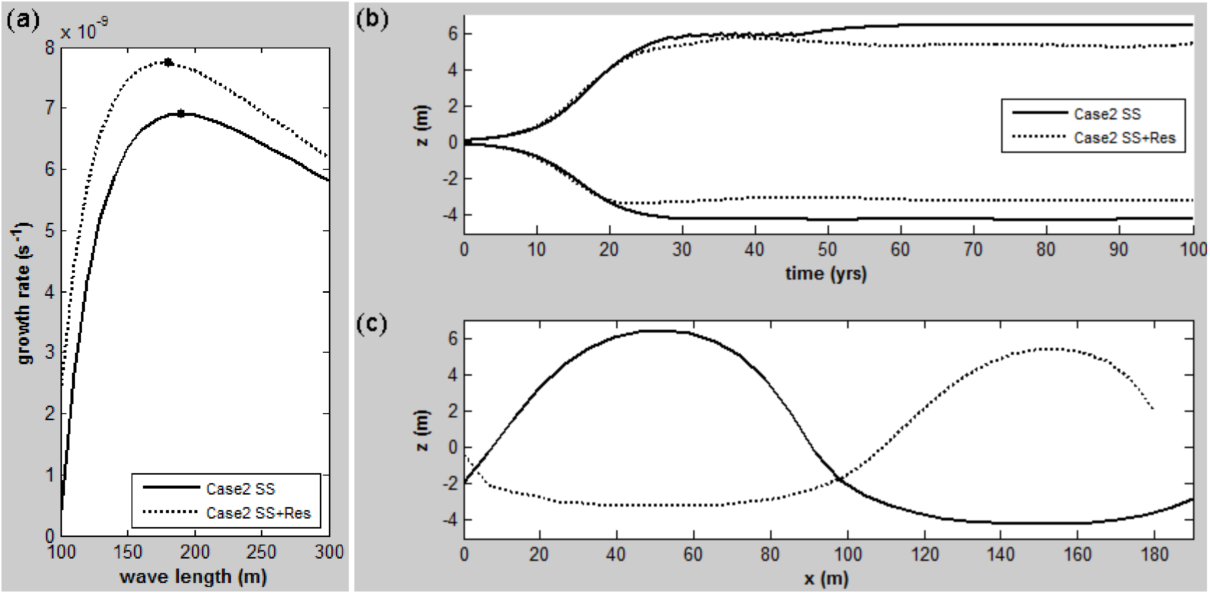

Figure 19: Influence of suspended sediment load on the sand waves for Case 2. (a) shows the initial growth rate for different wave lengths, where the dot indicates the FGM, (b) shows the crest and trough growth of the FGM in time and (c) shows the equilibrium sand wave shape for the two simulations. The shown legends apply to all three figures. The codes shown in the legends correspond with the codes shown in Tables 6 and 7.

To further elicit the effects of involving suspended sediment, in Figure 20a, b, c and d the sediment transport (upper panels), the divergence of sediment (shown as a gradient of the sediment transport in the middle panels) and the resulting seabed (lower panels) are shown in graphs. Each of the figures shows these graphs at a different time during the stage of the sand wave development, from a to d respectively after 1, 25, 40 and 80 years. These years were chosen so to show different stages in the sand wave development. This figure is only shown for Case 2, because showing it for all of the cases would be redundant, as the results are qualitatively the same.

Just like in the results of Sterlini (2009), the transport gradient initially follows the sand wave shape in both cases. A positive gradient occurs at the crest which causes deposition there and a negative gradient occurs at the trough which causes erosion there. As the sand wave develops, non-linear effects become more important and change the transport and thereby the sand wave shape. Eventually larger sediment transport gradients occur at the slopes of the sand waves. These slopes then become steeper and the crest becomes narrower.

The growth rate is higher in case of suspended sediment. This is mainly because the overall net transport increases in this case. Due to this, the sand wave evolution goes faster for the case with suspended sediment and consequently after 25 years the resulting sand wave is further developed than in the case without suspended sediment (Figure 20b). Just like in the results of Sterlini (2009), the bed load transport is often higher when suspended load is also present. The bed load transport is balanced by the suspended load transport after a while.

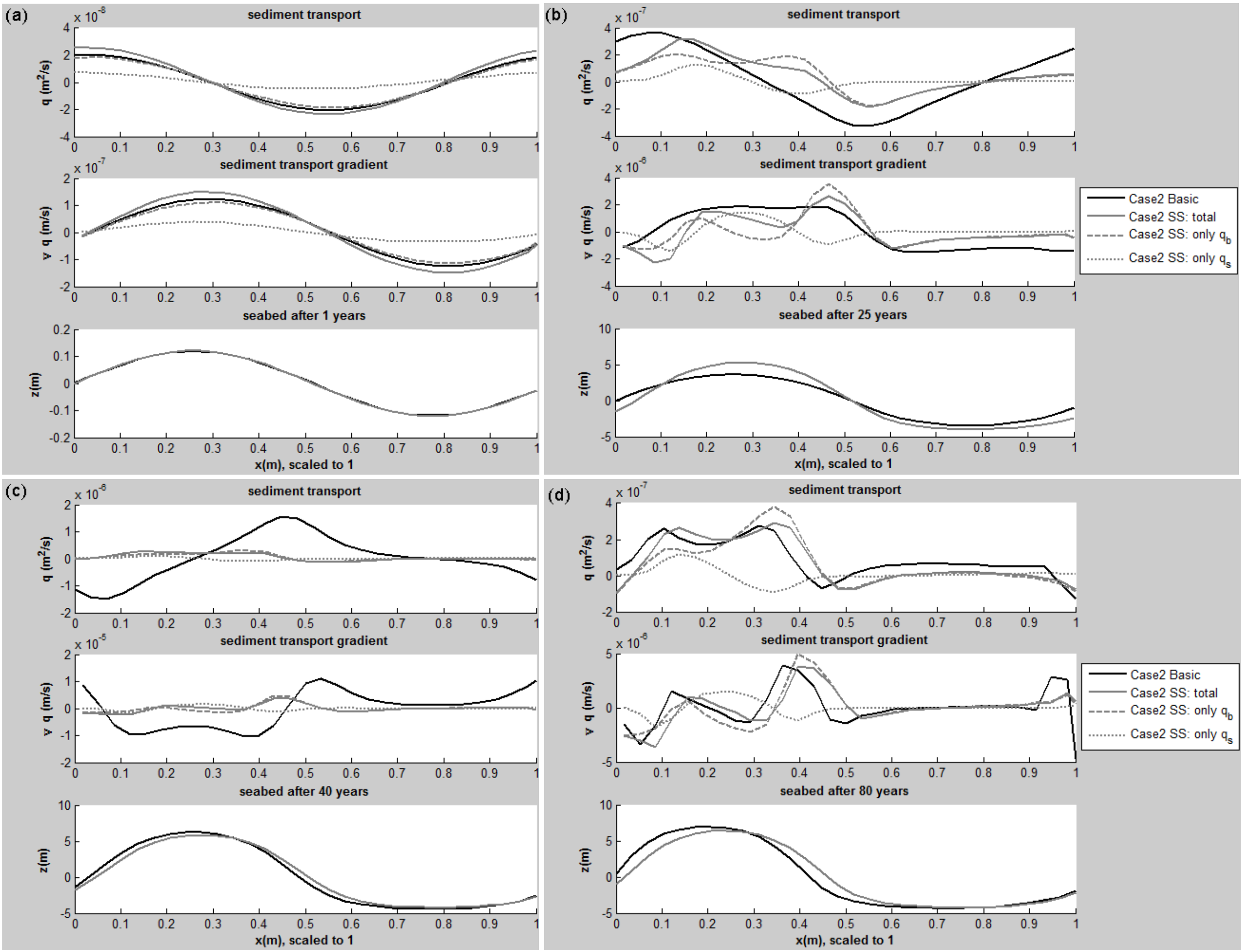

Figure 20: Sediment transport, sediment transport gradient and the sand wave shape at four times during the sand wave development for Case 2. The shown values are averaged over a tidal cycle. In (a) the values are shown after 1 year of simulation, in (b) after 25 years, in (c) after 40 years and in (d) after 80 years. For the simulation without suspended sediment, only the bed load transport and its gradient (black line) are shown respectively in the upper and middle panels. For the simulation with suspended sediment, both the bed load transport (dashed gray line) and the suspended load transport (dotted gray line) and their gradients are shown. The shown legends apply to all four figures. The codes shown in the legends correspond with the codes shown in Tables 6 and 7.

The results regarding Figure 20 are qualitatively the same as what Sterlini (2009) found. However, quantitatively some large differences can be distinguished. Sterlini (2009) reported that the bed load is approximately ten times larger than the suspended load in the initial stage, while here the suspended load transport was two times larger than the bed load transport after one year. This is very surprising, as under conditions where suspended sediment is dominant sand waves are expected to decay rather than grow (Tonnon et al., 2007). This will be discussed further in Section 7.1.2.

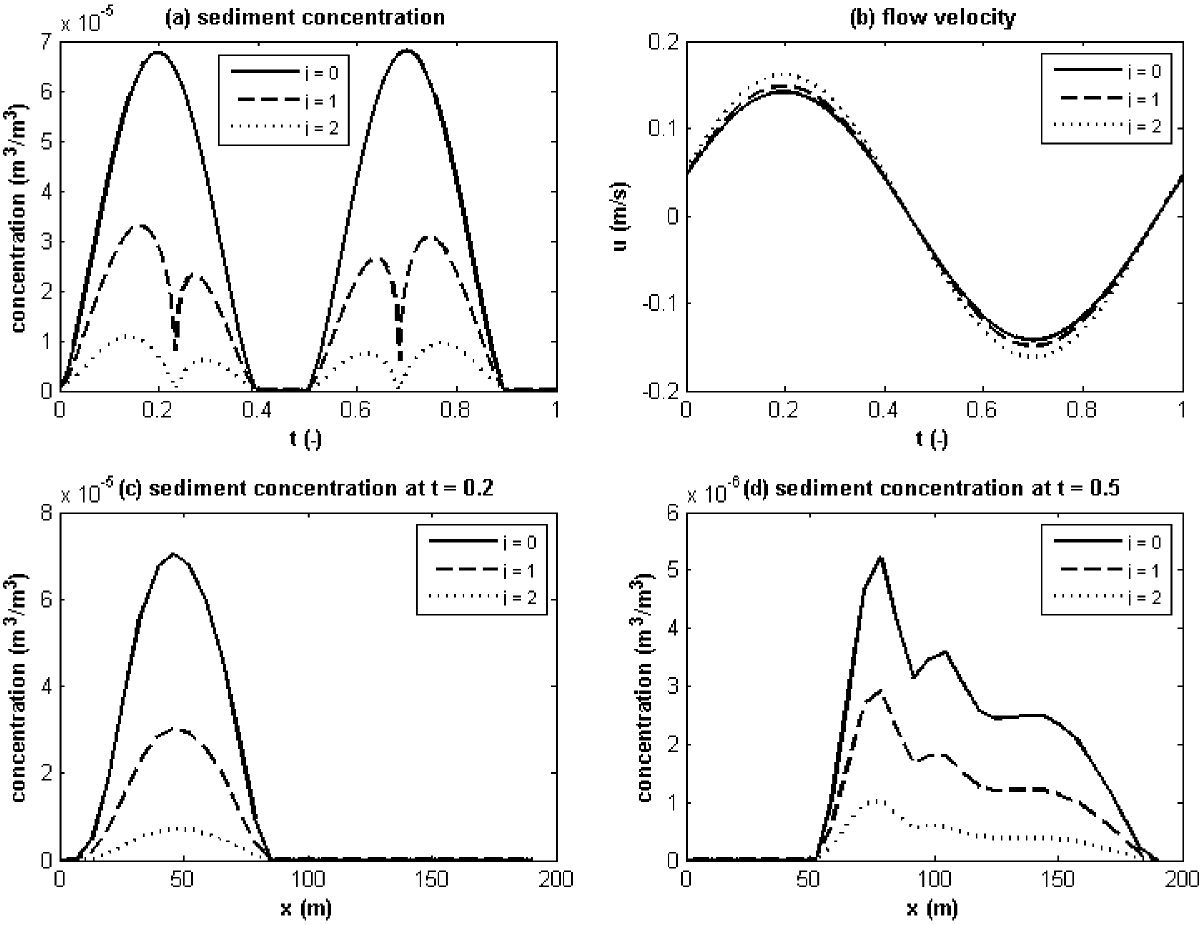

Figure 21: Sediment concentrations throughout the tidal cycle after 45 years for Case 2. In (a) the sediment concentration at the crest over a tidal cycle is shown. In (b) the horizontal flow velocity at the crest over a tidal cycle is shown. Graphs (c) and (d) show the sediment concentrations over a sand wave at two different times during the tidal cycle. Note that the graphs show the sediment concentrations at j = 0, j = 1 and j = 2, which correspond to about 0.30 m, 0.37 m and 0.57 m above the bed respectively. The time of a tidal cycle is scaled to 1.

In Figure 21 the sediment concentration and flow velocity at the crest are shown as a function of time in graphs (a) and (b) respectively. Graphs (c) and (d) show the sediment concentration at respectively t = 0.2 and t = 0.5 as a function of x. The time of a tidal cycle is scaled to 1 here. The times t = 0.2 and t = 0.5 represent a time with a high and a low flow velocity respectively. Only values near the bed are shown, at the bottom 3 cells in the SWC. The behavior of the suspended sediment is further elaborated in Figure 22 and Figure 23. The former shows the sediment concentration as a function of x and $\tilde{z}$ averaged over a tidal cycle after 1, 25, 40 and 80 years, while the latter shows the sediment concentration as a function of x and $\tilde{z}$ at two times during the tidal cycle after 80 years.

In Figure 21a a rather strange drop in the sediment concentration can be seen for $j = 1$ and $j = 2$. Why this drop occurs is not clear. It does not seem to occur at the bottom ($j = 0$). The sediment concentration profile at $t = 0.5$ is also rather irregular (Figure 21d), but this could just be because the shown values are very low and therefore rounding them off has a large influence.

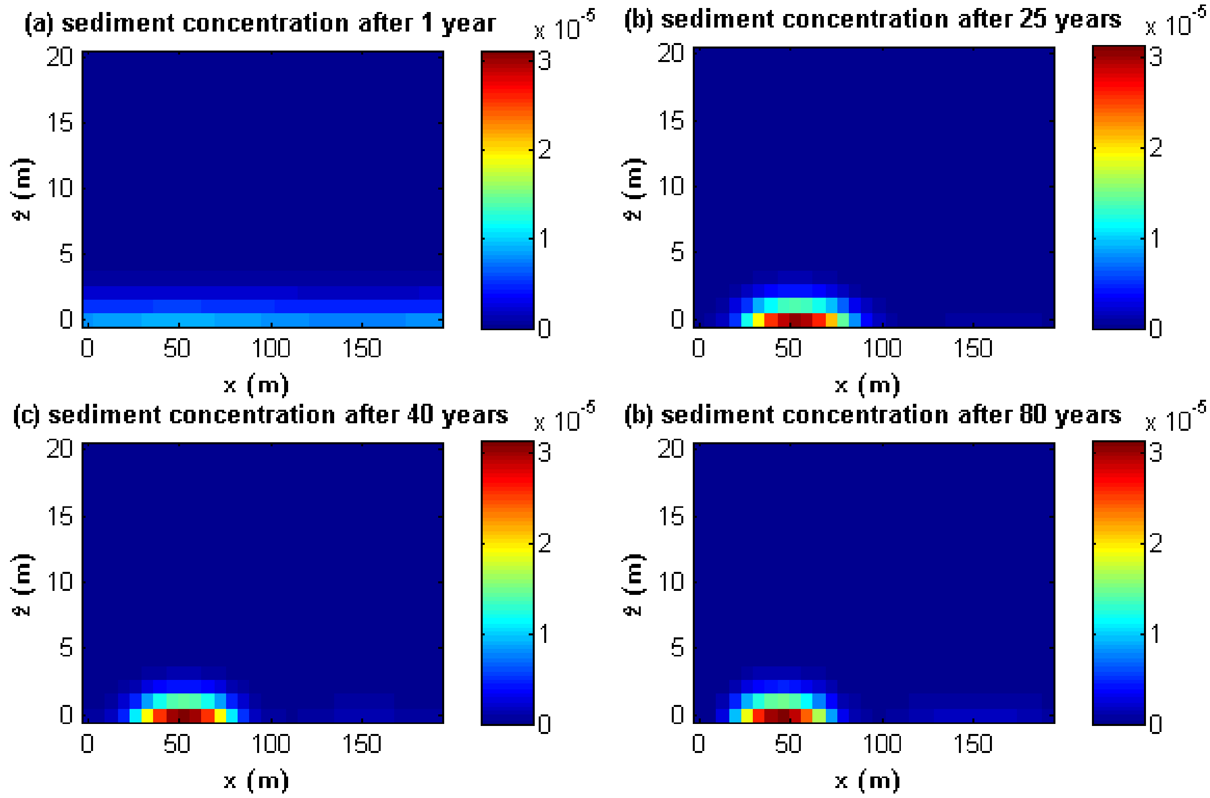

Figure 22: Sediment concentrations as a function of x and $\tilde{z}$ averaged over a tidal cycle. The graphs (a), (b), (c) and (d) show the sediment concentration after 1, 25, 40 and 80 years respectively. The color scales of all graphs are similar.

In Figure 22 it can be seen that initially the suspended sediment is quite evenly distributed over the entire domain, because the bottom is still approximately flat after one year. After 25 years the amount of suspended sediment is larger and mainly floats around the crest of the sand wave. As time progresses the concentrations diminish slightly. A small amount of suspended sediment can also be seen in the trough at 25, 40 and 80 years.

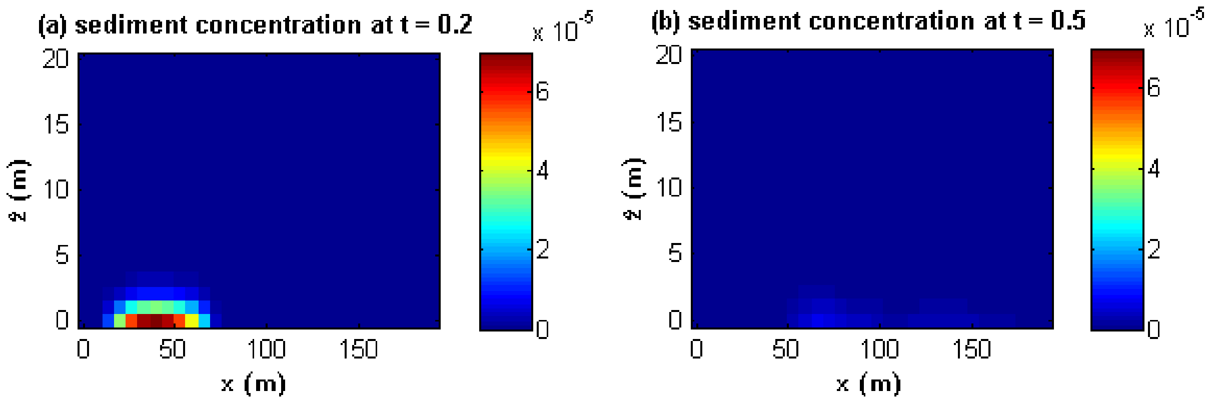

Figure 23: Sediment concentrations as a function of x and $\tilde{z}$ after 80 years of simulated time. The graphs (a) and (b) show the sediment concentration at two different times during the tidal cycle. The color scales in all graphs are similar.

In Figure 23 the same peaks can be identified as in graphs (c) and (d) of Figure 21. Apparently suspended sediment only occurs in the trough at low flow velocities. What also can be clearly seen in Figure 23 is that the sediment concentration is negligible in the top two thirds of the water column.

There seems to be zero to very little sediment concentrations between the crest and the trough, when looking at Figures 24 through 26. At first sight, it may therefore seem that there is no suspended sediment transport towards the crest or out of the trough. However, when looking at a video that shows all of the time steps (instead of only two, like in Figure 23), it can be seen that the suspended sediment moves from the outside of the crest to the inside of the crest. This could explain why steeper sand waves are observed in the results of simulations with suspended sediment. This issue is discussed further in Section 7.1.2.

6.4 Critical condition for bed load transport

Even though the new equation for bed load transport also works when surface waves are included, no surface wave climate has been taken into account in this research. There was no time for this and Sterlini (2009) already investigated the effect of surface waves in her research.

It should be noted that the bed load transport does depend on the grain size when the critical condition is turned on. This is because the grain size is used in the calculation of the critical bed shear stress (see equation (5.2.13)). This should be taken into account when analyzing the results of this section.

In Figures 24 and 25 it can be seen that the FGM is shorter in case of a critical condition. In Figure 25a it can be seen that for Case 2 an FGM lower than 100 m is reached both in case of a residual current and without it. A sand wave length of 100 m has been used in the long simulations, because otherwise the shallow water approximation would not hold. The actual values of the FGM are 90 m in absence of a residual current and 70 m when the residual current is included. Both the crest height and the trough depth reduce significantly when the critical condition is switched on for all cases. It should also be noted that the equilibrium is reached at a much later time when the critical condition is implemented (Figures 24b and 25b). This is quite logical, as the total bed load transport is lower, so therefore it should take longer to reach an equilibrium situation.

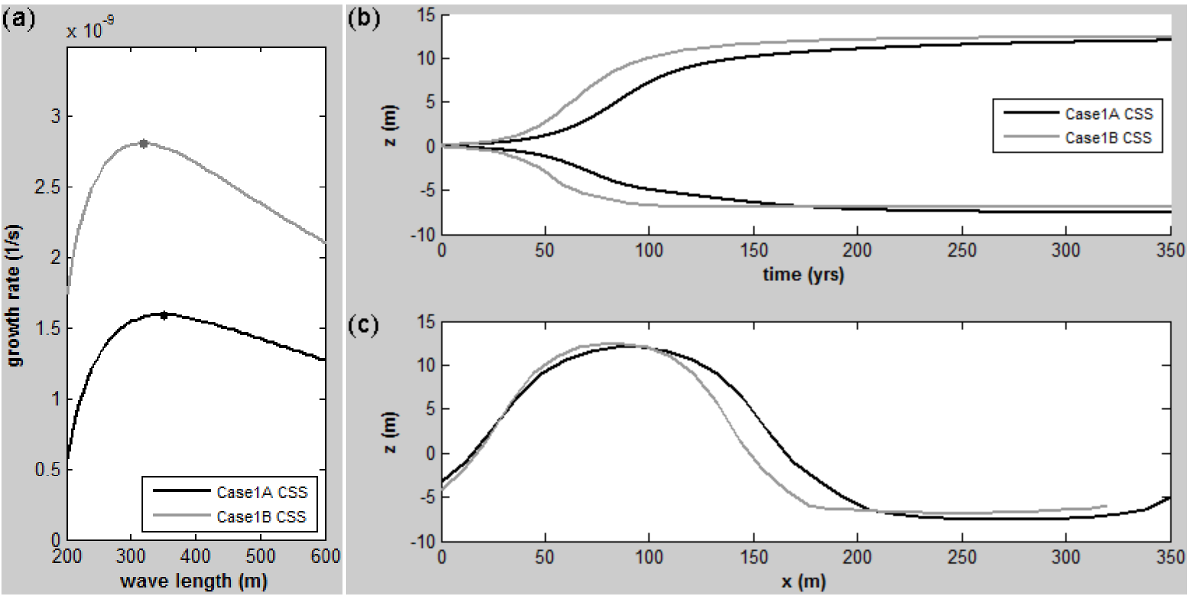

Figure 24: Influence of the critical condition for the initiation of bed load transport on the sand waves without suspended sediment for Case 1A and Case 1B. (a) shows the initial growth rate for different wave lengths, where the dot indicates the FGM, (b) shows the crest and trough growth of the FGM in time and (c) shows the equilibrium sand wave shape for the two simulations. The shown legends apply to all three figures. The codes shown in the legends correspond with the codes shown in Tables 6 and 7.

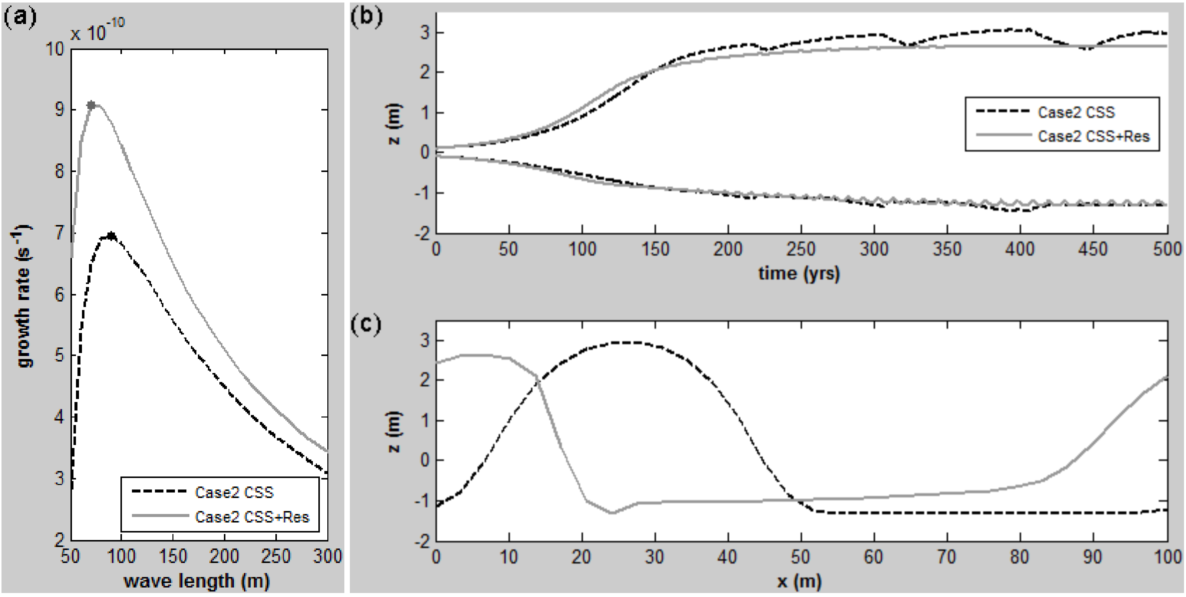

Figure 25: Influence of the critical condition for the initiation of bed load transport on the sand waves without suspended sediment for Case 2. (a) shows the initial growth rate for different wave lengths, where the dot indicates the FGM, (b) shows the crest and trough growth of the FGM in time and (c) shows the equilibrium sand wave shape for the two simulations. The shown legends apply to all three figures. The codes shown in the legends correspond with the codes shown in Tables 6 and 7.

In Figure 25b it can be seen that in case of a critical condition, a dynamic equilibrium is reached for Case 2. When the residual current is not involved it is mostly the crest that is influenced by the dynamic equilibrium, while the trough is mostly influenced by the dynamic equilibrium when the residual current is included.

Since the critical bed shear stress has a direct influence on the bed load transport, the sediment transport is also investigated in more detail here. Just like Figure 20, Figure 26 shows the sediment transport, the divergence of sediment and the resulting seabed at different times during the stage of the sand wave development. Note that Figure 26 also contains results from the case with both suspended sediment and a critical condition. Again this figure is only shown for Case 2.

When comparing Figure 26 with Figure 20, it can be seen that when the critical condition is implemented, the bed load transport becomes a lot smaller, while the suspended load transport remains approximately the same. This means that the suspended sediment transport becomes relatively more important. Furthermore, it can be seen that the run with suspended sediment stabilizes faster, while the run without suspended sediment is far from reaching an equilibrium after 80 years. In Figure 26 it can also be seen that the run with both suspended sediment and a critical condition is slightly unstable, which causes a very narrow crest to develop.

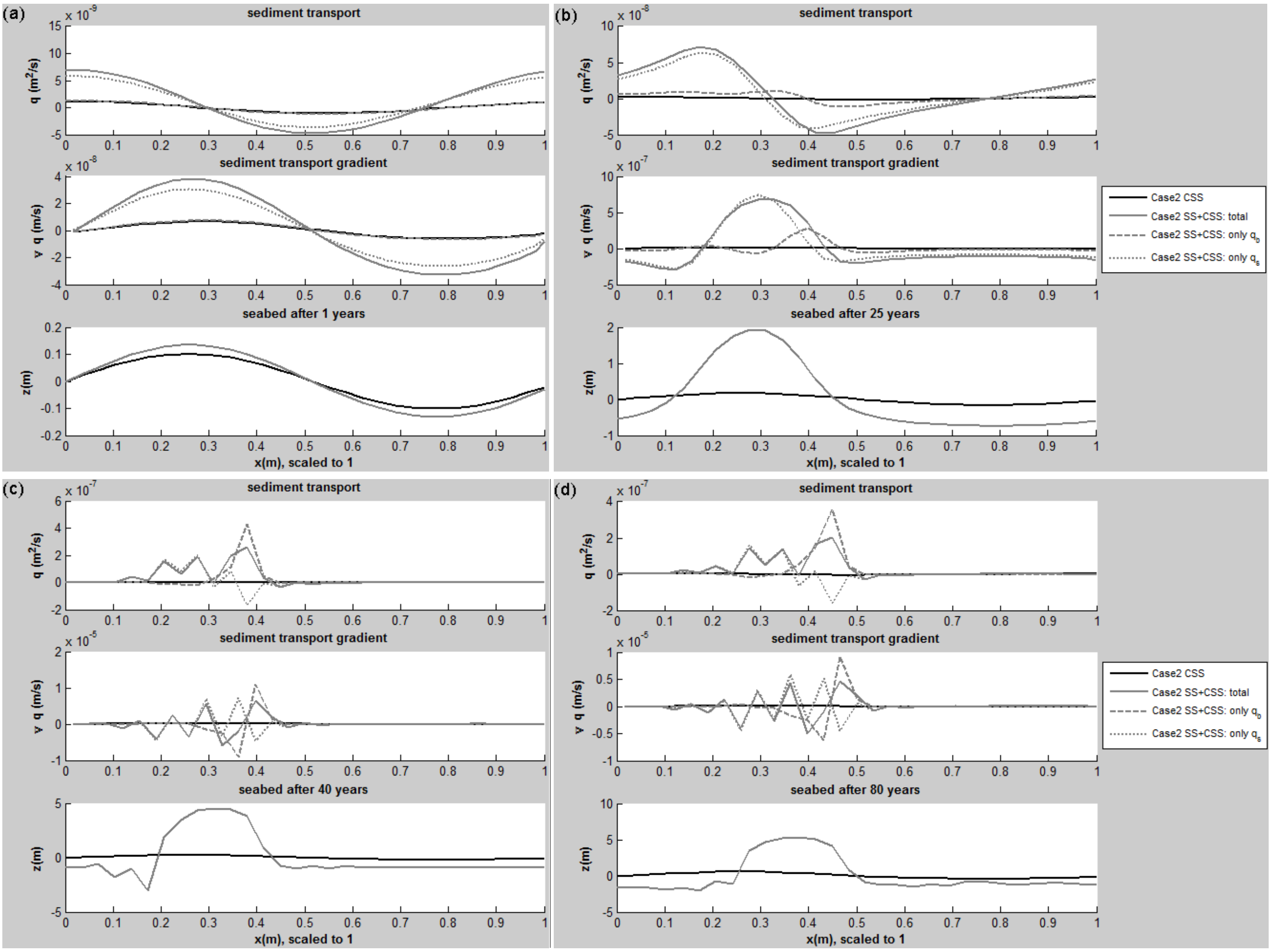

Figure 26: Sediment transport, sediment transport gradient and the sand wave shape after 1 year (a), 25 years (b), 40 years (c) and 80 years (d). The shown values are averaged over a tidal cycle. For the simulation without suspended sediment, only the bed load transport and its gradient (black line) are shown respectively in the upper and middle pannels. For the simulation with suspended sediment, both the bed load transport (dashed gray line) and the suspended load transport (dotted gray line) and their gradients are shown. The shown legends apply to all four figures. The codes shown in the legends correspond with the codes shown in Tables 6 and 7.

Of course the behavior of the bed load transport within a tidal cycle is also interesting. This is shown in Figures 27 through 29 for each case. The shown values are after 80 years of simulation. It can be seen that the bed load transport becomes much lower when the critical condition is implemented. Also, the bed load transport becomes zero when the bed shear stress gets below its critical value. It seems like the amount that the bed load transport gets reduced is very much dependent on the grain size. Case 2 has the largest grain size and the decrease in bed load transport in this case is very extreme. In Case 1A and Case 1B the bed load transport only reduces about 40 to 50% in amplitude.

From Figures 27 through 29 it can be said that the critical bed shear stress is properly implemented in the SWC. The reductions in bed load transport are as expected. In Case 2 the simulations with both suspended sediment and a critical condition were most troublesome. This is probably because the suspended sediment transport is very dominant in this case, as the bed load transport is reduced to a minimal amount.

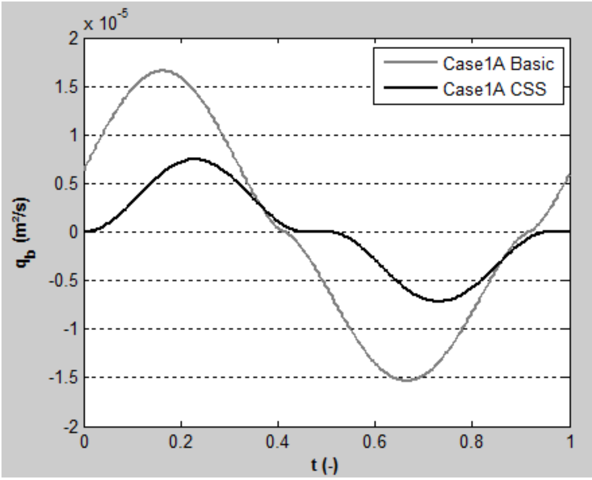

Figure 27: The bed load transport with and without a critical condition over a tidal cycle after 80 years of simulation for Case 1A. The time of a tidal cycle has been scaled to 1.

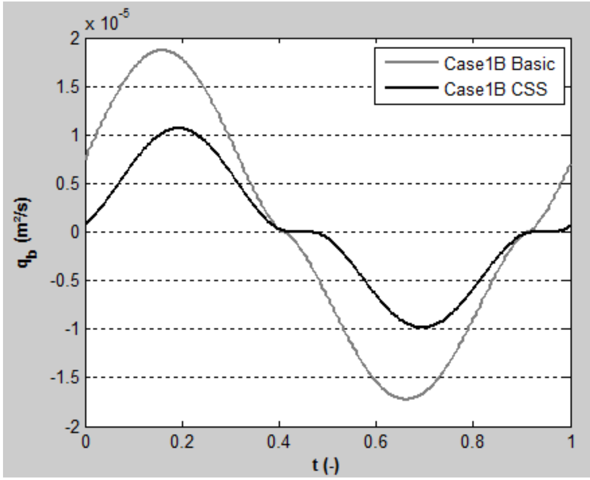

Figure 28: The bed load transport with and without a critical condition over a tidal cycle after 80 years of simulation for Case 1B. The time of a tidal cycle has been scaled to 1.

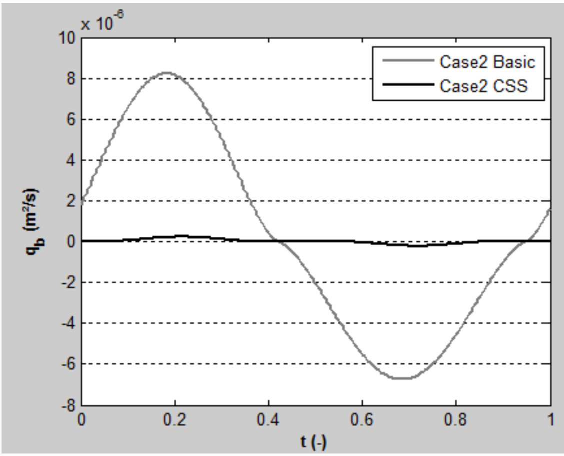

Figure 29: The bed load transport with and without a critical condition over a tidal cycle after 80 years of simulation for Case 2. The time of a tidal cycle has been scaled to 1.

The critical condition caused a much lower prediction of the fastest growing mode. A reduction in sand wave length often goes hand in hand with a reduction in sand wave height. This was seen in the results of Table 7, as large decreases in sand wave amplitudes could be seen and these were present for all measurement cases. This got me wondering if the sand wave amplitude would still decrease if the same FGM would be used as the one in the results of the basic model. Therefore, three more runs have been performed. The results of these runs are shown in Table 8. The runs are labelled "Long", because for all of the three cases the FGM had to be increased to the FGM of the basic model results.

In Table 8 it can be seen that the amplitude still reduces with respect to the basic model results for Case 1A and Case 2. For Case 1B the amplitude is slightly increased (by 0.7 m).

Run	FGM (m)	ampli-tude (m)	crest height (m)	trough depth (m)	crest/trough ratio (-)	maximum slope (°)
Case 1A CSS Long	520	22.5	+15.7	-6.8	0.45	17.6
Case 1B CSS Long	440	22.2	+15.8	-6.4	0.45	20.7
Case 2 CSS Long	210	7.3	+5.4	-1.9	0.30	20.4

Table 8: Results from the runs with a critical condition where the FGM of the basic model results was used.

In Figure 30 it can be seen that these simulations reached quite a steady equilibrium. However, the final sand wave shape does not look very pretty. Especially the transition between the crest and the trough seems strange, as it has a very low slope. The cause of this is not clear.

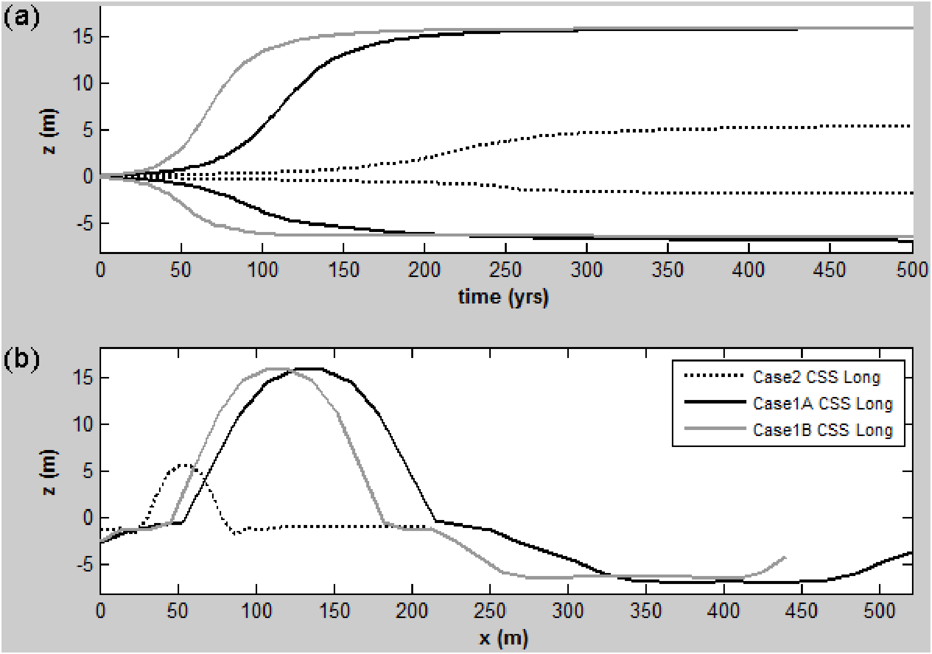

Figure 30: Influence of the critical condition for the initiation of bed load transport on the sand waves without suspended sediment for all three cases, when the FGM of the basic model results is used. (a) shows the crest and trough growth of the FGM in time and (b) shows the equilibrium sand wave shape for the three simulations. The shown legend applies to both figures. The codes shown in the legend correspond with the codes shown in Table 8.

6.5 Combining suspended sediment and the critical condition

Simulations have also been performed in which both suspended sediment and the critical conditions were included. The results of these simulations are presented in this section.

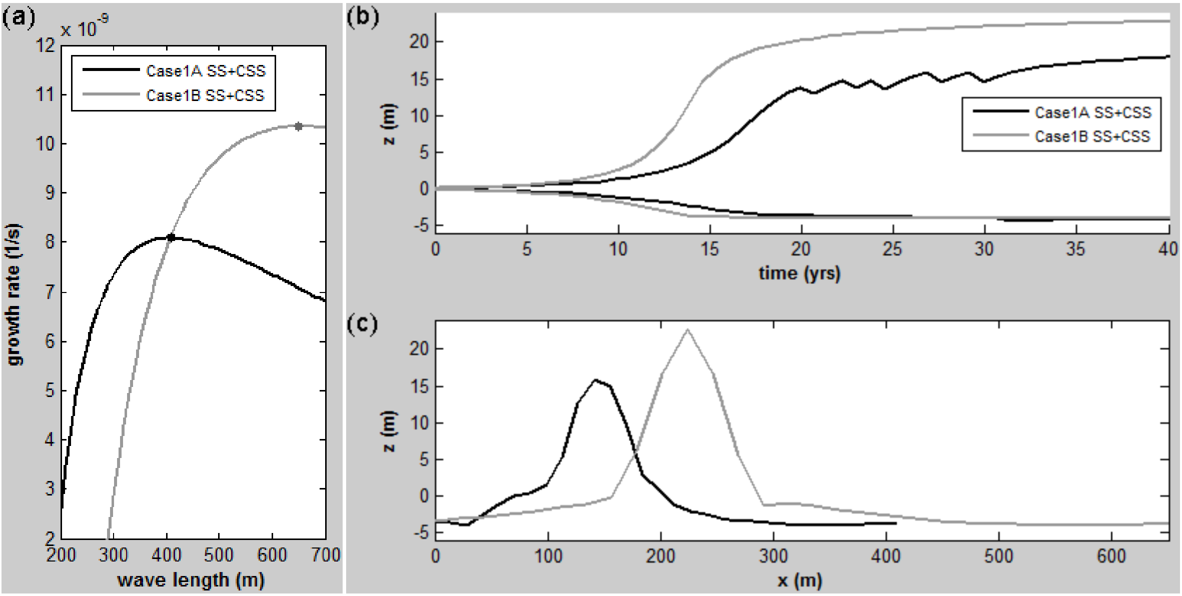

Figure 31: Influence of suspended sediment load on the sand waves. (a) shows the initial growth rate for different wave lengths, where the dot indicates the FGM, (b) shows the crest and trough growth of the FGM in time and (c) shows the equilibrium sand wave shape for the two simulations. The shown legends apply to all three figures. The codes shown in the legends correspond with the codes shown in Tables 6 and 7.

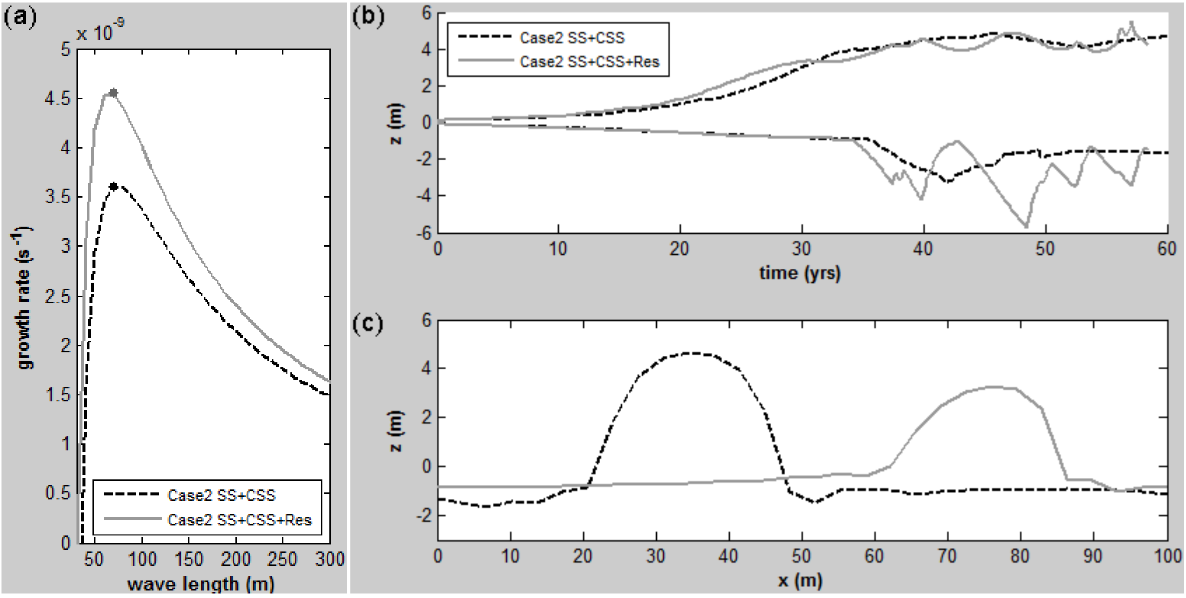

Figure 32: Influence of suspended sediment load on the sand waves. (a) shows the initial growth rate for different wave lengths, where the dot indicates the FGM, (b) shows the crest and trough growth of the FGM in time and (c) shows the equilibrium sand wave shape for the two simulations. The shown legends apply to all three figures. The codes shown in the legends correspond with the codes shown in Tables 6 and 7.

These simulations were the most unstable simulations. This can be clearly seen in Figure 31b and Figure 32b. In Case 1A the equilibrium situation shifts from dynamic to steady and in Case 2 the sand wave crest height and trough depth fluctuate a lot when the residual current is included. The equilibrium sand wave shape shown in Figure 32c is actually the shape at 35 years, just before the instability takes control. The final shapes shown in Figure 31c also look very strange, as they have very narrow crests with steep slopes. Most likely these instabilities were caused by the increased importance of the suspended sediment transport for these simulations, due to the reduction of bed load transport by the critical condition.

Nevertheless, some useful information can be obtained from the results of these simulations. It looks like the effects of including suspended sediment and adding a critical condition on the amplitude are superimposed. In Case 1A and Case 1B including suspended sediment increased the amplitude, while including the critical condition reduced the amplitude. Consequently, when both are included, the amplitude lies somewhere in between. It also looks like including the critical condition in case of suspended sediment amplifies the effect of the suspended sediment on the FGM. Consequently, in Case 1A the FGM is reduced more, while in Case 1B the FGM is increased more. For Case 2 these relations cannot be made so clear, as the FGM reached values below 100 m for these simulations.

7 Discussion

This chapter consists of two parts. In the first part will be discussed whether or not the results obtained in this research are in line with the measurements described in Chapter 2 and if adding suspended sediment and a critical condition for the initiation of bed load transport improve this. In the second part some remaining issues and limitations of the model will be discussed in further detail. Among these is the large slope that is found in all of the simulations.

7.1 Comparison with North Sea cases

In this section will be discussed whether the addition of suspended sediment and a critical condition for the initiation of bed load transport lead to a better prediction of the final sand wave shape. For this, the results in Chapter 6 will be analyzed and compared with the measurements shown in Chapter 2. First the basic model results will be discussed, then the new suspended sediment module and after that the critical condition for the initiation of bed load transport.

7.1.1 Basic model and residual current

The basic model results provided the best estimate for the length of the fastest growing mode. It can be argued that the good prediction of the fastest growing mode has a lot to do with the chosen values for the eddy viscosity (A_v), the slip parameter (S) and the slope factor (λ). However, realistic values have been chosen for these parameters, which were recommended by Besio et al. (2008) and Van Santen (2009).

The predicted final amplitude of the sand wave and the maximum slope are way too large in this case. This means that definitely some processes should be included to reduce these amplitudes and the corresponding maximum slopes. In the next two sections it is discussed whether including suspended sediment or a critical condition for the initiation of bed load transport can provide these reductions.

In Case 2 a residual current was also taken into account. The residual current caused a slight reduction in the prediction of the FGM along with a moderate reduction in the final amplitude. It could therefore be argued that a residual current might also be present at the locations of Case 1A and Case 1B. However, no residual current was reported by Van Santen (2009). For this reason it has not been taken into account for Case 1A and Case 1B.

7.1.2 Improved suspended sediment calculation

A lot has been changed in the suspended sediment calculation. The question here is if these changes have led to results that are better in line with our physical understanding of the system and if they lead to better predictions of the final sand wave shape. Differences between the three different cases will be discussed, as well as the physical significance of the profiles of sediment transport and concentrations that were provided for Case 2. Since these profiles were mostly qualitatively analyzed, also including this for Case 1A and Case 1B seemed redundant as the results were qualitatively comparable in these cases.

The effect of involving suspended sediment

First the addition of suspended sediment will be discussed. When suspended sediment is turned on, the FGM shortens for Case 1A and Case 2, while in Case 1B it causes an increase in the FGM. It is expected that this is due to the large tidal velocity amplitude that is present in Case 1B. The large water depth in Case 1B could also play a role in this, as a larger water depth is expected to allow for longer and higher sand waves.

With suspended sediment, the final amplitude of the sand waves was expected to diminish. However, an increase in the amplitude is observed both in Case 1A and in Case 1B. In Case 1B the increase goes hand in hand with the large increase of the FGM. That a larger amplitude is observed in Case 1A, where the FGM reduces as a result of the addition of suspended sediment, is more concerning. The reduction of the final amplitude in Case 2 is of the same order as the associated reduction of the FGM. Thus, including the suspended sediment as it is described in the current version of the SWC seems to increase the final amplitude rather than reduce it.

In the results of Case 1B with suspended sediment, it could be seen that the trough depth kept on dropping even though the crest height had reached an equilibrium (see Figure 18b). No clear explanation has been found yet for this continued decline. It keeps on declining even after 100 years of simulation, while it was expected to reach an equilibrium earlier than Case 1A.

Sediment transport rates and their gradients

The suspended sediment transport is now much larger than what Sterlini (2009) found. This is mainly due to one minor improvement in the suspended sediment calculation, namely the one discussed in Section A.2 (Appendix A), which reduced the bed shear velocity by about a factor 30. The direction of the suspended sediment transport is often opposite to the direction of bed load transport (Figure 20). This can be explained by the fact that the suspended sediment is brought into suspension at a high velocity and is deposited at a lower velocity when the direction of flow has changed.

The large suspended sediment transport rates found in the results of this research are not expected to occur in reality. The parameters chosen should not yield a dominance of suspended load transport. In offshore tidal regimes the bed load transport is namely assumed to be dominant (Besio and Blondeaux, 2003). Also, when the suspended load transport is dominant, it is expected that the sand waves decay instead of grow (Tonnon et al., 2007). When both the suspended sediment and the critical condition are included, a dominance of the suspended load transport occurs though (Figure Figure 26). It may not be that the suspended load transport is dominant when the critical condition is not taken into account, but the values are of the same order of magnitude as the bed load transport (Figure 20). The suspended sediment transport causes the sand waves to grow faster, while it is expected to cause some decay.

Furthermore, the sediment transport gradients as seen in Figure 20 were asymmetrical, while they were expected to be symmetrical around the top of the crest. The suspended load transport gradient and bed load transport gradient are both quite low around the downstream slope of the crest and high around the upstream side of the crest. What causes this asymmetry is not clear. The corresponding sand wave shapes don’t show any asymmetry, so this is very strange.

The suspended sediment concentration distribution

Figure 23 shows that most of the suspended sediment is entrained over the crest of the sand wave at a time when the flow velocity is high. At a low flow velocity, mostly low concentrations are present in the trough of the sand wave. When looking at a video that shows the suspended sediment concentrations for the whole course of a tidal cycle, it can be seen that the sediment clouds over the crest and the trough grow alternately. When the concentration peak over the crest grows, the peak in the trough shrinks, and vice versa. Between these two peaks, the sediment concentrations only reach very low values of $1 \cdot 10^{-5}$ m^3/m^3. At positive flow velocities there is a net suspended load transport from the slope on the left side of the crest to the top of the crest. When the flow velocity is negative, this net transport comes from the crest slope on the right side. Most of the time, the high flow velocities at the top of the water column only reach down to the crest of the sand wave. However, when these flow velocities are lower, an eddy seems to develop in the trough of the sand wave. This was only clear from a video showing the development of the flow velocity profiles, which can't be shown in a report unfortunately.

7.1.3 Critical condition for the initiation of bed load transport

In all three cases, the critical condition also causes the final amplitude to diminish. The equilibrium situation probably changes due to the decreased amount of bed load transport. It thus looks like the critical condition has the desired effect, a reduction in the final amplitude. However, this reduction goes hand in hand with a large decrease of the FGM. To check if the final amplitude would still be diminished in case of an unchanged FGM, simulations have been performed with the critical condition turned on and the FGM as found from the results of the basic model. These results still show a reduced amplitude in Case 1A and Case 2, while the amplitude for Case 1B increases only slightly. This indicates that the critical condition for the initiation of bed load transport can successfully diminish the final amplitude of the sand waves. This leads to outcomes that are closer to the measurements discussed in Chapter 2. However, only for Case 2 amplitudes are found that are within the range of the measurements. The latter occurs when both the critical condition and the residual current are taken into account.

When the critical condition for the initiation of bed load transport is implemented, less bed load transport will occur (Figure 26). Due to this, the relative importance of suspended sediment transport increases when suspended sediment is also taken into account. This amplifies the effect of suspended sediment transport on the FGM. In Case 1A this results in a larger reduction of the sand wave length and in Case 1B it causes a larger increase of the sand wave length (Table 7). In Case 2 the effect on the FGM is not significant.

7.2 Remaining issues and limitations of the model

As could be seen in the results, there were still some situations the SWC could not handle and some oddities occurred, these will be discussed here. Also some limitations of the model will be discussed, among which is the fact that the sand wave length cannot change during the development of the sand wave with the SWC. Another limitation is the fact that tidal conditions remain the same during the entire course of the sand wave development for all of the simulations in this research.

As can be seen in the results of Table 7, the maximum slopes that are found in the simulations of the three North Sea cases are very large. Maybe a process is lacking which should keep this slope within reasonable ranges. It could be that the slopes are increased to such high amounts due to the fact that the sand waves are often exposed to unchanging conditions in the simulations, which will be discussed later in this section. The maximum slopes in the sand wave fields shown by Besio et al. (2004) and Van Santen (2011) only reach about 5°, which indicates that the slopes here are indeed way too large.

It could be that the large slopes occur because a slope correction term is missing for suspended sediment transport. As the bed slope increases, the bed load transport will decrease, due to the bed slope correction term that is taken into account in its calculation. The suspended sediment transport aimed towards the crest of the sand wave can therefore cause an increase in slope and a resulting decrease in bed load transport directed towards the crest. Finally, the bed load transport will be away from the crest, while the suspended load transport is still directed towards the crest. This process is schematized in Figure X. It could be that the suspended sediment transport feels the bottom, since most of the suspended sediment remains close to the bottom. A slope correction term for suspended load transport would probably also reduce the final amplitude of the sand waves, as it would cause a reduction in the net sediment transport towards the crest of the sand wave.

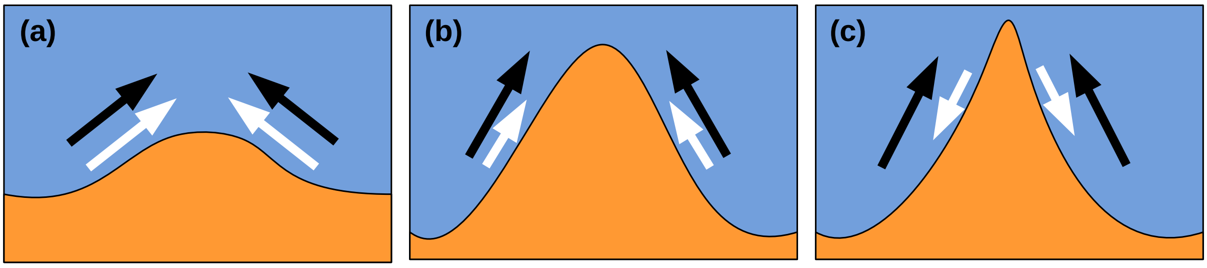

Figure 33: The suspended load transport and bed load transport in this schematization are indicated with black arrows and white arrows respectively. The length of the arrow indicates the amount of transport. In (a) the initial stage is shown in which the sand wave is still quite flat and the bed slope has little or no influence on the bed load transport. In (b) the bed slope has increased as a result of sand wave growth, resulting in a reduction of bed load transport directed towards the crest. In (c) the bed slope has become so large that the direction of bed load transport is away from the crest.

It could also be that flow separation plays a role in the development of sand waves in shelf seas. Paarlberg (2007) studied the effect of flow separation on subaqueous dunes in sandy river beds. They state that flow separation already occurs in a non-permanent form over dunes with maximum lower leeside slopes of 14°. In another article (Paarlberg et al., 2009), they use a critical leeside slope of 10°, which means that flow separation occurs in their model when the leeside slope is over 10°. This means that it is unlikely that flow separation should play a role here, as the measured maximum slopes are in the order of 5°. The flow in a river is unidirectional, while the flow in a coastal shelf sea is oscillating. This means that flow separation will possibly only occur when a large residual current is present, because it takes a while to develop and this will not happen when the flow is just oscillating.

Another small issue is that the shapes of the sand waves found in this research do not correspond with the shapes shown in the measurements. The measurements show sand waves that are more sharp-crested (Besio et al., 2004; van Santen et al., 2011). Németh et al. (2007) mentioned that sharper crested waves develop when $\lambda_1 > \lambda_2$. In this research only λ_2 has been used and it was named λ for simplicity. The value of λ_1 was set to zero in this research. The total slope factor (λ_{total}) consists of two components as follows:

$$\lambda_{total} = \frac{\lambda_1}{\tau_{bed}} + \lambda_2 \qquad (7.2.1)$$

To check the notion of Németh et al. (2007), the value of λ_2 has been set to zero and the value of λ_1 has been set to $1 \cdot 10^{-3}$ in the simulation of the basic model for Case 2. The results of this are shown in Figure 34, along with the earlier found results with the basic model and a slope factor λ_2 of 2.5.

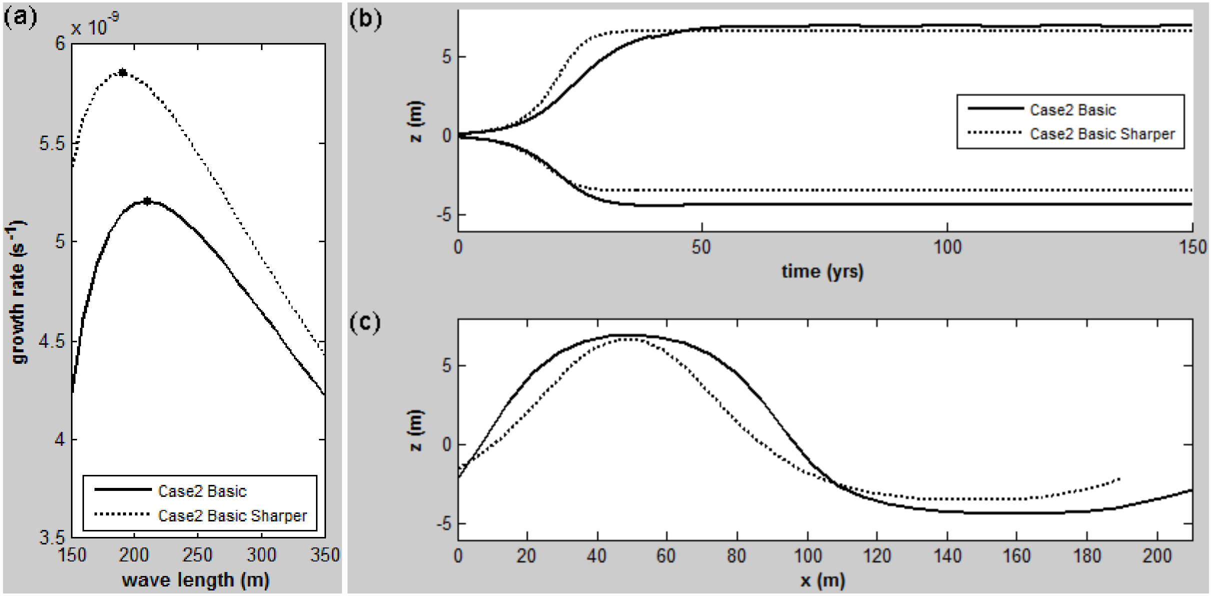

Figure 34: Basic model results for Case 2, including the results for the case with $\lambda_1 = 1 \cdot 10^{-3}$ and $\lambda_2 = 0$ (this case is labelled "Sharper"). (a) shows the initial growth rate for different wave lengths, where the dot indicates the FGM, (b) shows the crest and trough growth of the FGM in time and (c) shows the equilibrium sand wave shape for the two simulations. The shown legends apply to all three figures. The codes shown in the legends correspond with the codes shown in Tables 6 and 7.

Figure 17c shows that a sharper sand wave shape definitely develops when $\lambda_1 > \lambda_2$, while the sand wave length, growth rate and final amplitude don't change much.

Actually two cases from Besio et al. (2006) were considered in this research. However, it was not possible to find a value for the FGM for the model with suspended sediment for this case. This was most likely due to the high water depth of 40 m. Why this could not be determined from the graph can be seen in Figure 35. The graph looks like a seismograph and the values of the growth rate are about 3 to 4 orders of magnitude larger than normal, which makes them unreliable. Probably the water depth of 40 m was too large in combination with the other chosen conditions. The shallow water approximation might not have been valid in this situation. Note that Sterlini (2009) ran into the same issue, which is why she used a water depth of 39 m for one of her suspended sediment runs. Probably the issue was enhanced by the increased amount of suspended sediment transport in the improved suspended sediment calculation module.

Another issue occurs in Case 1B for the case with suspended sediment. In this simulation, the trough depth kept on dropping even though the crest height had reached an equilibrium (see Figure 18b). No reason for this strange behavior is found yet.

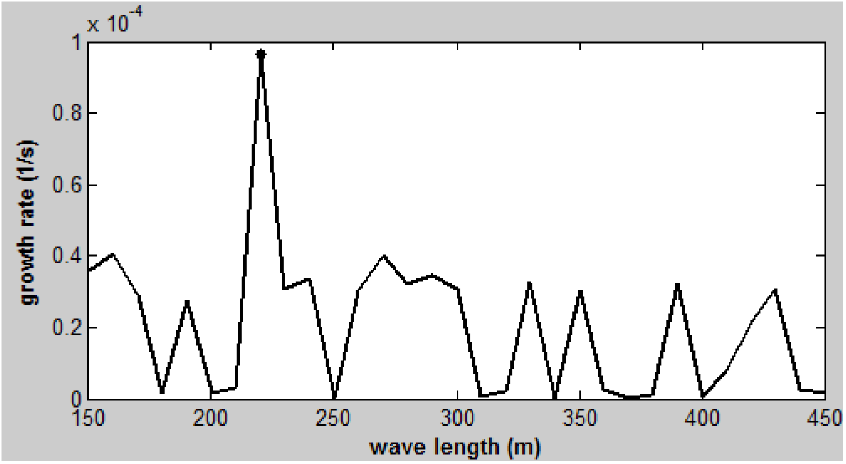

Figure 35: The initial growth rate at different wave lengths for the second case of Besio et al. (2006) with suspended sediment and a water depth of 40 m. As can be seen, no FGM can be safely determined from this graph. The growth rates are also much larger than usual (3 to 4 orders of magnitude larger).

In the current research, the parameters used are not changed during the entire course of development of the sand wave. This could mean that the sand wave is subject to such constant conditions that it can just keep growing. This could explain why sand waves with large amplitudes and steep slopes are resulting from the simulations. In reality, storms occur and flow conditions change, which could disrupt the development process by swiping away a part of the sand wave or changing the equilibrium situation. The model also has a surface wave module which does along for changing surface wave conditions over the course of the sand wave development. As the effects of this module have been explored by Sterlini (2009) already in quite some depth, this has not been repeated here. Also, this module could not be combined with the suspended sediment transport module yet.

The results indicate that the sand wave length and amplitude are often codependent. This means that when imposing a certain sand wave length (often the FGM), the amplitude of the sand wave will change long with this. A larger sand wave length often results in a higher amplitude. For the case with a critical condition for the initiation of bed load transport, this was investigated by imposing the same sand wave length as the one found in the basic model results. Results of this showed that the reduction in amplitude was not only due to the reduction in sand wave length, but that the amplitude was also mostly reduced when the sand wave length was kept constant.

Another limitation of the model used in this research is that the sand wave length cannot change during the development of the sand wave. Once a sand wave length is imposed, it stays that way. In reality however, sand waves can change both in length and in height. It could be that while the model results show that a sand wave changes in amplitude, it would actually be more likely to change in length in reality. Simulations on a large domain could also be used, but a disadvantage of this is that the sand waves then eventually evolve to one large bedform with the length of the domain (Sterlini, 2009). This is the whole reason why a domain of the length of the fastest growing mode is used here. It would be nice however, if there was a way to change the domain length during the course of the simulation to represent a change in sand wave length. This way, the final shape and growth rate of the sand wave could still be determined, while not making the assumption that the fastest growing mode remains the same throughout the entire process.

8 Conclusions

In this chapter the conclusions of this study are presented. First the research questions are answered, which helped to achieve the objective of this study. After this some recommendations for future research are given. These recommendations are based on the discussion of Chapter 7 and the conclusions of Section 8.1.

8.1 Answers to research questions

The objective of this research was to improve the Sand Wave Code (SWC) in order to make it predict the growth rate, final shape and migration speed of sand waves better, both by improving the suspended sediment transport module and by adding a critical condition for the initiation of sediment transport. To evaluate whether this objective has been reached, the two main research questions and their sub-questions will be answered.

8.1.1 How can the suspended sediment transport module be improved?

This research question has been divided into four sub-questions which will be answered first. After this, the main question is answered based on the answers of the sub-questions.

Which shortcomings does the suspended sediment module of the SWC have?

The suspended sediment calculation did not contain any kind of scaling. This meant in fact, that the bed level elevation was not properly taken into account. It was also found that a Neumann boundary condition was used at the surface for the suspended sediment concentration calculation, instead of a no flux boundary condition. This caused some strange results, which indicated it was not justified in a physical sense. Furthermore, the implementation of the suspended sediment module in the SWC seemed rather rushed overall, causing some minor shortcomings which are discussed in Appendix A. Some of these minor shortcomings influenced the results significantly.

How can the suspended sediment module be improved or expanded to overcome these shortcomings?

In order to incorporate both the bed level elevation and the reference height at which the reference concentration is applied, a new scaling has been composed. The new scaling is described in equation (4.2.9). For all terms in the suspended sediment calculation the discretization has been redone and these discretizations have been successfully implemented in the SWC. This meant in fact that the whole suspended sediment calculation in the SWC was revised. The Neumann boundary condition has been replaced with an actual no flux boundary condition, which led to a better representation of the physical understanding in the results. All of the minor shortcomings were also fixed, the corresponding improvements to the SWC can also be found in Appendix A.

To what extent does including the new suspended sediment module have a significant effect on the prediction of the growth rate, migration speed or final shape of the sand waves?

The effect of suspended sediment on the prediction of the growth rate is rather large. An equilibrium is often reached about 40% sooner than in the basic case. Suspended sediment can either increase or decrease the prediction of the FGM, depending on the local conditions. Also, the final amplitude is often increased in case of suspended sediment, which was against our expectations. The growth rate has not been considered in this research. This was because very long simulations are required for this and there was no time to run these. Also, the migration rate is not a direct output of the SWC, while other models may be able to give a prediction of the growth rate alongside the prediction of the FGM.

What do the results of the SWC with the improved suspended sediment transport module show when compared to measurements at three sites in the North Sea?

Including suspended sediment often results in either an overprediction or a slight underprediction of the FGM. The basic model seems to be able to give more adequate estimates of the FGM. Also, the final amplitude often increases, while a reduction is desired in order to more adequately predict it.

Summarizing, including suspended sediment does not in general give a better prediction of the final shape of the sand wave, even though a lot of minor improvements have been made to the suspended sediment transport module, alongside with applying a scaling to the calculations and by implementing a no flux boundary condition at the surface. Also, the three sediment diffusivity models have been re-evaluated, leading to another choice, namely the parabolic-constant profile instead of the linear profile. The new code is expected to give a better representation of the physical model. However, I do not believe it is physically justified yet. The suspended load transport rates that were found were rather high and should be expected to cause the sand waves to decay at least partially (Tonnon et al., 2007). However, the increase in suspended load transport and possibly the lack of a process that reduces the maximum slope cause higher and steeper sand waves to be simulated when suspended sediment is involved.

8.1.2 What is the effect of adding a critical condition for the initiation of bed load transport on the sand wave prediction?

This second main question has been divided into four sub-questions which will first be answered individually. After this, the main question is answered based on the answers of the sub-questions.

Which equations should be used to describe the critical condition?

The critical condition could be implemented in the equation describing the bed load transport. In Section 5.2 a detailed description of how it is derived can be read. This newly derived bed load transport equation also still incorporates the bed shear stress due to the presence of surface waves. It was checked that the model does work when surface waves are included, but no simulations with surface waves have been carried out for the results of this research.

How can these equations be implemented in the model?

Only the original equation for bed load transport had to be replaced in the SWC. This equation was divided into two components in the code however, but this did not cause any problems.

How significant is the effect of adding this critical condition on the prediction of the growth rate, migration speed or final shape of the sand waves?

The critical condition mainly causes shorter and lower sand waves to develop. Since the overall transport decreases, the growth rate also decreases. Furthermore, since the grain size determines the critical value of the bed shear stress, the grain size now influences the shape and growth rate of the sand wave even when only bed load transport is taken into account.

What do the results show when compared to measurements at three sites in the North Sea?

Due to the critical condition, the sand waves become much shorter and have lower crests. This causes an underprediction of the FGM, while the final sand wave amplitude reaches lower values that are more realistic. Even when the sand wave length is kept constant, the critical condition causes a reduction in the final sand wave amplitude in most of the cases. This indicates that the critical condition helps to predict the measured sand waves better, as the predicted amplitudes in the basic case are much too large. The migration speed has again not been checked, as very long simulations are required for this and this could not be done within the available time.

Concluding, adding a critical condition for the initiation of bed load transport leads to predictions of shorter sand waves with a smaller amplitude. The growth rate of the sand waves is also reduced significantly, except in the case with suspended transport. The resulting behavior of the bed load transport over a tidal cycle was as expected, with the bed load transport declining to zero for low flow velocities as shown in Figures 27 through 29. It can thus be said that the critical condition is properly implemented and that it helps predict the final amplitude of the sand waves better.

8.1.3 Evaluation of the research objective

I believe it can be said that the Sand Wave Code has been improved significantly. Especially the suspended sediment calculation has been improved. Many minor shortcomings have been improved and a new scaling has been successfully applied to the calculation. The critical condition has also been implemented successfully, even for the case with surface waves. All these changes have at least lead to significantly different predictions of the growth rate and final shape of the sand waves. When comparing the results to measurements at three locations in the North Sea, it can be seen that a better prediction of the final shape is obtained with the critical condition, but not with suspended sediment. However, it might still be that the improvements in the suspended sediment calculation have made the results more physically justified, but that more processes still have to be included to better balance out the role that suspended sediment plays.

8.2 Recommendations

The large slopes that were found in the results of this research give reason to believe that a process is lacking that makes sure the slope is kept within reasonable bounds. Perhaps a separation layer could also be present in shelf seas and not only in rivers. However, it would only be possible to occur when a very high residual current is present, because it takes a while to develop and this will not happen when the flow is just oscillating. In reality the high slopes are not found, so it is unlikely that this plays a role though. Therefore I would recommend to check for any missing processes in the Sand Wave code that would have prevented the sand wave from developing such steep slopes. The separation layer is only one example of such a process.

Another, probably more viable, example of such a process is a bed slope correction term in the calculation of the suspended load transport. Such a correction term is currently only present in the calculation of the bed load transport. This could have caused the sand waves to reach a steepness that is higher than what the bed load transport alone would allow. It might be possible that the suspended load feels the bottom, as most of the concentrations are very close to the bottom. It is therefore recommended to research this. For this, it should be investigated how the correction term can be implemented in this case and what this means for the development of the sand waves.

At the start of this research the idea was to combine two modules of the Sand Wave Code (SWC), namely the suspended sediment module and the surface wave module. However, improving the suspended sediment calculation had priority, since it contained many shortcomings and no scaling was applied yet. This took a lot of time and therefore there was no time to combine the two modules. However, I believe that it is a good idea to perform this combination of modules on the new version of the SWC in an upcoming research. Results of Sterlini (2009) showed that the surface wave module also has the capability to reduce the predicted final amplitude of the sand waves. When combining the modules regarding suspended sediment and surface waves, the suspended sediment transport could take on a better role in the whole physical process that the model describes.

It is also recommended to take a closer look into the problems regarding the water depth of 40 m in case of suspended sediment. No FGM could be found for a second case from Besio et al. (2006) with a water depth of 40 m. This could be due to some kind of resonance, an unknown problem in the SWC or due to this depth somehow being too large. It is possible that the shallow water approximation does not hold for certain situations with a water depth of 40 m. To get more clarity about this, a sensitivity analysis could be carried out for the water depth. Also the continued drop of the trough in Case 1B with suspended sediment could be further investigated, as the cause for this was also entirely unclear.

9 References

Allen, J. R. L., 1980, Sand-Wave Immobility and the Internal Master Bedding of Sand-Wave Deposits: Geological Magazine, v. 117, no. 5, p. 437-446.

Bartholdy, J., Ernstsen, V. B., Flemming, B. W., Winter, C., and Bartholoma, A., 2010, A simple model of bedform migration: Earth Surface Processes and Landforms, v. 35, no. 10, p. 1211-1220.

Beheshti, A. A., and Ataie-Ashtiani, B., 2008, Analysis of threshold and incipient conditions for sediment movement: Coastal Engineering, v. 55, no. 5, p. 423-430.

Besio, G., and Blondeaux, P., 2003, On the effect of the suspended load on the formation of sand waves, Proceedings 3rd IAHR Symposium on River, Coastal and Estuarine Morphodynamics, Volume I: Spain, RCEM 2003, p. 365-375.

Besio, G., Blondeaux, P., Brocchini, M., Hulscher, S. J. M. H., Idier, D., Knaapen, M. A. F., Nemeth, A. A., Roos, P. C., and Vittori, G., 2008, The morphodynamics of tidal sand waves: A model overview: Coastal Engineering, v. 55, no. 7-8, p. 657-670.

Besio, G., Blondeaux, P., Brocchini, M., and Vittori, G., 2004, On the modeling of sand wave migration: J. Geophys. Res., v. 109, no. C4, p. C04018.

Besio, G., Blondeaux, P., and Frisina, P., 2003, A note on tidally generated sand waves: Journal of Fluid Mechanics, v. 485, p. 171-190.

Besio, G., Blondeaux, P., and Vittori, G., 2006, On the formation of sand waves and sand banks: Journal of Fluid Mechanics, v. 557, p. 1-27.

Blondeaux, P., and Vittori, G., 2010, Formation of tidal sand waves: Effects of the spring-neap cycle: Journal of Geophysical Research-Oceans, v. 115, p. -.

Borsje, B. W., Hulscher, S. J. M. H., Herman, P. M. J., and de Vries, M. B., 2009, On the parameterization of biological influences on offshore sand wave dynamics: Ocean Dynamics, v. 59, no. 5, p. 659-670.

Coleman, N. L., 1970, Flume Studies of the Sediment Transfer Coefficient: Water Resour. Res., v. 6, no. 3, p. 801-809.

Davies, A. G., 1986, A model of oscillatory rough turbulent boundary layer flow: Estuarine, Coastal and Shelf Science, v. 23, no. 3, p. 353-374.

Dodd, N., Blondeaux, P., Calvete, D., De Swart, H. E., Falques, A., Hulscher, S. J. M. H., Rozynski, G., and Vittori, G., 2003, Understanding coastal morphodynamics using stability methods: Journal of Coastal Research, v. 19, no. 4, p. 849-866.

Franklin, E. M., and Charru, F., 2009, Morphology and displacement of dunes in a closed-conduit flow: Powder Technology, v. 190, no. 1-2, p. 247-251.

Habibzadeh, A., and Omid, M. H., 2009, Bedload resistance in supercritical flow: International Journal of Sediment Research, v. 24, no. 4, p. 400-409.

Hulscher, S. J. M. H., 1996, Tidal-induced large-scale regular bed form patterns in a three-dimensional shallow water model: Journal of Geophysical Research-Oceans, v. 101, no. C9, p. 20727-20744.

Lin, B., and Namin, M. M., 2005, Modelling suspended sediment transport using an integrated numerical and ANNs model: Journal of Hydraulic Research, v. 43, no. 3, p. 302-310.

Nemeth, A. A., Hulscher, S. J. M. H., and Damme van, R. M. J., 2007, Modelling offshore sand wave evolution: Continental Shelf Research, v. 27, no. 5, p. 713-728.

Németh, A. A., Hulscher, S. J. M. H., and de Vriend, H. J., 2003, Offshore sand wave dynamics, engineering problems and future solutions: Pipeline & Gas Journal, v. 230, no. 4, p. 67-69.

Paarlberg, A. J., Dohmen-Janssen, C. M., Hulscher, S. J. M. H., and Termes, P., 2007, A parameterization of flow separation over subaqueous dunes: Water Resources Research, v. 43, no. 12, p. -.

Paarlberg, A. J., Dohmen-Janssen, C. M., Hulscher, S. J. M. H., and Termes, P., 2009, Modeling river dune evolution using a parameterization of flow separation: J. Geophys. Res., v. 114, no. F1, p. F01014.

Sterlini, F. M., 2009, Modelling sand wave variation, 126 p.

Thomas, J. W., 1995, Numerical partial differential equations, Springer, v. v. 2.

Tonnon, P. K., van Rijn, L. C., and Walstra, D. J. R., 2007, The morphodynamic modelling of tidal sand waves on the shoreface: Coastal Engineering, v. 54, no. 4, p. 279-296.

van der Veen, H. H., Hulscher, S. J. M. H., and Knaapen, M. A. F., 2006, Grain size dependency in the occurrence of sand waves: Ocean Dynamics, v. 56, no. 3-4, p. 228-234.

van Rijn, L., 1984, Sediment Transport, Part II: Suspended Load Transport: Journal of Hydraulic Engineering, v. 110, no. 11, p. 1613-1641.

van Rijn, L. C., 1993, Principles of sediment transport in rivers, estuaries and coastal seas, Amsterdam, Aqua Publications

van Santen, R. B., 2009, Tidal sandwaves in the North Sea, data analysis and modellingMaster's thesis V09-07]: University of Utrecht.

van Santen, R. B., de Swart, H. E., and van Dijk, T., 2011, Sensitivity of tidal sand wavelength to environmental parameters: A combined data analysis and modelling approach: Continental Shelf Research, v. 31, no. 9, p. 966-978.

Verbanck, M. A., 2000, Computing near-bed solids transport in sewers and similar sediment-carrying open-channel flows: Urban Water, v. 2, no. 4, p. 277-284.

10 Appendices

Two appendices are attached to this report. In Appendix A a few minor improvements to the Sand Wave Code are discussed. Appendix B describes the discretization of the no flux boundary condition with a central difference approach by using a ghost point.

Appendix A: Minor improvements to the Sand Wave Code

A.1 Introduction

During the start of my research I encountered several shortcomings in the version of the Sand Wave Code (SWC) that was handed to me. I have adapted this version to a new version of my own, and will therefore refer to the version that was handed to me as the previous version. The current version is the version containing all the changes I have made to the SWC.

A.2 Minor improvements to the suspended sediment calculation module

Most of the shortcomings found were in the calculation of the suspended sediment concentration and transport. The reason for this is that this is the part of the SWC that I worked on the most, so this does not mean the other parts of the SWC are flawless. However, it has been made clear to me that the reason for the large amount of possible improvements to the suspended sediment calculation was probably a rushed implementation.

A.2.1 Correctly calculating the bed shear velocity

The bed shear velocity u_* should be determined using the following equation:

$$u_* = \frac{|\tau_b|}{\tau_b} \cdot \sqrt{\frac{|\tau_b|}{\rho_w}} \tag{10.1.1}$$

In the previous version of the SWC however, the water density ρ_w was not contained within the square root. The dimension of u_* should be m/s, which is not obtained when the water density ρ_w is not contained within the square root, since the dimension of τ_b is $N/m^2 = kg/(m \cdot s^2)$ and the dimension of ρ_w is kg/m^3, yielding the following dimension for u_*:

$$\frac{\sqrt{kg/(m \cdot s^2)}}{kg/m^3} = kg^{-\frac{1}{2}} \cdot m^{-\frac{7}{2}} \cdot s^{-1}$$

The above formula for the bed shear velocity (equation) does yield a dimension for u_* in m/s and it is a formula often found in the literature (e.g. (Beheshti and Ataie-Ashtiani, 2008; Davies, 1986; Franklin and Charru, 2009; Habibzadeh and Omid, 2009), which probably means the programmer made a mistake.

This mistake however had a significant effect on the results. This effect is illustrated in , which shows the initial growth rate for different wave lengths for several cases. The “old” case is the case in which u_* was wrongfully calculated and in the “new” case this error is fixed. A third plot was made to show what would happen if the whole suspended sediment module in the SWC was turned off.

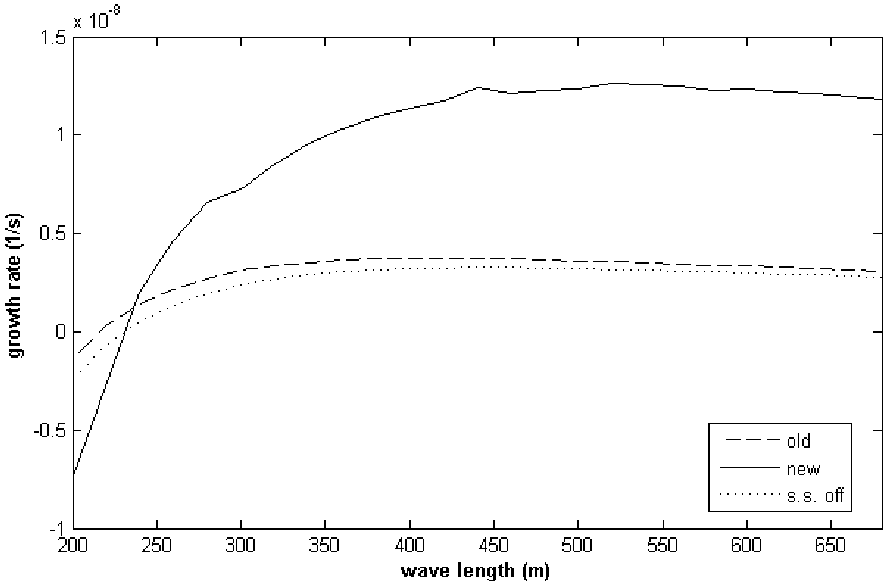

Figure 36: Initial growth rate for different wave lengths in case of a wrongfully calculated u_* ("old", with ρ_w outside the square root), a correctly calculated u_* ("new", equation) and in case the suspended sediment module in the SWC is switched off ("s.s. off"). Parameter Set 1 was used for obtaining these results.

As can be seen in above, when the mistake in the calculation of u_* is fixed, the wave length corresponding to the fastest growing mode increases from about 420 m to about 520 m. Of course these values depend on the chosen input parameters like water depth, tidal forcing, etc., but generally it can be said that the wave length corresponding to the fastest growing mode changes a lot. Also, the growth rate of the fastest growing mode becomes much larger, about four times for the case shown in Figure 36. Therefore, it can be said that fixing this mistake had a significant effect on the results.

Furthermore, it can be seen that the new curve is choppy, while a nice smooth graph with only one maximum is expected. This indicated that beside the error in calculating the bed shear velocity, more improvements to the suspended sediment module of the SWC were possible. Several more minor improvements to the SWC have carried out and they are described in the remainder of this chapter.

A.2.2 Improvement to the determination of the vertical coordinate

For the suspended sediment calculation, the points are distributed quadratically over the water depth. This means more points are close to the bottom and fewer points are close to the water surface.

In the previous version of the SWC, the location z of a certain point j was determined using the following formula:

$$z(j) = 0.99H \cdot \frac{j^2}{Npz^2} + 0.01H \tag{10.1.2}$$

This means that when j equals zero, the value of z is equal to $0.01H$, which is the value of the reference height for the sediment concentration, thus this is correct. However, the value of H is only obtained when j is equal to Npz. In the SWC, Npz points j are considered, and thus j ranges from 0 to Npz-1 instead of from 0 to Npz. This means that in the numerical calculations the highest point had a z-value lower than H, which caused a portion of the water depth to be forgotten. With 22 points (Npz = 22), this leads to forgetting about 9% of the water depth at the top of the water column. Therefore, the formula should be adjusted to the following:

$$z(j) = 0.99H \cdot \frac{j^2}{(Npz-1)^2} + 0.01H \qquad (10.1.3)$$

In this case the maximum value for z of H is attained at $j = Npz - 1$, while a value of $j = 0$ still yields $z = 0.01H$.

A.2.3 A fix in the interpolation of the velocity profile that prevented a hole from falsely forming in the sand wave trough

When the boundary condition at the surface was changed from Neumann to no flux (see Section 4.3), the SWC was expected to run properly when the suspended sediment module was turned on. However, there was still an error which caused a very deep hole to develop in the trough of the sand wave after around 29 years of simulated time. The parameters used here were those of Set 1 (see Table 4, Section 3.2.2) with a residual current of 0.05 m/s. This hole ultimately became so deep that the SWC was unable to handle it. When the suspended sediment module was turned off, this hole did not develop.

Figure 36 shows the sand wave with the hole at 29 simulated years and before the hole has started to develop at 28 simulated years. The chosen sand wave length was 250 m, which corresponds to the fastest growing mode of the model version used to simulate it.

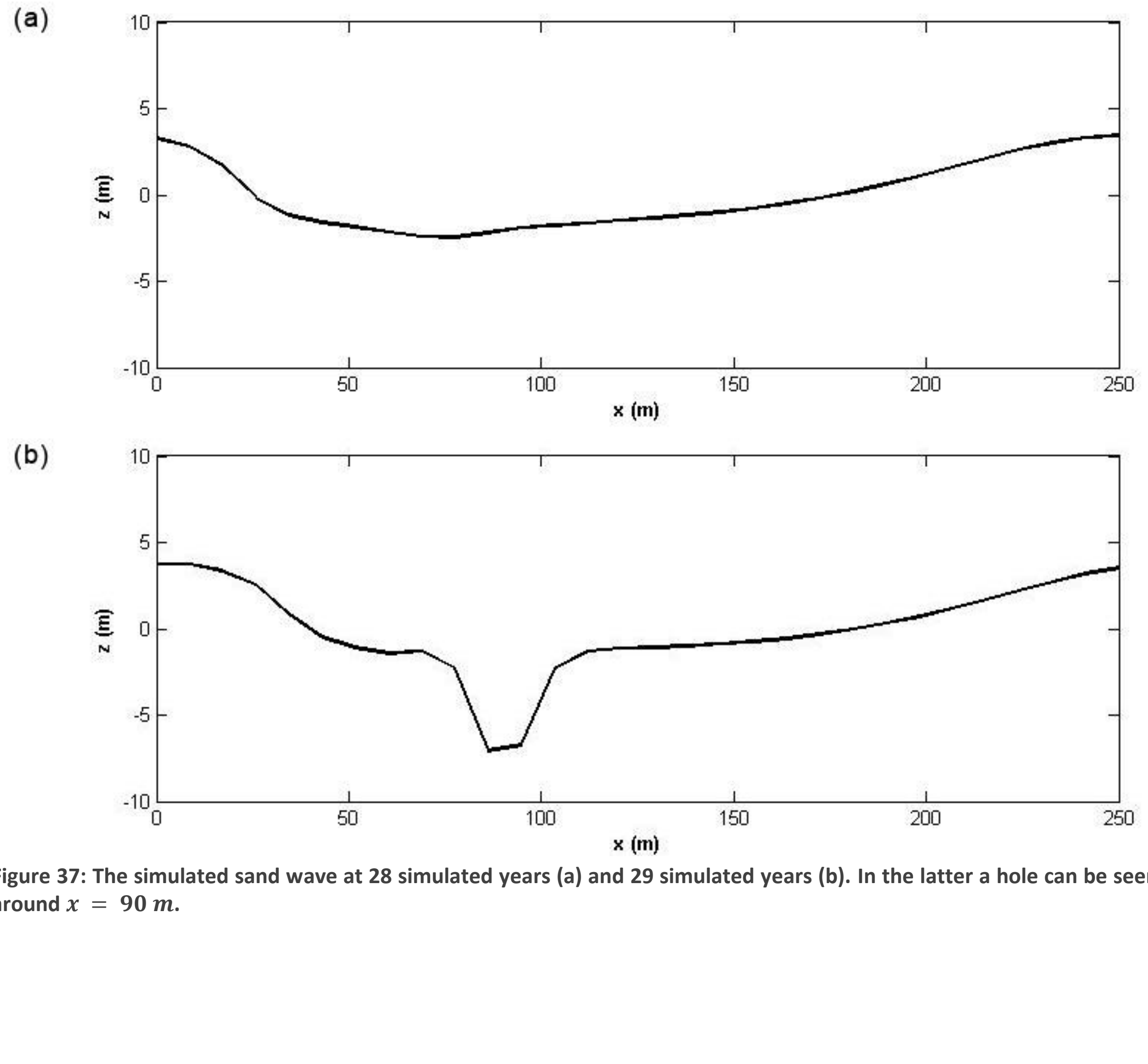

Figure 37: The simulated sand wave at 28 simulated years (a) and 29 simulated years (b). In the latter a hole can be seen around $x = 90\ m$.

The hole starts to develop for no apparent reason, when the trough reaches a depth of around $2.5\ \mathrm{m}$ with respect to $z = 0$. At the point where the trough is deepest, the vertical points z used in the calculation of the suspended sediment have the highest negative values. These negative z values are only used in the calculation of the diffusivity ϵ_v and in the determination of the horizontal flow velocity u for use in the suspended sediment calculation. In the calculation of the diffusivity the bottom elevation was already taken into account, so it could handle with the negative z values, which means the origin of the error was somewhere in the determination of u.

For the suspended sediment calculation, the calculation points are distributed quadratically over the water depth. In the calculation of the flow however, the calculation points are equally far apart. Because the value of the horizontal flow velocity u needs to be known at the quadratically distributed points, an interpolation is carried out. The values of u in the flow calculation are fitted to a polynomial. In generating this polynomial, the value of the vertical coordinate ranged from 0 to H, indicating that $\hat{z}$ was used instead of z. When calling the polynomial however, the value of z was used. Thus, to fix this, the value of $\hat{z}$ should be used instead when calling the polynomial. The simulation was redone after this fix. In the resulting sand wave at 29 simulated years is shown. No hole developed after this time either in this simulation.

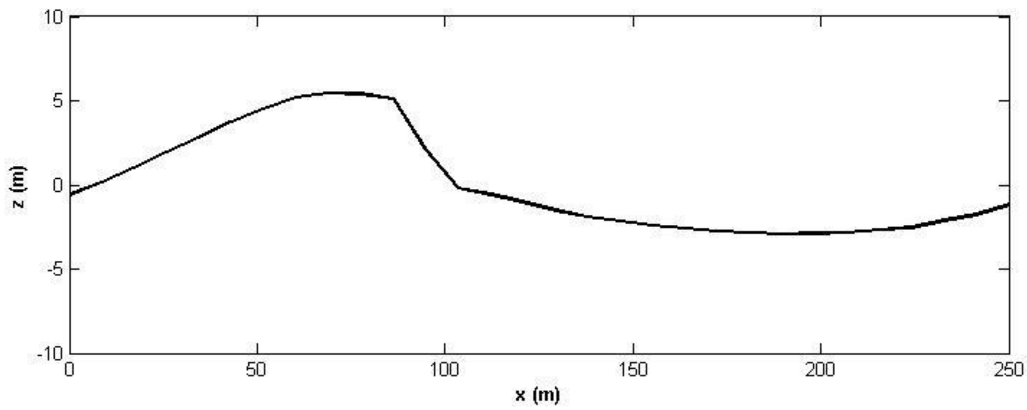

Figure 38: Newly simulated sand wave at 29 simulated years when the interpolation error is resolved.

This means that improving the interpolation of the velocity profile resolved this issue.

A.2.4 Improving the suspended sediment transport integration

In the previous version of the SWC, the suspended sediment transport was supposed to be calculated using the following:

$$q_s = \int_{z=a}^{H} u(z)c(z)dz \tag{10.1.4}$$

This can be discretized as follows:

$$[q_s]_i = \sum_{j=1}^{Npz-2} u_i(z_j) \cdot c_{i,j} \cdot \frac{z_{j+1} - z_{j-1}}{2} \tag{10.1.5}$$

However, in the implementation something went wrong as $u_i(z_j) \cdot c_{i,j}$ was multiplied with $\frac{z_{j+1}+z_{j-1}}{2}$, which meant that was integrated over $u(z)c(z)z$ instead of $u(z)c(z)dz$. This had a severe impact on the results and it could easily be corrected by changing the plus sign into a minus sign.

Furthermore, the concentration at the top of the water column (at the point with index $j = Npz$) and at the reference height (at the point with index $j = 0$) were not used for determining the suspended sediment transport. This could cause an underestimation of the sediment transport, as the concentration is the highest near the bottom. Therefore, the discretization of the suspended sediment transport equation has been changed to the following:

$$[q_s]_i = \sum_{j=0}^{Npz-2} u_i(z_j) \cdot \frac{c_{i,j} + c_{i,j+1}}{2} \cdot (z_{j+1} - z_j) \tag{10.1.6}$$

This way, the concentrations at the reference height and the surface both account for the transport in half a cell of height Δz. Note that this height Δz varies with depth (and thus with j) and bottom level.

A.2.5 Implementation of time in the tidal forcing

The velocity at the bed is calculated as a sum of three components, as follows:

$$u_{bed}(t) = U_0 + U_1 \sin(\omega t) + U_2 \cos(\omega t) \tag{10.1.7}$$

Where t is the time within the tidal cycle and U_0, U_1 and U_2 are constants that depend on the tidal velocity amplitude. The time t should range from zero to 44700 seconds for a full semi-diurnal tide. By accident the index of the time instead of the time was used in this equation in the previous version of the SWC. This resulted in only calculating the first 300 seconds of the semi-diurnal cycle. This had a severe impact on the results and could be easily corrected by changing the index of the time to the actual physical time.

A.3 Minor improvements to other parts of the code

Some other minor improvements have been carried out which have little to no effect on the results. One of them however did cause the SWC to crash on long simulations due to a memory leak.

A.3.1 Typing mistake in the calculation of the bed friction factor

The bed friction factor f_w is used in the calculation of the bed shear stress due to the surface waves. It is thus only used in the surface wave module of the SWC. It is calculated using the following equation:

$$f_w = \exp\left(-6 + 5.2\left(\frac{a}{2.5D_{50}}\right)^{-0.19}\right) \tag{10.1.8}$$

This equation is correctly formulated, but when implementing it in the SWC a dot had been mistaken for a comma. This led to an overestimation of the bed friction factor of about 25% for realistic values of the wave height and the sediment particle size. However, this overestimation caused no observable differences in model output.

A.3.2 Missing line for deletion of a temporary matrix

Another small mistake was causing quite some trouble while running the SWC. A temporary matrix is made containing all values of the current sediment concentrations. This temporary matrix however, was not deleted. This meant that every time step this rather large matrix containing values of the sediment concentrations was stored in the memory, causing a pile-up of memory when running the SWC. Eventually, the SWC would crash when using up all the memory that could be assigned to running it. This was solved by adding one line of code which deleted the temporary matrix after it had been used.

Appendix B: Discretization of the no flux boundary condition with a central difference approach by using a ghost point

In the SWC the surface lies at $j = Npz - 1$. For simplicity we define $J = Npz - 1$. When using a central difference approach, the numerical discretization of the equation above becomes:

$$c_{i,J} \cdot w_s + \tilde{\beta}\epsilon_{v_{i,J}} \frac{c_{i,J+1} - c_{i,J-1}}{\tilde{z}_{i,J+1} - \tilde{z}_{i,J-1}} = 0 \tag{10.2.1}$$

As can be seen, the terms $c_{i,J+1}$ and $\tilde{z}_{i,J+1}$ refer to points that don´t exist, at $j = Npz$. This means that for each point i along the x-axis a ghost point has been introduced. By definition, the distance $\Delta\tilde{z}$ between the ghost point and the surface is equal to the distance $\Delta\tilde{z}$ between the surface and the point just below the surface at $j = Npz - 2$, so:

$$\tilde{z}_{i,J+1} - \tilde{z}_{i,J} = \tilde{z}_{i,J} - \tilde{z}_{i,J-1} \tag{10.2.2}$$

This also means:

$$\tilde{z}_{i,J+1} - \tilde{z}_{i,J-1} = 2\left(\tilde{z}_{i,J} - \tilde{z}_{i,J-1}\right) \tag{10.2.3}$$

This way the $\tilde{z}$-term that refers to the ghost point can be eliminated:

$$c_{i,J} \cdot w_s + \tilde{\beta}\epsilon_{v_{i,J}} \frac{c_{i,J+1} - c_{i,J-1}}{2\left(\tilde{z}_{i,J} - \tilde{z}_{i,J-1}\right)} = 0 \tag{10.2.4}$$

The c term referring to the ghost point should also be eliminated from this equation, since it does not actually exist and should therefore not be used in the calculation. The only use of the ghost point is that we can use a central difference approach without actually using values at both sides (Thomas, 1995). In order to eliminate the c term referring to the ghost point, the transformed sediment transport equation is evaluated at $j = Npz - 1$:

$$\frac{1}{\tilde{\beta}}\frac{\partial c}{\partial \tilde{t}}\bigg|_{i,J} + \tilde{u}_{i,J}\frac{\partial c}{\partial \tilde{x}}\bigg|_{i,J} + \xcancel{\tilde{w}_{i,J}\frac{\partial c}{\partial \tilde{z}}\bigg|_{i,J}} = w_s\frac{\partial c}{\partial \tilde{z}}\bigg|_{i,J} + \xcancel{\frac{\partial \epsilon_v}{\partial z}\bigg|_{i,J}\frac{\partial c}{\partial \tilde{z}}\bigg|_{i,J}} + \tilde{\beta}\epsilon_{v_{i,J}}\frac{\partial^2 c}{\partial \tilde{z}^2}\bigg|_{i,J} \tag{10.2.5}$$

The third and fifth term can be immediately eliminated, as $\tilde{w} = 0$ at the surface and ϵ_v is constant at the upper half of the water column with a parabolic-constant distribution so its derivative is zero. When a linear distribution is used, this does not apply and the derivation is different. The equation above can be expressed in discretized terms:

$$\frac{1}{\tilde{\beta}}\frac{\mathrm{c_{i,J}}\big|_{\mathrm{t}} - \mathrm{c_{i,J}}\big|_{\mathrm{t-1}}}{\Delta \mathrm{t}} + \tilde{u}_{i,J}\frac{c_{i,J} - c_{i-1,J}}{\Delta x} = w_s\frac{c_{i,j+1} - c_{i,j}}{\tilde{z}_{i,j+1} - \tilde{z}_{i,j}} + \tilde{\beta}\epsilon_{v_{i,J}}\frac{\left(\frac{c_{i,J+1} - c_{i,J}}{\tilde{z}_{i,J+1} - \tilde{z}_{i,J}} - \frac{c_{i,J} - c_{i,J-1}}{\tilde{z}_{i,J} - \tilde{z}_{i,J-1}}\right)}{\left(\frac{\tilde{z}_{i,J+1} - \tilde{z}_{i,J-1}}{2}\right)} \tag{10.2.6}$$

Since $\tilde{z}_{i,J+1} - \tilde{z}_{i,J} = \tilde{z}_{i,J} - \tilde{z}_{i,J-1}$ (by definition), we can write:

$$\frac{1}{\tilde{\beta}}\frac{\mathrm{c_{i,J}}\big|_{\mathrm{t}} - \mathrm{c_{i,J}}\big|_{\mathrm{t-1}}}{\Delta \mathrm{t}} + \tilde{u}_{i,J}\frac{c_{i,J} - c_{i-1,J}}{\Delta x} = w_s\frac{c_{i,J+1} - c_{i,J}}{\tilde{z}_{i,J} - \tilde{z}_{i,J-1}} + \tilde{\beta}\epsilon_{v_{i,J}}\frac{c_{i,J+1} - 2c_{i,J} + c_{i,J-1}}{\left(\tilde{z}_{i,J} - \tilde{z}_{i,J-1}\right)^2} \tag{10.2.7}$$

Note that in this equation it is assumed that $\tilde{u}_{i,J}$ is positive. If it were negative, the point to the right would be used instead of the point to the left. At the end of this paragraph, two versions of the equation will be given, one for positive and one for negative values of $\tilde{u}_{i,J}$. We rearrange the above equation to attain an expression for $c_{i,J+1}$, which is the concentration at the ghost point.

$$w_s \frac{c_{i,J+1}}{\tilde{z}_{i,J} - \tilde{z}_{i,J-1}} + \tilde{\beta}\epsilon_{v_{i,J}} \frac{c_{i,J+1}}{\left(\tilde{z}_{i,J} - \tilde{z}_{i,J-1}\right)^2} = \frac{1}{\tilde{\beta}} \frac{\mathrm{c_{i,J}}\big|_{\mathrm{t}} - \mathrm{c_{i,J}}\big|_{\mathrm{t-1}}}{\Delta \mathrm{t}} + \tilde{u}_{i,J} \frac{c_{i,J} - c_{i-1,J}}{\Delta x} + w_s \frac{c_{i,J}}{\tilde{z}_{i,J} - \tilde{z}_{i,J-1}} + \tilde{\beta}\epsilon_{v_{i,J}} \frac{2c_{i,J} - c_{i,J-1}}{\left(\tilde{z}_{i,J} - \tilde{z}_{i,J-1}\right)^2} \tag{10.2.8}$$

$$c_{i,J+1}\left(\frac{w_s}{\tilde{z}_{i,J} - \tilde{z}_{i,J-1}} + \frac{\tilde{\beta}\epsilon_{v_{i,J}}}{\left(\tilde{z}_{i,J} - \tilde{z}_{i,J-1}\right)^2}\right) = \frac{1}{\tilde{\beta}} \frac{\mathrm{c_{i,J}}\big|_{\mathrm{t}} - \mathrm{c_{i,J}}\big|_{\mathrm{t-1}}}{\Delta \mathrm{t}} + \tilde{u}_{i,J} \frac{c_{i,J} - c_{i-1,J}}{\Delta x} + w_s \frac{c_{i,J}}{\tilde{z}_{i,J} - \tilde{z}_{i,J-1}} + \tilde{\beta}\epsilon_{v_{i,J}} \frac{2c_{i,J} - c_{i,J-1}}{\left(\tilde{z}_{i,J} - \tilde{z}_{i,J-1}\right)^2} \tag{10.2.9}$$

$$c_{i,J+1} = \left(\frac{\frac{1}{\tilde{\beta}} \frac{\mathrm{c_{i,J}}\big|_{\mathrm{t}} - \mathrm{c_{i,J}}\big|_{\mathrm{t-1}}}{\Delta \mathrm{t}} + \tilde{u}_{i,J} \frac{c_{i,J} - c_{i-1,J}}{\Delta x} + w_s \frac{c_{i,J}}{\tilde{z}_{i,J} - \tilde{z}_{i,J-1}} + \tilde{\beta}\epsilon_{v_{i,J}} \frac{2c_{i,J} - c_{i,J-1}}{\left(\tilde{z}_{i,J} - \tilde{z}_{i,J-1}\right)^2}}{\left(\frac{w_s}{\tilde{z}_{i,J} - \tilde{z}_{i,J-1}} + \frac{\tilde{\beta}\epsilon_{v_{i,J}}}{\left(\tilde{z}_{i,J} - \tilde{z}_{i,J-1}\right)^2}\right)}\right) \tag{10.2.10}$$

In order to remove the ghost point from the boundary condition, this expression can be entered into the equation that describes the no flux condition:

$$c_{i,J} w_s + \tilde{\beta}\epsilon_{v_{i,J}} \frac{\left(\frac{\frac{1}{\tilde{\beta}} \frac{\mathrm{c_{i,J}}\big|_{\mathrm{t}} - \mathrm{c_{i,J}}\big|_{\mathrm{t-1}}}{\Delta \mathrm{t}} + \tilde{u}_{i,J} \frac{c_{i,J} - c_{i-1,J}}{\Delta x} + w_s \frac{c_{i,J}}{\Delta \tilde{z}} + \tilde{\beta}\epsilon_{v_{i,J}} \frac{2c_{i,J} - c_{i,J-1}}{(\Delta \tilde{z})^2}}{\left(\frac{w_s}{\Delta \tilde{z}} + \frac{\tilde{\beta}\epsilon_{v_{i,J}}}{(\Delta \tilde{z})^2}\right)}\right) - c_{i,J-1}}{2(\Delta \tilde{z})} = 0 \tag{10.2.11}$$

The equation above has been made readable by replacing $\tilde{z}_{i,J} - \tilde{z}_{i,J-1}$ with $\Delta\tilde{z}$. Since the Sand Wave Code stores values of the concentration c of different locations separately, the equation above has been rewritten as follows:

$$\begin{aligned} &c_{i,J} \cdot \left(w_s + \tilde{\beta}\epsilon_{v_{i,J}} \frac{\left(\frac{\frac{1}{\tilde{\beta}\Delta \mathrm{t}} + \frac{\tilde{u}_{i,J}}{\Delta x} + \frac{w_s}{\Delta \tilde{z}} + \frac{2\tilde{\beta}\epsilon_{v_{i,J}}}{(\Delta \tilde{z})^2}}{\left(\frac{w_s}{\Delta \tilde{z}} + \frac{\tilde{\beta}\epsilon_{v_{i,J}}}{(\Delta \tilde{z})^2}\right)}\right)}{2(\Delta \tilde{z})}\right) + c_{i,J-1} \cdot \left(\frac{\left(\frac{-\frac{\tilde{\beta}^2 {\epsilon_{v_{i,J}}}^2}{(\Delta \tilde{z})^2}}{\left(\frac{w_s}{\Delta \tilde{z}} + \frac{\tilde{\beta}\epsilon_{v_{i,J}}}{(\Delta \tilde{z})^2}\right)}\right) - 1}{2(\Delta \tilde{z})}\right) \\ &\quad + c_{i-1,J} \cdot \left(-\frac{\left(\frac{\frac{\tilde{\beta}\epsilon_{v_{i,J}}\tilde{u}_{i,J}}{\Delta x}}{\left(\frac{w_s}{\Delta \tilde{z}} + \frac{\tilde{\beta}\epsilon_{v_{i,J}}}{(\Delta \tilde{z})^2}\right)}\right)}{2(\Delta \tilde{z})}\right) + \mathrm{c_{i,J}}\big|_{\mathrm{t-1}} \cdot \left(-\frac{\left(\frac{\frac{\epsilon_{v_{i,J}}}{\Delta \mathrm{t}}}{\left(\frac{w_s}{\Delta \tilde{z}} + \frac{\tilde{\beta}\epsilon_{v_{i,J}}}{(\Delta \tilde{z})^2}\right)}\right)}{2(\Delta \tilde{z})}\right) \\ &\quad = 0 \end{aligned} \tag{10.2.12}$$

Equations (10.2.11) and (10.2.12) only count for positive values of $\tilde{u}_{i,J}$, for negative values of $\tilde{u}_{i,J}$ the expressions become:

$$c_{i,J}w_s+\tilde{\beta}\epsilon_{v_{i,J}}\frac{\left(\frac{\frac{1}{\tilde{\beta}}\frac{\mathrm{c_{i,J}}|_{\mathrm{t}}-\mathrm{c_{i,J}}|_{\mathrm{t-1}}}{\Delta\mathrm{t}}+\tilde{u}_{i,J}\frac{c_{i,J}-c_{i+1,J}}{\Delta x}+w_s\frac{c_{i,J}}{\Delta\tilde{z}}+\tilde{\beta}\epsilon_{v_{i,J}}\frac{2c_{i,J}-c_{i,J-1}}{(\Delta\tilde{z})^2}}{\left(\frac{w_s}{\Delta\tilde{z}}+\frac{\tilde{\beta}\epsilon_{v_{i,J}}}{(\Delta\tilde{z})^2}\right)}\right)-c_{i,J-1}}{2(\Delta\tilde{z})}=0 \tag{10.2.13}$$

$$\begin{aligned}&c_{i,J}\cdot\left(w_s+\tilde{\beta}\epsilon_{v_{i,J}}\frac{\left(\frac{\frac{1}{\tilde{\beta}\Delta\mathrm{t}}+\frac{\tilde{u}_{i,J}}{\Delta x}+\frac{w_s}{\Delta\tilde{z}}+\frac{2\tilde{\beta}\epsilon_{v_{i,J}}}{(\Delta\tilde{z})^2}}{\left(\frac{w_s}{\Delta\tilde{z}}+\frac{\tilde{\beta}\epsilon_{v_{i,J}}}{(\Delta\tilde{z})^2}\right)}\right)}{2(\Delta\tilde{z})}\right)+c_{i,J-1}\cdot\left(\frac{\left(-\frac{\frac{\tilde{\beta}^2\epsilon_{v_{i,J}}{}^2}{(\Delta\tilde{z})^2}}{\left(\frac{w_s}{\Delta\tilde{z}}+\frac{\tilde{\beta}\epsilon_{v_{i,J}}}{(\Delta\tilde{z})^2}\right)}\right)-1}{2(\Delta\tilde{z})}\right)\\&\quad+c_{i+1,J}\cdot\left(-\frac{\left(\frac{\frac{\tilde{\beta}\epsilon_{v_{i,J}}\tilde{u}_{i,J}}{\Delta x}}{\left(\frac{w_s}{\Delta\tilde{z}}+\frac{\tilde{\beta}\epsilon_{v_{i,J}}}{(\Delta\tilde{z})^2}\right)}\right)}{2(\Delta\tilde{z})}\right)+\mathrm{c_{i,J}}|_{\mathrm{t-1}}\cdot\left(-\frac{\left(\frac{\frac{\epsilon_{v_{i,J}}}{\Delta\mathrm{t}}}{\left(\frac{w_s}{\Delta\tilde{z}}+\frac{\tilde{\beta}\epsilon_{v_{i,J}}}{(\Delta\tilde{z})^2}\right)}\right)}{2(\Delta\tilde{z})}\right)\\&\quad=0\end{aligned} \tag{10.2.14}$$

Unfortunately, this does not make things look any less complicated. It is very hard to implement this into the SWC. Also, it is of a higher order than most things implemented in the SWC, meaning that it is probably safer to implement the no flux condition without a ghost point. Implementing the no flux condition with a ghost point could thus cause instabilities in the SWC that are hard to predict. Furthermore, mistakes are bound to be made when implementing such a large equation.